A TRANSLATIONAL APPROACH TO IDENTIFY MICRORNA THAT REGULATE THE VOLTAGE-GATED POTASSIUM CHANNEL, KCNH2

by

Abdullah Assiri

A Dissertation

Submitted to the Faculty of Purdue University

In Partial Fulfillment of the Requirements for the degree of

Doctor of Philosophy

Department of Pharmacy Practice

West Lafayette, Indiana

May 2019

THE PURDUE UNIVERSITY GRADUATE SCHOOL
STATEMENT OF COMMITTEE APPROVAL

Dr. Brian R. Overholser Chair
Department of Pharmacy Practice
Dr. David R. Foster
Department of Pharmacy Practice
Dr. James E. Tisdale
Department of Pharmacy Practice
Dr. Kevin M. Sowinski
Department of Pharmacy Practice
Dr. Todd Skaar
Department of Pharmacy Practice

Approved by:

Dr. Buck Doe
Head of the Graduate Program

This work is dedicated to my parents, Ayde and Fatima, and my daughter Layan, with love and gratitude

ACKNOWLEDGMENTS

I would like to thank all the individuals who contributed to my progression throughout the years in this program and made this work possible. Firstly, I would like to express my sincere gratitude to my major advisor, Dr. Brian Overholser, for his guidance and continuous support during my PhD. His continuous motivation, patience, and guidance were the reasons behind me being able to write this thesis. I could not imagine having a better mentor for my PhD; I am really blessed and grateful to have had the opportunity to work with him, and will never forget everything he has made and done for me.

Besides my mentor, I would like to thank the rest of my committee members, Dr. Tisdale, Dr. Sowinski, Dr. Foster, and Dr. Skaar for their support, their insightful comments and input, and their encouragement and motivating advice.

Lastly, I would like to thank my family for their eternal support. I would like to thank my parents and their patience with me being away from them for almost ten years. In addition, I would like to thank my brothers Moshabab, Khalid, Saleh, Abdulaziz, and Ahmed, as well as my sister, Jamelah, for supporting me throughout my journey. I would also like to thank my daughter, Layan, for being patient with me being away from her for almost two years and for caring about me all the time.

TABLE OF CONTENTS

LIST OF TABLES

LIST OF FIGURES

ABSTRACT

Author: Assiri, Abdullah. PharmD, PhD
Institution: Purdue University
Degree Received: May 2019
Title: A Translational Approach to Identify microRNA that Regulate the Voltage-Gated Potassium Channel, KCNH2
Committee Chair: Brian Overholser

The human ether-a-go-go-related gene (hERG, KCNH2) potassium channel has been implicated in diverse physiological and pathological processes. The *KCNH2* gene encodes a rectifier voltage-gated potassium channel (Kv 11.1) that governs the chief repolarizing current, I_{Kr}, which is essential for normal electrical activity in excitable cells such as cardiomyocytes. It is also involved in cell growth and apoptosis regulation in non-excitable cells, such as tumor cells. Dysfunction of hERG is associated with potentially lethal complications, including diseases and sudden death under certain circumstances. While the mechanisms regulating *KCNH2* expression remain unclear, recent data suggested that microRNAs (miRNAs) are involved, particularly in the context of several pathologic effects.

miRNA is a class of RNA defined by its conserved, short, non-coding nature. miRNAs are important regulators of gene expression at the post-transcriptional level that bind through complimentary annealing to the 3' untranslated regions (3' UTRs) of target mRNAs, resulting in mRNA destabilization and translational repression. The primary objectives of this research were to 1) identify miRNAs regulating *KCNH2* expression in cancer, 2) investigate the potential association between miR-362-3p expression and risk of drug-induced QT interval lengthening, and 3) identify miRNAs potentially regulating *KCNH2* expression and function in cardiac cells.

Through bioinformatics approaches, five miRNAs were identified to potentially regulate *KCNH2* expression and function in breast cancer cells. The five identified miRNAs were validated

through a Dual-Luciferase Assay using the *KCNH2* 3′ UTR. Only miR-362-3p was validated to bind to the *KCNH2* 3' UTR, decreasing luciferase activity by 10% ± 2.3 ($P < 0.001$, n = 3) when compared to cells transfected with luciferase plasmid alone. miR-362-3p was also the only miRNA that its expression positively correlated with overall survival of patients with breast cancer from The Cancer Genome Atlas-Cancer Genome (TCGA) database by log-rank test (HR: 0.39, 95% CI: 0.18 to 0.82, $P = 0.012$). Cell proliferation was assessed by MTS assay (3-(4,5-dimethylthiazol-2-yl)-5-(3-carboxymethoxyphenyl)-2-(4-sulfophenyl)-2H-tetrazolium) 48 hours following transfection in breast cancer cell lines, including SK-BR-3 and MCF-7. miR-362-3p significantly decreased proliferation of SK-BR-3 and MCF-7 cells by 23% ± 8.7 ($P = 0.014$, n = 3) and 11.7% ± 1.0 ($P < 0.001$, n = 3), respectively. Cell cycle phases in SK-BR-3 and MCF-7 cells were differentiated by flow cytometry 48 hours following transfection. miR-362-3p and hERG siRNA (positive control) significantly increased the accumulation of cells in G0/G1 phase in MCF-7 by 11.7% (from 51.1% ± 0.64 to 57.1 ± 0.96, $P = 0.002$, n = 3) and 10% (from 51.1% ± 0.64 to 56.8 ± 0.96, $P < 0.001$, n = 3), respectively.

The demonstrated ability of miR-362-3p to regulate hERG in breast cancer cells coupled with previously published data that indicated an alteration of miR-362-3p expression during HF and a potential association between its expression and QT interval prolongation suggesting an important role for this miRNA in regulation of hERG function during HF. Therefore, the contribution of miR-362-3p to hERG function was investigated in patients administered the QT prolonging drug ibutilide, known to inhibit hERG. A total of 22 patients completed a prospective, parallel-group comparative study during which they received subtherapeutic doses (0.003 mg/kg) of ibutilide. The study was originally designed to investigate the influence of heart failure with preserved ejection fraction (HFpEF) on response to drug-induced QT prolongation. Blood for

determination of serum Ibutilide concentrations and miR-362-3p expression, along with electrocardiograms (ECGs) were serially collected over a span of 12 hours. ΔΔ-Fridericia-heart rate corrected QT ($\Delta\Delta QT_F$) intervals were utilized for all analyses to account for baseline and diurnal variation.

To assess the ability of miR-362-3p to predict ibutilide QT-induced $\Delta\Delta QT_F$ changes, nonlinear mixed effects pharmacokinetic/ pharmacodynamic (PKPD) modeling was performed to assess the contribution of miR-362-3p to drug-induced QT interval lengthening. The model that best fit serum ibutilide concentrations versus time was a 3-compartment model with first order elimination and proportional residual errors, while the model that best described the ibutilide concentration- $\Delta\Delta QT_F$ relationship was an E_{max} model with an effect compartment. In addition to miR-362-3p expression, several demographic and clinical data were evaluated as potential covariates on PK and PD parameter estimates. Of tested covariates, heart failure (HF) status on E_{max} (ΔOFV = -4.1; $P < 0.05$), and miR-362-3p expression on EC_{50} (ΔOFV = -9.9; $P < 0.05$) were incorporated in the final PKPD model. The mean individual E_{max} was significantly higher in HF patients when compared to non-HF patients ($P = 0.015$), while EC_{50} was negatively correlated with miR-362-3p expression ($P < 0.0001$, R^2 0.93).

Previous evidence indicates that miR-362-3p is altered in patients with HF. In addition, several miRNAs commonly regulate the same ion channel. Therefore, we have developed a large-scale high-throughput bioassay (HT-bioassay) to explore and identify other miRNAs potentially involved in *KCNH2* expression and function in human induced pluripotent stem cell-derived cardiomyocytes (hiPS-CM) during sustained β-adrenergic receptor (βAR) stimulation or overexpression of activated calcium/calmodulin-dependent protein kinase 2 (CaMKII), which are classical consequences of HF.

Through bioinformatic approaches, putative miRNA binding sites (n=327) were identified in the *KCNH2* 3′ UTR. Fragments containing these putative binding sites were synthesized, cloned into linearized plasmids, and amplified. The plasmid pool was transfected into hiPS-CM cells either treated with βAR stimulation or overexpressing CaMKII. Next-generation sequencing was performed to identify: 1) expression of putative miRNA binding sites and 2) endogenous miRNAs versus control. Eight predicted binding sites were found to be significantly downregulated in the CAMKII group (P <0.05, log fold change -0.287 to -0.59), and six significantly downregulated in the sustained βAR group (P <0.05, log fold change -0.29 to -0.72). Two binding sites were significantly reduced in both treatment groups (P < 0.05, log fold change between -0.38 and -0.61).

Thirty-one miRNAs were predicted to bind to the 16 binding sites identified from the bioassay. Of these, seven were selected for further screening using dual luciferase assays. None of the putative miRNAs reduced luciferase activity. However, hERG expression was assessed by immunoblot analysis following transfection of the seven miRNAs into HEK293 cells stably expressing hERG (HEK293-hERG). Six of the seven miRNA mimics reduced hERG protein expression. An additional validation step was performed by assessing hERG-related current density by whole cell electrophysiology, in which three of the six miRNAs inhibited hERG protein transfected into HEK293-hERG cells. Those same three miRNA mimics significantly decreased I_{kr} current (P <0.05).

Finally, expression of the miRNAs identified by HT-bioassay was examined in the patients enrolled in the clinical trial in which genome-wide next generation sequencing was performed on miRNAs extracted from whole blood samples. Of the 31 miRNAs identified from HT-bioassay, six were found to be expressed in patients (n = 12). A correlation analysis was performed between

levels of the expressed miRNAs and corresponding QT_F interval lengthening with ibutilide. Of the six miRNAs, only miR-4665-5p was significantly associated with QT_F interval ($P = 0.0379$).

In summary, miR-362-3p was identified to regulate hERG, and reduces proliferation of breast cancer cells through a mechanism that may be partially mediated by hERG inhibition. While miR-362-3p may have modest effects in cancer, in Aim 2 we demonstrated that it along with HF status accounts for a significant amount of variability in QT_F prolongation following ibutilide administration. However, it is common for several miRNAs to regulate a single ion channel. Therefore, an HT-bioassay was developed to identify all miRNAs that potentially regulate *KCNH2* during HF. In addition to miR-362-3p, thirty-one miRNAs were predicted to regulate *KCNH2*; one miRNA (miR-4665-5p) was significantly associated with QT_F prolongation. The potential for miR-362-3p and HT-bioassay-identified miRNAs to reduce hERG-related current and influence susceptibility to drug-induced QT interval prolongation warrants further investigation.

CHAPTER 1. INTRODUCTION

1.1 KCNH2 definition

KCNH2 is the official name for the human ether-a-go-go related gene (hERG), which encodes the pore-forming subunit of the rapid component of the delayed rectifier voltage-gated potassium channels (Abbott, et al. 1999). These channels are generally referred to as hERG, IKr, or Kv11.1. In this work, KCNH2 refers to the gene or mRNA and hERG refers to the pore-forming subunit protein expression (Vandenberg, et al. 2012). Kv11.1 would refer to the full protein with all the auxiliary subunits that confer the physiological I_{Kr}. While the physiological function of hERG is best characterized in the heart, hERG is also expressed in several other cell types including smooth muscle, endocrine cells, and a wide range of tumor cell lines. These potassium channels have a variety of roles depending on the specific cell or tissue type context (Akbarali, et al. 1999).

1.2 Gene and protein structure

The human *KCNH2* gene is located in region q36.1 on chromosome 7, spans approximately 33 kb, and contains 15 exons. It contains three alternative transcription start sites and two alternative termination sites, resulting in five *KCNH2* transcript variants (Itoh, et al. 1998). The full-length transcript, *KCNH2-1a*, is the predominant transcript expressed in the heart, and gives rise to a 1,159 amino acid protein. Use of an alternate transcription start site in intron 5 of the full-length transcript produces *KCNH2-1b*, which lacks the first five exons. Both *KCNH2-1a* and *KCNH2-1b* are identical from exon 6 and onwards. The third transcript is *KCNH2-1c*, which has its transcription start site in intron 2; it lacks the first two exons but is thereafter identical to

KCNH2-1a. These three transcripts can form functional channels with distinct gating properties. An alternative stop codon in exon 9 results in a transcript with a premature COOH-terminal truncation, referred to as $KCNH2_{USO}$ *(Lees-Miller, et al. 1997; London, et al. 1997)*. The three *KCNH2* isoforms (a-c) are functional and mediate I_{Kr} current while the $KCNH2_{USO}$ isoforms are not functional but can modulate the channel characteristics.

Functional hERG channels are tetramers with a pore domain formed by the coassembly of four α-subunits. Each α-subunit consists of six transmembrane α-helical segments (S1-S6) along with large cytoplasmic NH2- and COOH- terminal domains. The S1-S4 segments form the voltage sensor domain, while S5, S6, and the pore loop from each of the four subunits form the ion-conducting pore domain. These pore domains line the central potassium ion conduction pathway (Morais Cabral, et al. 1998; Warmke and Ganetzky 1994).

Exon 1 of *KCNH2* encodes the 5'UTR, which plays a critical role in channel deactivation kinetics. Exons 2 and 3 encode the Per-Arnt-Sim (PAS) domain of the protein's NH2 terminus. Exon 6 encompasses the NH2 terminus and 1-3 transmembrane segments. Segment 4 and the pore domain are mostly encoded by exon 7, while the remaining exons encode the c-linker, the cyclic nucleotide binding domain, and the distal COOH terminal domain (Jiang, et al. 2002; Liu and Grigoriev 2004).

The accessory β-subunits *KCNE1* and *KCNE2* are single transmembrane proteins that can interact with a hERG α-subunit. These accessory subunits are not essential components of the I_{Kr} current, but are essential for the slow delayed rectifier potassium (I_{Ks}) (Anantharam and Abbott 2005; McDonald, et al. 1997). However, previous literature has shown that *KCNE1* and *KCNE2* may interact with hERG and alter its gating kinetics in mammalian cells (Anantharam and Abbott 2005).

1.3 Physiological role of hERG channels

While hERG are expressed in various tissues (Guasti, et al. 2005; Huffaker, et al. 2009; Rosati, et al. 2000), their physiological roles are best characterized in cardiac cells (Carmeliet 1992; Lees-Miller, et al. 1997; London, et al. 1997). Similar to other voltage-gated potassium channels, the S4 segment contains two basic Arg residues (R528, R531) and one Lys residue (K525) that contribute to the activation gating charge and acts as the primary voltage sensor for channel activation (Aggarwal and MacKinnon 1996; Liman, et al. 1991; Tristani-Firouzi, et al. 2002). The channels can exist in the following states: closed, open, or inactivated. Transitions between these states are voltage-dependent. Furthermore, the transition between closed and open in response to membrane depolarization is very slow, while that between open and inactivated is much faster(Piper, et al. 2005; Subbiah, et al. 2004; Zhang, et al. 2004). The slow activation and deactivation of hERG channels coupled with their rapid, voltage-dependent inactivation kinetics make them ideally suited for the physiological role of I_{Kr} in cardiac repolarization (Sanguinetti and Tristani-Firouzi 2006).

The I_{Kr} current plays a critical role in determining the duration of the plateau phase of atrial and ventricular action potentials, which is key to allowing sufficient time for calcium release to enable cardiac contraction. The plateau phase is terminated when repolarization (phase 3) begins as a result of I_{Kr} outward current coupled with other outward potassium channels, including I_{Ks} current. As repolarization begins, the hERG channels rapidly recover from inactivation, allowing more I_{Kr} current to pass and resulting in an outward tail current that further repolarizes the cell (Sanguinetti and Tristani-Firouzi 2006; Smith, et al. 1996).

Pharmacological inhibition and other factors including genetic defects in hERG channels can result in reduction in I_{kr} current and subsequently lead to hereditary or acquired long QT

syndromes; these are characterized by increased action potential duration, lengthened QT interval, and increased risk for life-threatening ventricular arrhythmia and sudden cardiac arrest. The increase in QTc of 60 ms or QTc interval prolongation to greater than 500 ms are generally considered a major determinant of the risk of drug induced torsades de pointes *(*TdP). Loss of function mutations in *KCNH2* result in reduction of I_{kr} currents, which produces long QT syndrome type 2 (LQTS2). LQTS2 is the second most common type of long QT syndrome, making up about 25% of all QT syndrome cases(Anderson, et al. 2006; Smith, et al. 2016). Acquired LQTS can be due to drugs or other diseases (El-Sherif, et al. 2018; Yap and Camm 2003). Most drugs are believed to prolong QT interval by inhibiting I_{kr} current resulting in increasing the action potential duration and hence increase susceptibility to early afterdepolarizations and the development of life-threatening arrhythmias, including TdP (Drici and Barhanin 2000; El-Sherif, et al. 2018; Roden and Viswanathan 2005; Sanguinetti, et al. 1995). TdP is a distinctive form of polymorphic ventricular tachyarrhythmia that appears on an ECG as continuous twisting of the QRS complex around the ECG baseline. TdP can degenerate into sustained ventricular tachycardia or ventricular fibrillation resulting in sudden cardiac death (El-Sherif, et al. 2018; Yap and Camm 2003).

1.4 KCNH2 in cancer

In addition to the important role of KCNH2 in cardiac cells, there is increasing evidence that hERG channels are involved in the development and pathophysiology of cancer (D'Amico, et al. 2013; Lastraioli, et al. 2015). *KCNH2* has been implicated as an oncogene that is overexpressed in several types of cancer, including breast cancer, glioblastoma, and colorectal cancer (Fiore, et al. 2013; Pointer, et al. 2017; Staudacher, et al. 2014; Wang, et al. 2015). Furthermore, several pieces of evidence indicate that membrane potential changes during cellular differentiation and cell cycle

progression (Staudacher, et al. 2014). Therefore, it is unsurprising that voltage-gated channels such as hERG are expressed more frequently in tumors than their corresponding normal tissues. High expression of *KCNH2* in cancer tissue correlates with the fact that membrane potentials in cancer cells are more depolarized at a membrane potential, in which hERG channels usually closed; noncancerous cells display more negative membrane potentials, suggesting lower *KCNH2* expression levels.

In proliferating cells, the resting membrane potential varies from -40 to -90 mV. Differences in membrane potential between cells correlate to their respective proliferative potentials, ranging from -70 to -90 mV (slowly proliferative) to -40 to -55 mV (highly proliferative) (Binggeli and Weinstein 1986). During the G1 phase, cycling cells are depolarized, which can be largely attributed to the fact that hERG channels close at membrane potentials below -60 mV(Shapovalov, et al. 2011); the predominance of hERG channels in these cells maintains a more depolarized membrane potential that facilitates cell cycle progression, and thus accelerates the growth and invasiveness of tumors (Bianchi, et al. 1998).

The first study investigating the role of hERG channels in cancer examined hERG expression and function in 17 different tumor cell lines using northern blot analysis and the patch clamp technique (Bianchi, et al. 1998). The examined tumor cells had much higher hERG expression than their corresponding non-cancerous cells. The findings of this study suggest that hERG over-expression results in depolarized resting membrane potential in cancer cell lines that may facilitate cell proliferation and enhance cell survival, while hERG similar current (K+ inward-rectifier current) was not detected in non-cancerous cells. Another study showed that the hERG channel blocker E4031 reduced cell migration in the FLG29.1 leukemic cell line, which expresses hERG channels. Cell cycle analysis following treatment with E4031 revealed accumulation of cells in the

G1 phase (Smith, et al. 2002). However, cell cycle arrest in the G1 phase was not observed with other hERG blockers such as terazosin or in other cell lines expressing hERG channels (Benning and Kyprianou 2002), indicating that hERG function varies between cells.

In human colorectal cancer, hERG channels were identified as regulators of tumor invasion, and their expression was observed more frequently in patients with poor prognosis and metastatic cancers than in those with less aggressive cancers (Lastraioli, et al. 2004), suggesting a potential role for hERG in colorectal cancer growth.

In breast cancer, hERG channels are expressed in various cell lines, including SK-BR-3, MCF-7, and MDA-MB-231 (Bianchi, et al. 1998). Wang et al. investigated the role of hERG in MCF-7 cells and showed that arsenic trioxide induces the apoptosis of MCF-7 cells through inhibition of hERG channels and activation of caspase-3 (Wang, et al. 2015). In addition, hERG channels have been thoroughly studied in many other cancers, including esophageal, gastric, pancreatic, endometrial, and ovarian cancers. Ongoing findings concerning hERG channels and their functions in different cancers, including breast cancer, suggest importance for these channels and their potential use as a novel target in cancer therapy.

1.5 miRNA definition and function

miRNAs are small, evolutionarily conserved, single-strand non-coding RNA molecules with an average length of 22 nucleotides. miRNAs regulate target mRNAs negatively and post-transcriptionally by cleaving them or just repressing their translation (Lee, et al. 1993; O'Brien, et al. 2018; Perron and Provost 2008). It has been shown that miRNAs tend to target and regulate the expression of more than one mRNA, and mRNA target can be regulated by a set of miRNAs rather than one specific miRNA alone. In most cases, miRNAs regulate mRNAs through binding to

sequence motifs in the target's 3'UTR (Ha and Kim 2014). However, miRNAs can interact with other regions including the coding sequence, 5'UTR, or promoters (Broughton, et al. 2016). Additionally, several studies showed that miRNAs can induce gene expression under certain conditions (Vasudevan 2012).

miRNAs are critical for nearly all development and growth in humans. Aberrant expression of miRNAs has been demonstrated to be involved in a variety of pathological processes and other clinically important diseases (Ardekani and Naeini 2010). Several mechanisms can lead to dysregulation of miRNA expression and impairment of miRNA function, including single point mutations in miRNAs or their corresponding targets(Lee, et al. 2011).

1.6 miRNA biogenesis and regulation

The biogenesis of a miRNA starts with transcription of its host gene by RNA polymerase II/III, then the production of a primary miRNA (pri-miRNA) that contains a local hairpin structure. The pri-miRNA is subsequently processed into precursor miRNA (pre-miRNA) by a microprocessor consisting of ribonuclease III and Drosa (Cullen 2004; Denli, et al. 2004). After the pre-miRNA is generated, it is exported to the cytoplasm by the exportin 5 complex, then further processed into a mature miRNA by the RNase III endonuclease Dicer (Chendrimada, et al. 2005). About half of identified miRNAs are intragenic and encoded within the introns of coding and non-coding transcripts; relatively few are processed from the exons of protein-coding genes. Both of these types of miRNA are co-expressed with and in some cases share the same promoter as the corresponding protein-coding sequence. Still other miRNAs are intergenic, in which they are transcribed from independent transcription units and regulated by their own promoters (de Rie, et

al. 2017). Sometimes, miRNAs are co-transcribed as a cluster; these miRNAs may have similar seed regions and are considered a family of miRNAs (Tanzer and Stadler 2004).

1.7 Mechanisms of miRNA-mediated gene regulation

Once a miRNA duplex has been generated by Dicer, it is subsequently loaded in the Argonaute (AGO) complex to form an effector complex known as the pre-minimal miRNA-induced silencing complex (pre-miRISC). After loading, the passenger strand is quickly removed from the miRNA duplex, resulting in mature miRISC. This complex operates by base pairing the miRNA with a target mRNA, with the AGO protein recruiting factors to facilitate binding and induce translational repression or mRNA decay (Dueck, et al. 2012).

The recognition of a mRNA target and the specificity of binding by miRISC are based on Watson-Crick pairing of the miRNA's 5' seed region (nucleotides 2-8) to the corresponding site in the target mRNA's 3'UTR (Bartel 2009). The miRNA-mRNA interaction is also called a miRNA response element (MRE). The degree of MRE complementarity determines whether miRISC induces translational inhibition or degradation of the target mRNA. If perfectly complementary, the interaction between miRNA and target mRNA induces cleavage of the mRNA by the AGO2 endonuclease. However, the majority of miRNA-mRNA target interactions in animals are not perfectly complementary, which results in resistance to AGO2 endonuclease activity and associated degradation (Meister and Tuschl 2004; O'Brien, et al. 2018).

While most studies have focused on miRNA mediated downregulation, evidence indicates that miRNAs may upregulate gene expression under some conditions. This effect can result from a direct interaction between mRISC and a target mRNA or indirectly through stopping miRNA-mediated repression. Several studies have provided evidence that miRNA-mediated upregulation

is a result of the presence/absence of factors that are required for miRISC function. One example is the let-7 miRNA, which has been found to activate translation during cell cycle arrest but induce translational repression in proliferating cells (Vasudevan and Steitz 2007). Gene activation by miRNAs may also occur through interactions with regions other than the 3' UTR, as reported in a study by Orom et al. in which miR-10a binds to the 5′ UTRs of ribosomal protein mRNAs, resulting in upregulation of these proteins (Orom, et al. 2008). These examples and many others indicate that miRNA-mediated upregulation can happen under some circumstances.

1.8 Dysregulation of miRNAs in cardiovascular diseases

miRNAs are expressed in the cardiovascular system, have been identified as critical regulators of cardiovascular function, and play important roles in the pathogenesis of cardiovascular diseases including HF, cardiac arrhythmia, myocardial infarction, atherosclerosis, and coronary artery disease(Romaine, et al. 2015).

1.8.1 Dysregulated miRNAs in HF

Mounting evidence suggests that miRNA dysregulation is associated with HF and comorbid pathologies. Both miR-1 and miR-210 alteration have been associated with the New York Heart Association Class functional classification (Endo, et al. 2013; Sygitowicz, et al. 2015). In addition, Andrew et al. showed that declining expression of the miRNAs let-7i, miR-18b, miR-18a, miR-223, miR-301a, miR-652, and miR-423 are associated with increased risk of mortality in HF patients (Ovchinnikova, et al. 2016). Conversely, increased levels of miR-1254 and miR-1306 are associated with death and hospitalization, while increased levels of miR-208b and miR-499 are strongly associated with death and development of HF (Bayes-Genis, et al. 2018).

Deep sequencing and bioinformatics tools have been used to examine miRNA expression profiles in healthy and failing human hearts. In failing hearts, over 250 miRNAs were differently expressed; among these, miR-362-3p was found to be highly expressed in patients with refractory end-stage HF when compared with controls (Leptidis, et al. 2013). This finding was further supported in our laboratory (unpublished data). miR-362-3p expression in the left ventricular tissue of with HF patients with reduced ejection fraction (HFrEF) was significantly higher when compared to controls. Overall there is evidence to suggest acritical role of miRNAs in HF pathogenesis and their potential use as a biomarker or target in HF therapy.

1.8.2 Dysregulated miRNAs in cardiac arrhythmia

Similar to role of miRNAs in HF, changes in circulating miRNA expression levels have been associated with arrhythmia. Dysregulation of miR-29 was documented in cardiac tissue and found to contribute to atrial fibrillation (AF) development and progression(Dawson, et al. 2013). Upregulation of miR-208b has been identified in human cardiac tissue with AF (Nishi, et al. 2013). Elevated levels of miR-483 predict the risk of post-operative AF (Harling, et al. 2017), while miR-23a and miR-26a have been shown to contribute to the development of post-operative AF (Feldman, et al. 2017).

More evidence suggests that miRNAs may regulate the protein expression of several important ion channels, including the L-type calcium channel, calcium voltage-gated channels, and the K+-inwardly-rectifying channel, subfamilyJ3 (KCNJ3). In particular, miR-328 was identified to regulate cardiac protein expression of L-type calcium channel and as a result contribute to electrical remodeling in AF (Li, et al. 2014). Another important miRNA is miR-30d, which was found to regulate the expression and function of both calcium voltage-gated channels and K+-inwardly-rectifying channels (Morishima, et al. 2016).

Recently, our group has identified miR-362-3p as an important regulator of hERG channel expression and hERG-related current (unpublished). Its effects were assessed in cancer cells endogenously expressly hERG and in HL-1 cardiomyocytes which were originally derived from murine atrial cardiomyocytes. At 48 hours following miR-362-3p transfection, the hERG-related current density was reduced in both cell lines, indicating a potential role for miR-362-3p in regulating hERG current in the human heart.

1.9 Dysregulation of miRNAs in cancer

Dysregulation of miRNA expression has been shown to affect hallmarks of cancer including cell proliferation, evading growth suppressors, and activating invasion and metastasis. Based on these effects, miRNAs have been classified as oncomirs or tumor suppressors. Upregulation of oncomirs promote tumorigenesis, invasion, and metastasis while the downregulation of tumor suppressor miRNAs contributes to initiation and progression of tumors in susceptible tissues. There is a long list of miRNAs that have potential roles in cancer therapy.

As discussed previously, *KCNH2* has been implicated as a potential oncogene, and recently was identified as a direct target of miR-96 and miR-493. The expression of miR-96 is downregulated in pancreatic cancer tissues, and its ectopic expression reduces hERG expression, which subsequently inhibits the proliferation, migration, and invasion of pancreatic cancer cells (Feng, et al. 2014). Similarly, Zhi et al. demonstrated that miR-493 acts as a tumor suppressor by reducing hERG expression, leading to inhibition of malignant behavior in pancreatic cancer (Zhi, et al. 2017). These results call for further investigation and more thorough screening of mRNAs targeting *KCNH2* in order to better understand the roles of both miRNAs and hERG channels in cancer.

1.10 Population Pharmacokinetic/Pharmacodynamics (PKPD)

Population PK/PD studies are conducted to quantify the drug concentration and its effect on a population of patients. They allow explaining and predicting variability in drug concertation profiles, and how this variability can subsequently contribute to drug PD response. Understanding the source of variability helps optimization of drug regimen, and provide precise and accurate dosing recommendations for patients based on their own characteristics. Statistical models are utilized to develop of population PKPD model to enable describing drug disposition and corresponding effect following drug administration, and to provide some outlines of the underlying biological process contributing to patients' variability in drug disposition or response.

PK models characterize drug disposition using compartmental analysis approach. In this approach, the drug is assumed to be distributed uniformly in compartments which are virtual spaces representing the distribution of drug inside the body in which it is distributed into different tissues and organs. Each compartment is characterized by its clearance and apparent volume of distribution. The developed population PK model is then used to study and identify the source of specific drug variability in which identified covariates incorporated in the final model, which is thenceforth used for PD analysis.

PD models on the other hand allows to relate the drug concentration at site of effect to drug effect (PD effect). Given the difficulty of measuring drug concentration at site of effect, plasma concentration measurement used and linked to PD effect, assuming no delay between drug concentration and PD effect, implying that drug concentration at site of action has reached an equilibrium with plasma. This model is the simplest model and is called a direct model. Conversely, when plasma drug concentration is not in equilibrium with drug concentration at site of action, a notable delay between concentration and response can be observed when plot effect vs plasma

concentration resulting in a hysteresis curve. In this situation, a more complicated model taking into account the detected delay in effect can be built to better describe the relationship between drug concentration and PD response. This model called indirect model. Either direct or indirect model is linked to the developed final PK model to develop a final PKPD model. The final PKPD model is used to identify covariates contribute to variability in PD response.

In this work, we used nonlinear-mixed effect model (NONMEM) software to develop a PKPD model for ibutilide, a QT prolonging drug. This model allowed for describing the ibutilide disposition and its QT interval lengthening effect. The final PKPD model was eventually used to test and describe the contribution of identified KCNH2-miRNAs in ibutilide PD effect.

1.11 Screening of miRNA-mRNA interaction

The process of miRNA target identification is complex due to several reasons, including the ability for one miRNA to regulate a set of target mRNAs, one mRNA target potentially being regulated by multiple miRNAs, the sharing of common seed sequences between miRNAs, and incomplete knowledge of the rules governing miRNA-mRNA target binding. A number of techniques can be performed to determine individual miRNA-mRNA interactions and to indicate the ability of such an interaction to regulate targeted gene expression and function, including quantitative reverse transcription-polymerase chain reaction (qRT-PCR), luciferase reporter assays, and western blotting. However, these techniques are limited to characterizing a single miRNA-mRNA interaction. Therefore, methods for large-scale miRNA identification and screening have been developed to screen and identify miRNA targets.

Crosslinking immunoprecipitation sequencing (CLIP-seq) and crosslinking, ligation, and sequencing of hybrids (CLASH) of isolated RNA are examples of a high-throughput identification

technique that has been used for transcriptome-wide mapping of miRISC-binding sites on mRNAs in order to identify miRNA-mRNA interactions. CLIP-seq and CLASH are very powerful techniques that provides insight into the location of miRNA target sites. In this work, we developed a novel HT-bioassay to validate the bioinformatically predicted binding of miRNAs to the 3'UTR of *KCNH2*. Unlike CLIP-seq or CLASH techniques, HT-bioassay allows to determine miRNAs target site with the ability to modify these target sequencing to test the influence of sequencing variants on miRNAs bindings. The goal is to explore and identify all miRNAs that potentially regulate *KCNH2* expression and function under specific conditions. Coupled with population PKPD models, the HT-bioassay is a very strong tool for the identification of novel miRNAs that potentially contribute to specific drug response and may provide promising biomarkers that warrant further investigation.

1.12 Research objectives:

Specific Aim I: *Identify and determine the role of miRNAs in regulating KCNH2 gene expression and function in cancer.*

In this aim, we utilized bioinformatics prediction tools to identify and explore the miRNAs that potentially target and regulate hERG channels expression and function in breast cancer cells. additional in-vitro assays were performed to quantify miRNAs expression and characterize their function in culture breast cancer cells.

Specific Aim II: *Investigate the contribution of miR-362-3p to drug associated QT interval changes in HF.*

In this aim, we hypothesized that miR-362-3p predicts drug induced QT interval lengthening in HF. To test this hypothesis, a PKPD model was developed for Ibutilide to describe the relationship between ibutilide disposition and its PD response. The final developed model was further used to explore the contribution of miR-362-3p in ibutilide QT interval lengthening.

Specific Aim III: *Identify miRNAs regulating KCNH2 expression and function in HF*.

In this aim, we developed a novel HT-bioassay to identify all miRNAs potentially regulate *KCNH2* gene expression and function in hiPS-CM cells. The bioassay-identified miRNAs were further validated using luciferase assay and patch clamp technique.

CHAPTER 2. METHODS

2.1 SPECIFIC AIM I

Identify and determine the role of miRNAs in regulating KCNH2 gene expression and function in cancer cells.

2.1.1 Bioinformatics approaches

miRNAs predicted to regulate *KCNH2* were initially identified using the miRWalk database (http://zmf.umm.uni-heidelberg.de/apps/zmf/mirwalk2/). miRWalk is an open-source, comprehensive online algorithm that generates and provides information on miRNAs and their predicted and validated binding sites in genes (Sticht, et al. 2018). The four default algorithms were used to predict miRNAs that putatively regulate *KCNH2* transcripts 1a and 1b: miRWalk, RNA22, miRanda, and TargetScan. Only human data were searched. The input parameters used the 3' UTR as the target location and required putative miRNAs to have a minimum seed length of 7 and/or a *p*-value of 0.05.

The predicted miRNAs were further screened using the mirCancer database (www.mircancer.ecu.edu) (Xie, et al. 2013), which provides a comprehensive collection of miRNA and gene expression profiles along with their known roles in human breast cancer. The combination of both databases was chosen to improve prediction accuracy and reduce false positives. The overlap of miRNAs identified by a prediction algorithm and having a reported benefit in human breast cancer in the mirCancer database was used for subsequent analysis.

OncoLnc (http://www.oncolnc.org) was used to interactively explore survival correlations related to the identified miRNAs (Anaya 2016). The OncoLnc dataset contains expression data for

mRNAs and miRNAs coupled to clinical data for 198 patients from breast invasive carcinoma (BRCA) studies performed by The Cancer Genome Atlas (TCGA).

2.1.2 Cell culture and transfection

Human breast cancer cell lines (SK-BR-3, MCF-7) were obtained and grown in McCoy's 5A medium (ATCC® 30-2020™) or minimum essential medium (EMEM medium; ATCC® 30-2003™) containing 10% (v/v) fetal bovine serum (FBS; ATCC® 30-2020™) and penicillin/streptomycin 1% (v/v). The SK-BR-3 line consists of *TP53*-mutated invasive ductal carcinoma cells derived from a pleural effusion and has been shown to overexpress *KCNH2 (Engel and Young 1978)*. MCF-7 is an invasive ductal carcinoma cell line derived from a pleural effusion and has been shown to express estrogen receptors as well as *KCNH2* (Kao, et al. 2009; Soule, et al. 1973).

Human embryonic kidney 293 cells stably expressing *KCNH2* (HEK293-hERG) were obtained from Dr. Craig T. January (Zhou, et al. 1998). HEK293-hERG cells were cultured and grown in EMEM medium (ATCC® 30-2003™) containing 10% (v/v) fetal bovine serum (FBS; ATCC® 30-2020™) and penicillin/streptomycin 1% (v/v). Cells were maintained at 37°C in an atmosphere containing 5% CO_2.

Negative control miRNAs, MISSION miRNAs mimics, and siRNAs were purchased from Sigma Aldrich® (St. Louis, MO, USA) and Santa Cruz Biotechnology (Dallas, TX, USA). Cells were seeded in 6-well plates for 24 hours before transfection. On the next day, cells were transfected with 100 μM of negative control, MISSION miRNA mimic, or siRNA in 5 μL of Lipofectamine 2000 (Thermo Fisher Scientific®, Waltham, MA, USA) per well. Transfected cells were incubated for 48 hours before the experiment was performed.

2.1.3 Luciferase assays

Putative miRNAs identified through the bioinformatics approach were quantitatively screened for *KCNH2* 3' UTR activity using Dual-Luciferase Assays (Promega, Madison, WI, USA). The *KCNH2* 3′ UTR reporter clone (pLenti-UTR-LUC) was purchased from Applied Biological Materials (Richmond, BC, Canada; MT-h11487). SK-BR-3 cells were plated 24 hours before transfection of cells with the control reporter plasmid (Renilla), 100 µM of MISSION miRNA mimic, or the pLenti-UTR-LUC (negative control) using 5 µL of Lipofectamine 2000 (Thermo Fisher Scientific®, Waltham, MA, USA) per well. Forty-eight hours following transfection, luciferase reporter activity, which was normalized to that of Renilla luciferase in the same well, was measured using a 96-well plate-reader (BioTek, Winooski, VT, United States). The firefly luciferase activity was measured using a TD-20/20 Luminometer. Experiments were performed in triplicate and repeated under independent conditions. Relative luciferase activity was normalized to Renilla to control for transfection efficiency.

2.1.4 Quantitative reverse transcriptase-Polymerase Chain Reaction (q-PCR) analysis

A total of 500 ng RNA from each sample was reverse transcribed using the High Capacity RNA-to-cDNA Kit (Applied Biosystems, Foster City, CA, USA) according to the manufacturer's protocol. The extracted RNA was mixed with 10 µL 2x RT Buffer, 1 µL 20x enzyme mix, 1 µL of a mixture of random-sequence oligonucleotide primers, and 4 µL nuclease-free water. For cDNA synthesis, the thermal cycler (GeneAmp® PCR System 2700, Applied Biosystems, Foster City, CA, USA) was programmed as follows: 37°C for 30 minutes, 95 °C for five minutes, and the final holding step at 4 °C. The TaqMan® Gene Expression Kit (Life Technology, Carlsbad, CA, USA) was used with the $2^{-\Delta\Delta Ct}$ method (Livak and Schmittgen 2001) to quantify expression of

KCNH2 mRNA 48 hours after transfection in cell lines transfected with miRNA mimics or negative controls (Sigma Aldrich®, St.Louis, MO, USA). Threshold cycle (Ct) values were determined for both *KCNH2* and *GAPDH*. The Ct value is the PCR cycle number required for the fluorescent signal of PCR reaction to cross the threshold. The Ct value inversely related to the amount of target in the sample. *GAPDH* was used to normalize Ct values for *KCNH2*. Using the normalized Ct values, the relative expression was calculated as $2^{-\Delta\Delta Ct}$ as follow:

$\Delta\Delta Ct$ = ((Ct *KCNH2* Ct – Ct *GAPDH* Ct) mimic miRNAs – (Ct *KCNH2* Ct – Ct *GAPDH* Ct) Control)

The $2^{-\Delta\Delta Ct}$ was calculated to determine expression fold change.

Specific primers targeting either *KCNH2* mRNA (Product# 4351372) or the endogenous control for normalization, *GAPDH* (Product# 4331182), were purchased from Applied Biosystems (TaqMan® assays, Foster City, CA, USA). The PCR reactions consisted of 1 µL cDNA, 1 µL specific primers, 10 µL of TaqMan® Universal Master Mix II (Applied Biosystems, Foster City, CA, USA), and 8 µL nuclease-free water. The QuantStudio 12K Flex Real-Time PCR system (Applied Biosystems, Foster City, CA, USA) was used to quantify expression changes between all groups, and cycling conditions were set as follows: 50 °C for ten minutes, 95 °C for ten minutes, and 40 cycles consisting of 95 °C for 15 seconds and 60 °C for one minute.

2.1.5 Western blot analysis

For the Western blot analysis, the cells were washed with phosphate- buffered salt solution (PBS; Thermo Fisher Scientific®, Waltham, MA, USA) and then lysed with RIPA lysis buffer (Beyotime, Shanghai, China). Protein concentrations were determined for each sample using the Bradford method with BSA (Pierce®, Rockford, IL, USA) as the standard. Protein samples were then fractionated on a 6-12% sodium dodecyl sulfate-polyacrylamide gradient gel (Novex® Bis-

Tris Bolt® SDS-PAGE gel; Thermo Fisher Scientific, Waltham, MA, USA) through electrophoresis for 1.5 hours at a constant voltage of 125 V. The electrophoresed proteins were transferred to nitrocellulose membranes (Thermo Fisher Scientific®, Waltham, MA, USA) at 4 °C in a 25 Mm Trisma base/190 Mm glycin/20% methanol transfer buffer for one hour at a constant voltage of 100 V. After one hour blocking at room temperature with 5% bovine serum albumin (BSA; Sigma Aldrich®, St. Louis, MO, USA) in Tris-buffered saline with 0.1% (v/v) Tween 20 (TBST; Sigma Aldrich®, St. Louis, MO, USA), the membrane was probed with hERG-specific primary antibodies (Product# 12889S, Cell Signaling, Danvers, MA, USA), and primary GAPDH antibodies (Product# sc-47724,Santa Cruz Biotechnology, Dallas, TX, USA) overnight at 4 °C. The membrane was then washed in TBST and probed with secondary antibody (Santa Cruz Biotechnology, Dallas, TX, USA) for one hour at room temperature. Lastly, the membrane was washed and then developed using Pierce ECL Western Blotting Substrate (Thermo Fisher Scientific, Waltham, MA, USA). The Li-Cor Odyssey imaging system was used to quantify and detect hERG protein expression. Images were analyzed with ImageJ®.

2.1.6 Cell proliferation assay

Cell proliferation was determined using the CellTiter Aqueous One Solution Cell Proliferation Assay (MTS; Promega®, Madison, WI, USA). Cultured cancer cells transfected with miR-362-3p mimic or negative control (Sigma Aldrich®, St. Louis, MO, USA) were harvested and seeded in 96-well plates (Coring Incorporated®, Corning, NY, USA) then dissociated into single-cell suspensions by digestion with 0.9% trypsin for 2 min at 37 °C followed by pipetting 30 times. After 48 hours, the medium was replaced with 100 µl of culture medium and 20 µl of CellTiter Aqueous One Solution, followed by incubation for four hours at 37 °C. Finally, the absorbance was measured at a wavelength of 490 nm (with 630 nm as the reference wavelength) using an

ELISA microplate reader (Shenzhen Highcreation Technology Co®, Turku, Finland). All proliferation assays were repeated in triplicate.

2.1.7 Cell cycle analysis

Flow cytometry was used to differentiate cell cycle phases following transfection with MISSION mimic for miR-362-3p, MISSION mimic negative control, or *KCNH2* siRNA (Sigma Aldrich®, St.Louis, MO, USA). Cell cycle progression was examined using propidium iodide staining to assess DNA amounts in the G0/G1, S, and G2/M phases of the cell cycle. Cells were trypsinized 48 hours following transfection, fixed and permeabilized using 70% ethanol, rinsed in phosphate-buffered saline (PBS; Thermo Fisher Scientific®, Waltham, MA, USA), and treated with RNase A. DNA was then quantitatively stained with propidium iodide for 30 minutes at room temperature while protected from light. Fluorescence was analyzed using a BD LSRFORTESSA flow cytometer and ModFit LT software.

2.1.8 Statistical analysis

Data were expressed as mean ± standard deviation (SD) from at least three independent experiments. All statistical analyses were performed using GraphPad Prism version 8.0.0 for Windows (GraphPad Software, San Diego, CA, USA, www.graphpad.com). Student's *t*-test was used for comparisons of two groups. Analysis of variance (ANOVA) was used when comparing more than two groups, with Bonferroni correction as a post-hoc analysis. Differences between groups were considered significant if the *P*-value was less than 0.05. Multivariate Cox regressions were followed by a Kaplan–Meier survival analysis for miRNA expression, with *p*-values calculated by log-rank test.

2.2 SPECIFIC AIM II

Investigate the contribution of miR-362-3p to drug associated QT interval changes in HF.

2.2.1 Study design

The data utilized for the development of the pharmacokinetic-pharmacodynamics (PKPD) model were collected from a prospective, parallel-group comparative study. The study consists of three groups of volunteer subjects ≥ 18 years of age. The purpose was to enroll a population of patients with heart failure with preserved ejection fraction (HFpEF), a population with heart failure with reduced ejection fraction (HFrEF), and a control population matched to the HFpEF and HFrEF groups for age and sex. The original goal of this clinical study was to establish the influence of HFpEF on sensitivity to drug induced QT prolongation. Patients were excluded if have any of the following: weight < 60 or > 130 kg; serum potassium < 3.8 mEq/L; serum magnesium <1.8 mg/dL; hematocrit <26%; aspartate aminotransferase/alanine aminotransferase > 3x the upper limit of normal; creatinine clearance < 20 mL/minute; received any Vaughan Williams class IA or III antiarrhythmic agent within five half-lives of ibutilide infusion; baseline \QTc interval > 450 ms; history of TdP; New York Heart Association class IV heart failure; personal or family history of congenital long QT syndrome or sudden cardiac death outside the setting of an acute myocardial infarction; concomitant use of any QT interval-prolonging drugs; pregnancy; permanently paced ventricular rhythm; any sustained arrhythmias including atrial fibrillation, 2nd or 3rd degree atrioventricular block, junctional rhythm; premature ventricular complexes or premature atrial complexes requiring treatment.

The study consisted of two phases. First was a screening phase in which subjects stayed 12 hours at the Indiana Clinical Research Center (ICRC). They underwent three 12-lead ECGs

(Marquette Mac 5500, GE Healthcare Bio-Sciences, Pittsburgh, Pennsylvania) approximately one minute apart at pre-specified time points that were matched during the treatment (second) phase: 0, 15, and 30 minutes and 1, 2, 4, 6, 8, and 12 hours. In the treatment phase, blood samples and three baseline (pre-ibutilide) 12-lead ECGs approximately one minute apart were obtained for each subject. Afterward, all subjects received a single intravenous dose of ibutilide 0.003 mg/kg diluted in 50 ml normal saline and infused over ten minutes via infusion pump. Three ECGs (approximately one minute apart) and venous blood samples for determination of serum ibutilide concentrations were obtained serially immediately at the end of infusion and at 5, 10, 15, 20, 30, and 45 minutes and 1, 2, 4, 6, 8, and 12 hours' post-infusion. The study was approved by the Indiana University (IU) Institutional Review Board. All patients provided written informed consent.

2.2.2 QT Interval measurements and baseline QT_F interval correction

ECGs were collected before administration of ibutilide, at the end of infusion, and at 5, 10, 15, 20, 30, and 45 minutes and 1, 2, 4, 6, 8, and 12 hours following infusion. At least three ECGs were recorded per time point, 1-3 minutes apart. QT and RR intervals were determined from leads II, V1, and V5 by a study investigator blinded to time and the subjects' assigned groups. QT intervals were measured using the MUSE automated system (GE Healthcare Bio-Sciences, Pittsburgh, PA) using electronic calipers as QRS deflection to the end of the T wave. The end of the T wave was defined as the intersection of the steepest last limb of the presumed T wave and the isoelecteric line. QT and RR intervals were averaged over ≥ 3 consecutive beats, and the average of three QT intervals was taken to obtain a single mean QT interval at each time point for each lead. QT intervals were corrected for heart rate using the Fridericia correction method (QT_F), and corrected intervals were used in analyses. Time-matched QT_F interval measurements from the

treatment phase before ibutilide administration and a pre-randomization phase without ibutilide were subtracted from corresponding measurements from the ibutilide phase, which allowed the determination of a time-matched baseline (no-ibutilide) and placebo-corrected QT_F interval ("$\Delta\Delta QT_F$") for the PKPD model.

2.2.3 Ibutilide concentration assays

Blood samples (10 ml) were obtained from the indwelling catheter in the contralateral arm to determine serum ibutilide concentration. Briefly, serum was separated from whole blood and then stored at -70°F until analysis. Serum ibutilide concentrations were determined using reverse-phase high-performance liquid chromatography with mass spectrometry detection (HPLC-MS/MS; Agilent 1290 HPLC, Eksiegent Autosampler, and AB Sciex 5500 MS/MS) in the IU Clinical Pharmacology Analytical Core Laboratory.

2.2.4 PKPD analysis model building

Population PK and PKPD modeling was performed with a nonlinear mixed-effects approach using NONMEM (Version 7.2.1, GloboMax LLC, Hanover, Maryland). Models were estimated using first order conditional estimation with interaction methods throughout model development under subroutine ADVAN 11 (TRANS 4) for the PK model and ADVAN 13 (TOL9) for the PKPD model. Modeling was conducted using NONMEM with Pirana software (Certara, Princeton, NJ, United states) as the user interface. In conjunction with Pirana software, the R package *Xpose4* was used for generating diagnostic plots. The change in Akaike's information criterion (AIC) or the objective function value (OFV), and goodness of fit diagnostic plots (GOF) (individual plots, residual plots, and observed versus predicted plasma concentration) were used to assess and select the best representative structural models.

2.2.4.1 Structural PK model

The basic population PK model was developed using ibutilide serum concentrations from 22 subjects to describe ibutilide pharmacokinetic profiles. In this analysis, both 2 and 3-compartment models were tested. The AIC, GOF plots, and PK parameter estimates, were compared to ensure appropriate model selection for this study population.

2.2.4.2 Structural PKPD model

The population PKPD model was developed and constructed using sequential PKPD analysis strategies on ibutilide PK individual estimated parameters from the final PK model and QT_F interval data. The initial structure of the PD model was determined from exploratory plots of $\Delta\Delta QT_F$ intervals. Additional exploratory plots of individual and mean $\Delta\Delta QT_F$ and serum ibutilide concentrations versus time were created to investigate possible equilibration delays. The effect of ibutilide concentration on the QT_F interval was fitted to linear (Equation 1), E_{max} (Equation 2), and sigmoid E_{max} models with and without hypothetical effect compartments. The model equations are given below:

$E = S*C$ (equation 1)

$E = E_0 + Emax*C^h/EC_{50}^h + C^h$ (equation 2)

Where E is the QT_F interval lengthening, S is the slope that describes the concentration-effect relationship, C is the serum ibutilide concentration, E_0 is the baseline effect of ibutilide, E_{max} is the maximum effect of ibutilide, EC_{50} is the serum concentration required to produce 50% of the maximum effect, and h is the Hill coefficient defining the sigmoid shape of the curve. For the E_{max} model, h was 1, indicating independent drug binding. For the effect compartment model, C represents the ibutilide concentration in the hypothetical effect compartment.

2.2.4.3 Random effects

For both PK and PD parameters, inter-subject variability was modeled using a log-normal distribution of the between-subject variability in population parameter estimates (Equation 3). The below equations were used to relate individual estimates to population estimates:

$P = TVP * \exp(\eta_P)$ (equation 3)

Where P is the individual parameter estimate, TVP is the population estimate, and $\exp(\eta_P)$ is the inter-individual variability for parameter P.

The residual unexplained variability (RUV) (ε) was tested using additive, proportional, and combined models as described in equations 4, 5, and 6. The ε was assumed to be normally distributed with a mean of zero and a variance of σ^2. For the final PK model, a proportional error term (equation 5) was chosen, whereas for the final PKPD model, an additive error term (equation 4) was utilized. Below are the equations for tested residual error models.

Additive error model: $Y = IPRED + \varepsilon 2$ (equation 4)

Proportional error model: $Y = IPRED + IPRED*\varepsilon$ (equation 5)

Combined error model: $Y = IPRED + IPRED*\varepsilon 1 + \varepsilon 2$ (equation 6)

Where Y is the observed concentration, IPRED is the individual predicted concentration, and ε1 and ε2 are additive and proportional error, respectively. The final PK/PKPD model was developed in two steps: first, building the basic structural PK/PKPD model that describes the disposition of ibutilide for PK mode, or the ibutilide-$\Delta\Delta QT_F$ relationship, followed by selection of the significant covariates to be included in the final model.

2.2.5 Covariate analysis

The potential contributions of individual specific covariates to the observed variability in the pharmacokinetics of ibutilide, and in the ibutilide induced QT_F interval lengthening were evaluated using the structural base model. Potential tested covariates included individual age, sex, weight, race, and heart failure status (HFpEF or HFrEF) for both PK and PKPD models. In addition, miR-362-3p expression was tested as a potential predictor of ibutilide induced QT_F interval lengthening in the PKPD model. Covariates were considered significant if the difference in OFV (ΔOFV) between the structural model and the covariate model was greater than 3.84, α=0.05. Covariates were tested and incorporated based on ΔOFV magnitude; only significant covariates were used for stepwise forward addition to develop the final model. The final model was then assessed using stepwise backward elimination. Covariates were removed from the model if ΔOFV > 7.88, α=0.05. Additive, proportional, and exponential inter-individual variability structure models for continuous covariates, and binary string structure models for categorical covariates, were tested as follows:

2.2.5.1 Continuous covariates

Additive model: P = THETA1+ (COV-COV median) *THETA2 (equation 7)

Proportional model: P = THETA1 *(COV/COV median)**THETA2 (equation 8)

Exponential model: P = THETA1 *EXP(COV*THETA2) (equation 9)

2.2.5.2 Categorical covariates

Binary string model: P = THETA1*COV+THETA2*(1-COV) (equation 10)

Where P is the individual value of the parameter, THETA1 represents the population value of the parameter estimate, COV is the covariate, and THETA2 is an estimated parameter describing the magnitude of the COV-parameter relationship.

2.2.6 Model evaluation

Adequacy of model fit was evaluated by assessing individuals predicted versus observed concentrations and weighted residuals versus predicted concentrations. The predictive performance of the final model on the observed data was evaluated through visual predictive checks (VPC) using *xpose* in R. The final model stability and its precision in estimating PK parameters were evaluated using bootstrapping with Pirana for NONMEM software. The median and 95% confidence intervals of final model parameter estimates obtained from bootstrap were compared with final model parameter estimates.

2.2.7 Simulations

The effects of miR-362-3p expression on ibutilide-induced $\Delta\Delta QT_F$ interval lengthening were evaluated through Monte Carlo simulations performed in NONMEM using the final population PKPD model with covariates. For each miR-362-3p expression group, 1000 patients were simulated.

2.2.8 Statistical analysis

Data was expressed as mean ± standard deviation (SD). All statistical analyses were performed using GraphPad Prism version 8.0.0 for Windows (GraphPad Software, San Diego, CA, USA, www.graphpad.com). Analysis of variance (ANOVA) was used when comparing more than

two groups, with Bonferroni correction as a post-hoc analysis. Differences between groups were considered significant if the *P*-value was less than 0.05.

2.3 SPECIFIC AIM III

Identify miRNAs regulating KCNH2 expression and function in HF.

A miRNA screening bioassay was developed to validate the putative binding of miRNAs to the *KCNH2* 3' UTR. This HT-bioassay was adapted from the PASSPORT-seq assay originally developed by Ipe et al. to functionally test polymorphisms in miRNA target sites (Ipe, et al. 2018). Figure 2.1 summarizes assay development. The ability of validated miRNAs to regulate *KCNH2* expression was further evaluated utilizing different assays as described below.

2.3.1 Experimental groups

Three experimental groups were used in this assay as follow: βAR Group: Sustained βAR stimulation with isoproterenol 1.0 μM for 48h; CaMKII Group: Transfected with activated CaMKII; Control Group: Treated with vehicle. All experiments were conducted in hiPS-CMs.

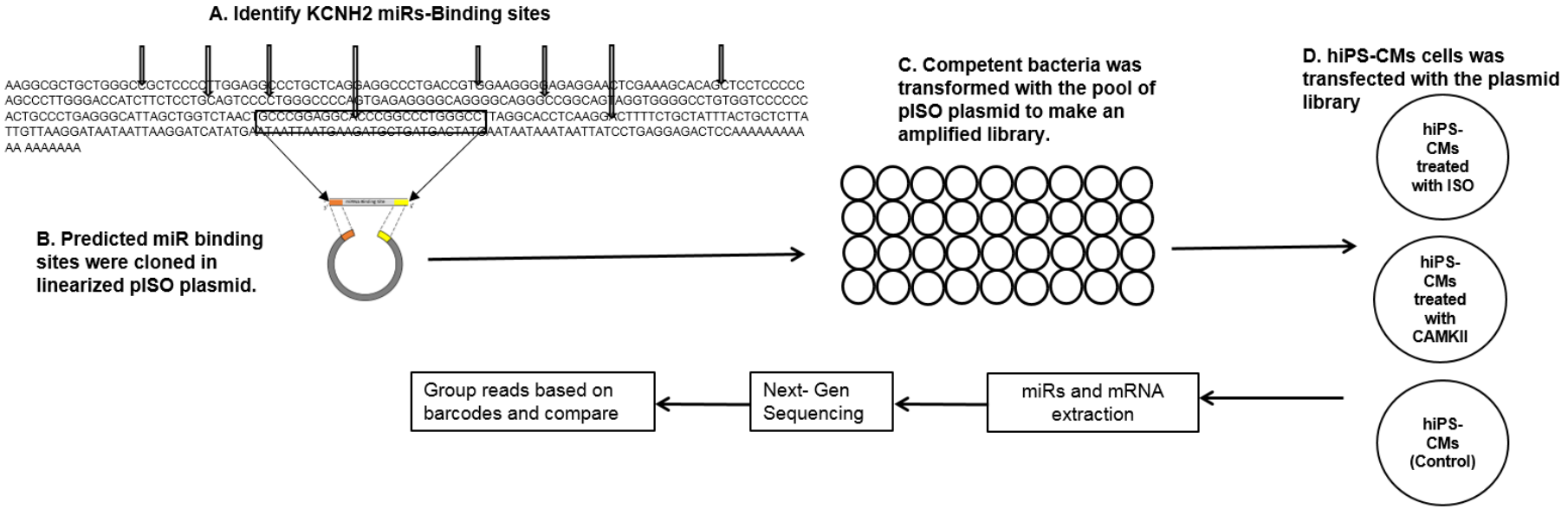

Figure 2:1. Approaches to identify potential miRNAs binding sites regulating hERG expression and function. This figure illustrates the modes used in this work to identify miRNAs that regulate hERG.

2.3.2 High throughput bioassay analysis

2.3.2.1 Identification of putative miRNAs and corresponding binding sites in KCNH2 mRNA

miRNAs predicted to regulate *KCNH2* were initially identified using the miRWalk database (Sticht, et al. 2018). The four default algorithms were used to predict miRNAs that putatively regulate *KCNH2* transcripts 1a and 1b: miRWalk, RNA22, miRanda, and TargetScan. Only human data were searched. The input parameters used the 3' UTR as the target location and required putative miRNAs to have a minimum seed length of 7 and/or a *p*-value of 0.05.

Fragments (35 bp) of the *KCNH2* 3' UTR containing binding sites for each putative miRNA identified from miRWALK and TargetScan were synthesized and sequenced. Each binding site fragment started 5 bp before the seed region (seed region length ~8bp) and ended 22 bp after the seed region.

2.3.2.2 miRNA Target Sequence Fragment Design

A total of 327 miRNA target site sequence fragments were identified and used for the HT-bioassay analysis. Each fragment was flanked by universal primers, in which GCCGTGTAATTCTAGGAGCTC was added to the fragment start and CGTTCTAGAGTCGGGC to the end. The final test fragments were 73 nucleotides in length (Figure 2.2). All miRNAs target fragments were commercially synthesized as pooled single-stranded DNA oligonucleotides (OligomixR , LC Sciences, Houston, TX, United States). The pool contained 10–50 attomoles of each sequence. One µL of the diluted OligomixR (1:5) was made double-stranded and amplified in a 50 µL PCR reaction using 0.3 µM universal primers and 25 µL

2X CloneAmpTM HiFi PCR premix (Takara, Mountain View, CA, United States). The PCR conditions used were: 98 °C (10 s), 53 °C (5 s), and 72 °C (5 s) for 35 cycles.

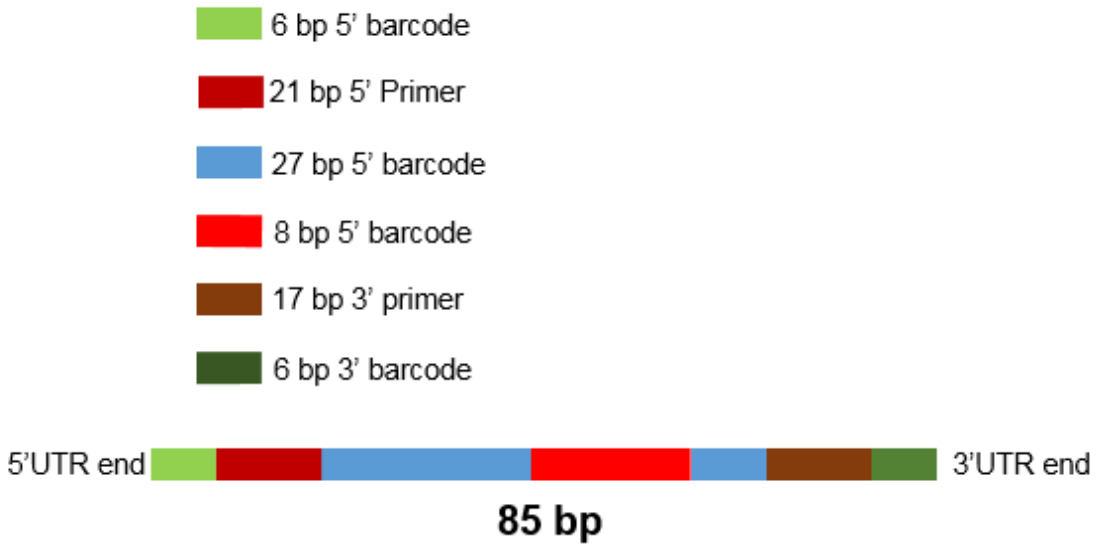

Figure 2:2. miRNA target fragment diagram

2.3.2.3 Plasmid library preparation

Plasmids containing the miRNA target sites were constructed from the pIS-0 vector (plasmid 12178; Addgene, Cambridge, MA, United States) (Yekta, et al. 2004). Briefly, 2 µL of PCR product containing the double-stranded oligoneuclotide pool was mixed with 40 ng of linearized plasmid using the NEBuilderR HiFi DNA assembly kit (New England Biolabs, Ipswich, MA, United States). Competent *Escherichia coli* (*E. Coli*) Cells were transformed with 2 µL of the plasmid using the heat shock method and plated on 20 LB-agar plates containing 100 µg/ml ampicillin. All colonies were harvested after overnight incubation, pooled together in LB broth, and incubated for 5 h at 37 °C. The plasmid DNA was then isolated and purified using QIAprepR Spin miniprep columns (Qiagen, Germantown, MD, United States) as per manufacturer's

instructions. The final plasmid DNA concentration was quantified using a Quant-iTTM DNA Broad Range kit (Thermo Fisher Scientific, Waltham, MA, United States).

2.3.2.4 Sanger sequencing

Twenty randomly-selected colonies transformed with plasmids from the target fragment library were harvested and separately grown in LB broth containing 100 µg/ml ampicillin. The final plasmid DNA was isolated using QIAprepR Spin miniprep columns (Qiagen, Germantown, MD, United States) as per manufacturer's instructions. The plasmid DNA was then Sanger sequenced using a primer (GTGGTTTGTCCAAACTCATC) with complementary sequence near the miRNA target sequence insert (ACGT, Inc., Wheeling, IL, United States).

2.3.2.5 Transfection of cells in culture

The plasmid library was used to transfect hiPS-CMs cells (Cellular Dynamics, Madison, WI, United States). The cells were thawed and maintained in 12-well plates for four days per manufacturer's instructions. On day four, the cells were transfected with 600 ng/well of the plasmid library and 600 ng/well of CAMKII plasmid or empty vector. Transfection was performed using 4 µL of ViaFect transfection reagent (Promega, Madison, WI, United States) and 50 µL transfection mix in Opti-MEMR (Life Technologies, Carlsbad, CA, United States).

2.3.2.6 RNA isolation and cDNA synthesis

Total RNA was isolated from transfected hiPS-CMs cells after 48 hours using a RNeasyR purification kit with the optional DNase treatment (Qiagen, Germantown, MD, United States). Isolated RNA was quantified using the Quant-iTTM RNA Broad Range kit (Thermo Fisher

Scientific, Waltham, MA, United States), and reverse transcribed to make cDNA using the QuantiTectR Reverse Transcription kit (Qiagen, Germantown, MD, United States).

2.3.2.7 Molecular barcoding

Each experiment group contained four biological replicates. Using cDNA synthesized from the hiPS-CMs transfected cells, miRNA binding site inserts were amplified in 50 µL PCR reactions using 0.3 µM flanking universal primers and 25 µL 2X CloneAmpTM HiFi PCR premix (Takara, Mountain View, CA, United States). Inserts from the input plasmid pool were also amplified. PCR conditions were set as follows: 98 °C (10 s), 54 °C (5 s), and 72 °C (5 s) for 25 cycles. To ensure that transfection and isolation of the plasmids were successful in hiPS-CMs cells, the final PCR product was confirmed by agarose gel electrophoresis (Figure 2.3). The presence of multiple bands indicating that there are some plasmids with duplicate inserts. Bands that represent single inserts are indicated by the blue arrow. The plasmid with more than one insert was informatically removed.

2.3.2.8 Next-generation sequencing

The miRNA binding sites were amplified using universal primers that incorporated unique 6-nt barcodes on the 5' end, as displayed in Table 2.1. All groups were given different sets of barcodes, including their biological replicates, allowing them to be pooled together and with the input plasmid library for sequencing. Sequencing was performed using an ion-proton sequencing system. Expression of miRNAs was assessed in the treatment groups with their respective binding sites through sequencing of RNA and cDNA isolated from the transfected hiPS-CMs cells. The reads from each treatment group, including biological replicates, were grouped based on barcodes.

The effect of treatment was determined by comparing read numbers between groups. Read numbers were normalized to the input plasmid pool to ensure precise RNA-seq analysis.

2.3.3 Electrophysiology

A set of whole-cell recordings of I_{Kr} current were performed in HEK293-hERG cells using a HEKA® EPC 9 amplifier in voltage-clamp mode. All functional experiments were performed at room temperature. Data were recorded and analyzed with HEKA® Patchmaster and Fitmaster software. Currents were recorded using two silver electrodes, in which a reference electrode was placed in the bath solution and a patch electrode inside the glass micropipette filled with the internal solution. The micropipette tip moved toward the cell membrane, allowing for a high resistance seal (~1 GΩ) between the cell membrane surface and the micropipette tip. This seal is referred to as a gigaseal. Gentle suction was applied to break the membrane patch enclosed by the micropipette tip and allow whole cell access.

2.3.3.1 Electrophysiology solutions and chemicals

The electrophysiology solutions were prepared to mimic the physiologic intracellular and extracellular environments of cells, with potassium concentration being higher inside the cell. At the time of recording, the cell culture medium was replaced with the external (bath) solution, which contained (in mM): 137 NaCl, 4 KCl, 1.8 $CaCl_2$, 1 $MgCl_2$, 10 HEPES, and 10 glucose (Sigma Aldrich®, St. Louis, MO, USA), with pH adjusted to 7.4 using NaOH. The patch pipette was filled with internal solution, which contained (in mM): 130 KCl, 1 $MgCl_2$, 10 HEPES, 5 Mg-ATP, and 5 EGTA (Sigma Aldrich®, St. Louis, MO, USA), with pH adjusted to 7.2 using KOH. The osmolarity of each solution ranged between 285-295 milliOsm/L.

2.3.3.2 Experimental protocols

The effects of bioassay miRNAs on hERG channel conductivity were assessed through measurement of I_{Kr} inward tail currents via a voltage clamp protocol in miRNA-transfected cells and control cells 48 hours following transfection. Membrane voltage was increased from a holding potential of -80 mV to +60 mV using one-second depolarizing steps, followed by a series of five-second repolarizing steps between -100 mV and +40 mV to elicit tail current.

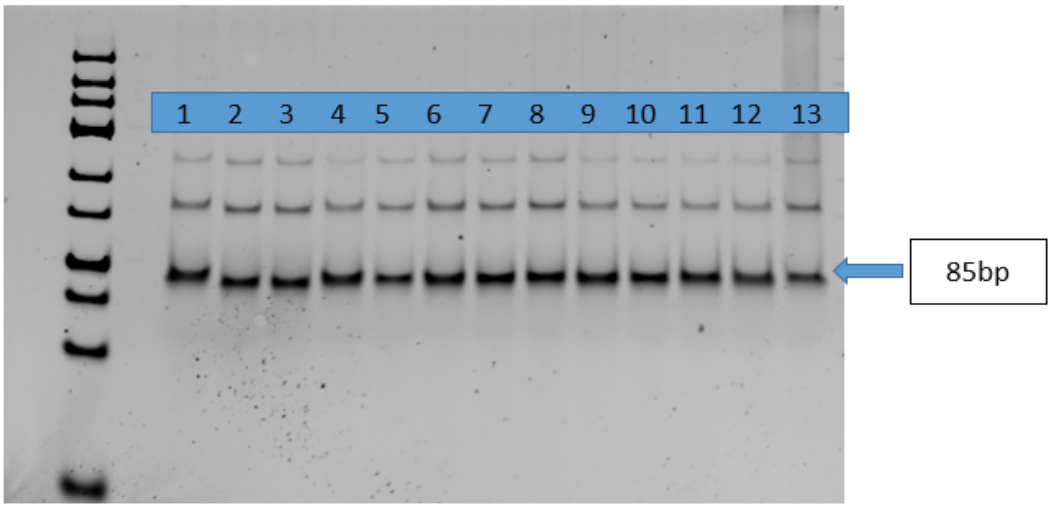

Figure 2:3. cDNA of miRNAs target site fragments on agarose gel. This figure illustrates the band that contains amplified cDNA of miRNA target site insert after successful transfection. The band of interest is indicated by blue arrow in which the fragment is single and 85 bp in length.

Table 2.1. Barcode & primers sequences used to prepare plasmid library.

Sample#	Group	5' Barcode *and Primer* (27 nt)	3' Barcode *and Primer** (25 nt)
1	ISO (1)	**GTAGAG**GCCGTGTAATTCTAGGAGCTC	**GTTAGT**CGTTCTAGAGTCGGGGC
2	ISO (2)	**TAACCC**GCCGTGTAATTCTAGGAGCTC	**TACAGA**CGTTCTAGAGTCGGGGC
3	ISO (3)	**TAGAAC**GCCGTGTAATTCTAGGAGCTC	**TATGCC**CGTTCTAGAGTCGGGGC
4	ISO (4)	**TCAAAG**GCCGTGTAATTCTAGGAGCTC	**TCCATA**CGTTCTAGAGTCGGGGC
5	CTR (1)	**TCGATT**GCCGTGTAATTCTAGGAGCTC	**TCTACC**CGTTCTAGAGTCGGGGC
6	CTR (2)	**TGCTAG**GCCGTGTAATTCTAGGAGCTC	**TGAACC**CGTTCTAGAGTCGGGGC
7	CTR (3)	**TTCGAA**GCCGTGTAATTCTAGGAGCTC	**TTAACG**CGTTCTAGAGTCGGGGC
8	CTR (4)	**AAACAC**GCCGTGTAATTCTAGGAGCTC	**TTCTGG**CGTTCTAGAGTCGGGGC
9	CAMK (1)	**TAAGAC**GCCGTGTAATTCTAGGAGCTC	**TGCTCA**CGTTCTAGAGTCGGGGC
10	CAMK (2)	**TGGGAT**GCCGTGTAATTCTAGGAGCTC	**TCTTAG**CGTTCTAGAGTCGGGGC
11	CAMK (3)	**TCTGCT**GCCGTGTAATTCTAGGAGCTC	**AAGAAC**CGTTCTAGAGTCGGGGC
12	CAMK (4)	**AACGGT**GCCGTGTAATTCTAGGAGCTC	**AACTTC**CGTTCTAGAGTCGGGGC
13	INPUT	**AATGTG**GCCGTGTAATTCTAGGAGCTC	**GCAGAA**CGTTCTAGAGTCGGGGC

ISO= hiPS-CMs cells treated with isoproterenol, CTR= Control, CAMKII= hiPS-CMs cells transfected with a plasmid containing active Calcium/calmodulin-dependent protein kinase II.

CHAPTER 3. RESULTS

3.1 SPECIFIC AIM I

Identify and determine the role of miRNAs in regulating KCNH2 gene expression and function in cancer cells.

In this aim, we utilized bioinformatics prediction tools to identify and explore the miRNAs that potentially target and regulate the expression and function of hERG channels in breast cancer. The putative miRNAs were screened and validated using dual luciferase assays. The expression levels of validated miRNAs were further assessed in cultured breast cancer cells, and in data for patients with breast cancer. Of the five miRNAs, miR-362-3p was confirmed to significantly regulate *KCNH2* expression and its expression positively correlated with overall patient survival.

3.1.1 microRNAs predicted to regulate KCNH2 channels

The number of miRNAs predicted to bind *KCNH2* were: 432 by miRWalk, 266 by miRanda, 436 by RNA22, and 432 by TargetScan. To minimize false positive predictions, these sets were intersected with the miRcancer database, which contains 256 dysregulated miRNAs that have been previously associated with beneficial effects in breast cancer. Among these 256 miRNAs, five (miR-199b-5p, miR-362-3p, miR-494-3p, miR-497-5p, and miR-625-5p) were predicted by at least one algorithm to regulate the *KCNH2* 3'UTR (Table 3.1). Two of these (miR-362-3p & miR-625-5p) were predicted to bind *KCNH2* by at least two of the prediction algorithms.

Table 3.1. Bioinformatics approaches to identified miRNAs predicted *KCNH2* binding with known beneficial effect in breast cancer.

	miRWALK database (http://zmf.umm.uni-heidelberg.de/apps/zmf/mirwalk2/)			
Prediction algorithms	miRWALK	miRANDA	RNA22	Targetscan
Putative miRNAs identified by each algorithm	432 miRNAs	266 miRNAs	436 miRNAs	375 miRNAs
mirCancer database	256 miRNAs associated with benefit in human breast cancer			
KCNH2-putative miRNAs associated with breast cancer benefits (mirCancer database)	miR-494-3p miR-497-5p miR-625-5p	miR-362-3p	miR-625-5p miR-199b-3p	miR-362-3p miR-625-5p
miRNAs identified by at least 2 algorithms	miR-362-3p miR-625-5p			

3.1.2 Lower expression of miR-362-3p is associated with longer survival in breast cancer

Kaplan–Meier survival analyses were performed using the OncoLnc online tool to examine the strength of association between the expression of five putative *KCNH2*-regulating miRNAs (miR-199b-5p, miR-362-3p, miR-494, miR-497, and miR-625-5p) and clinical outcomes in the form of survival data from The Cancer Genome Atlas-Cancer Genome (TCGA). Expression distributions of the five miRNAs in breast cancer patients (n = 988) are presented in Figure 3.1. To examine the influence of these miRNAs on survival, survival rates were compared by log-rank test between patients with the highest expression (90^{th} percentile; n = 98) and those with the lowest expression (10^{th} percentile; n = 98). Patients with low miR-362-3p expression had significantly reduced survival rates (HR: 0.39, 95% CI: 0.18 to 0.82, $P = 0.012$), as displayed in Figure 3.2. For the other four miRNAs, no statistically significant difference in overall survival was found between patients with low and high expression, including for miR-625-5p (HR: 0.93, 95% CI: 0.43 to 2, $P = 0.36$), which was the only other miRNA predicted by more than algorithm.

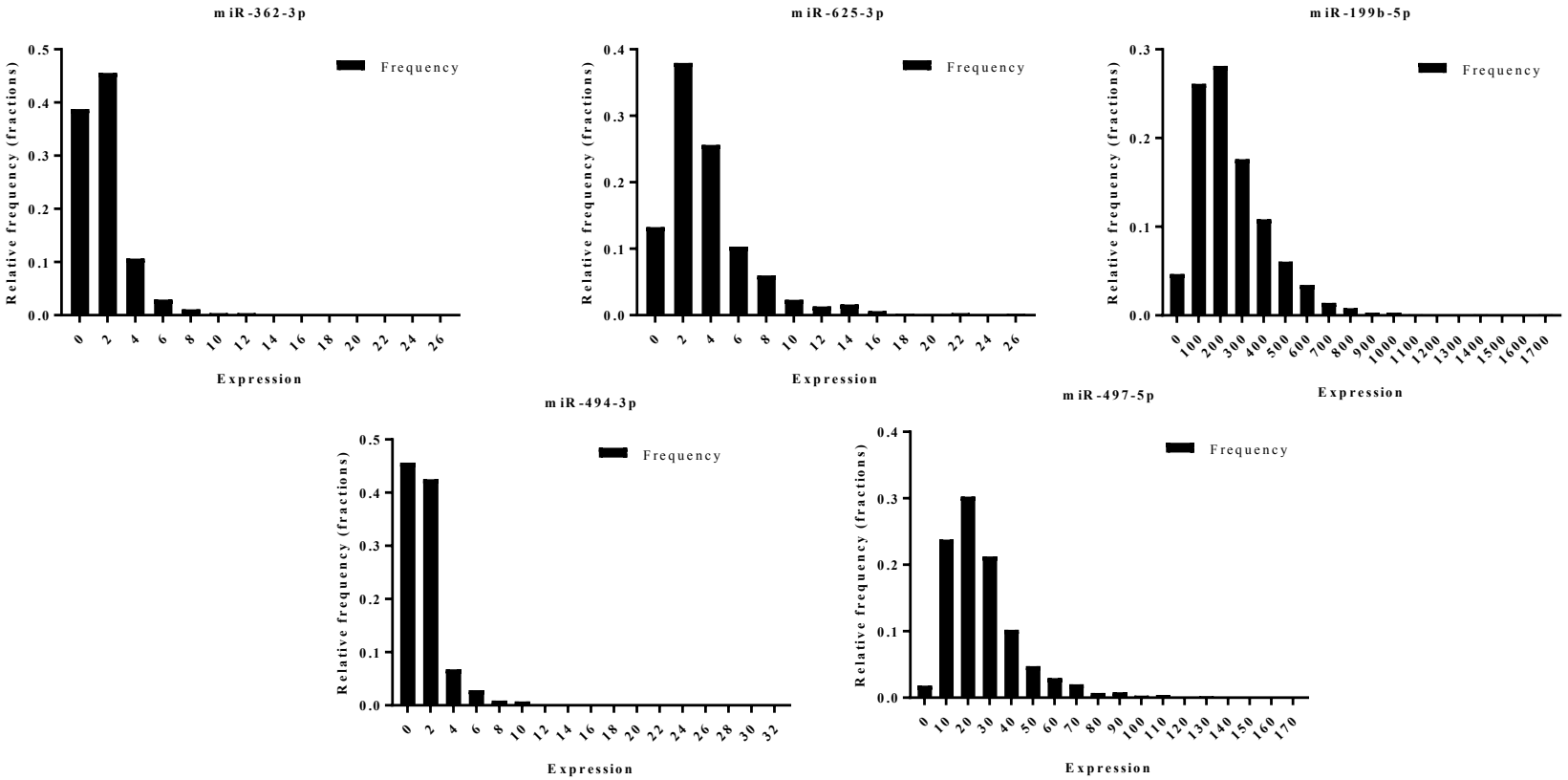

Figure 3:1. Histogram of miRNA expression. This figure represents expression of miRNA-199b-5p, miR-362-3p, miR-494-3p, miR-497-5p, and miRNAs-625-5p in 988 breast cancer patients from The Cancer Genome Atlas-Cancer Genome (TCGA) database.

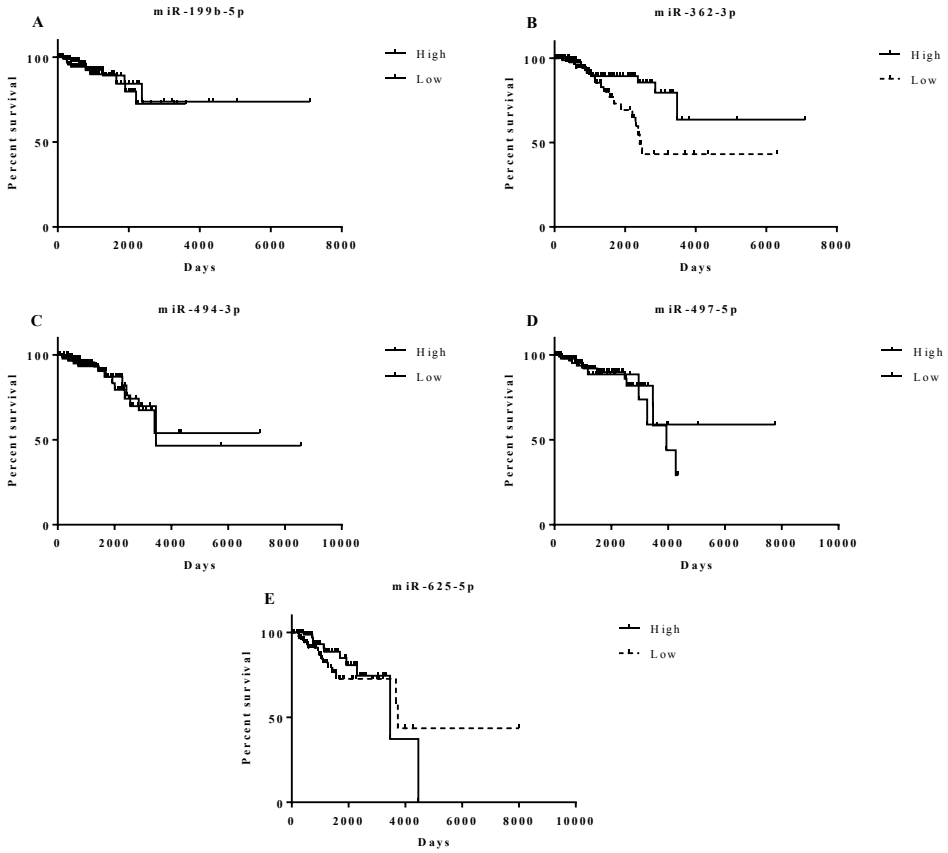

Figure 3:2. Kaplan-Meier survival curves for expression of the identified miRNAs in breast cancer. (A) Survival data of patients highly expressing miR-199b-5p (647±184) versus those with low expression (49.6±17.9). (B) Survival data of patients highly expressing miR-362-3p (5.9±2.8) versus those with low expression (0.01±0.05). (C) Survival data of patients highly expressing miR-494-3p (6.19±3.88) versus those with low expression (0±0). (D) Survival data of patients highly expressing miR-497-5p (73.15±24.27) versus those with low expression (6.52±1.74). (E) Survival data of patients highly expressing miR-625-5p (12.28±5.22) versus those with low expression (0.45±0.3). Only patients with low expression of miR-363-3p had significantly shorter overall survival rate than their counterparts with high expression by log-rank test (HR: 0.39, 95% CI: 0.18 to 0.82, P = 0.012).

3.1.3 miR-362-3p decreases *KCNH2* 3'UTR activity

The five putative *KCNH2*-regulating miRNAs (miR-199b-5p, miR-362-3p, miR-494, miR-497 and miR-625-5p) were screened for *KCNH2* 3′ UTR activity using luciferase assays (Figure 3.3A). miR-362-3p significantly decreased luciferase activity (10% ± 2.3, $P < 0.001$) when compared to cells transfected with luciferase plasmid alone, while the four other miRNAs did not reduce luciferase activity, including miR-625-5p (0.66% ± 3.56, $P = 0.55$).

3.1.4 miR-362-3p decreases *KCNH2* expression in breast cancer cells

Based on the results of the bioinformatics approach, survival analysis, and luciferase screening, miR-362-3p was selected for additional screening to verify its regulation of *KCNH2*. Both SK-BR-3 and MCF-7 cancer cells have been reported to express *KCNH2*. miR-362-3p and *KCNH2* siRNA (positive control) significantly decreased *KCNH2* mRNA expression in SK-BR-3 cells, by 15.9% ± 6.0 ($P < 0.001$, n = 3) and 42.3% ± 4.0 ($P = 0.01$, n = 3) respectively. Similarly, miR-362-3p and *KCNH2* siRNA significantly decreased *KCNH2* mRNA expression in MCF-7 cells, by 25.7% ± 11.1 ($P = 0.02$, n = 3) and 23.7% ± 6.4 ($P = 0.03$, n = 3) respectively. Screening results are displayed in Figure 3.3B.

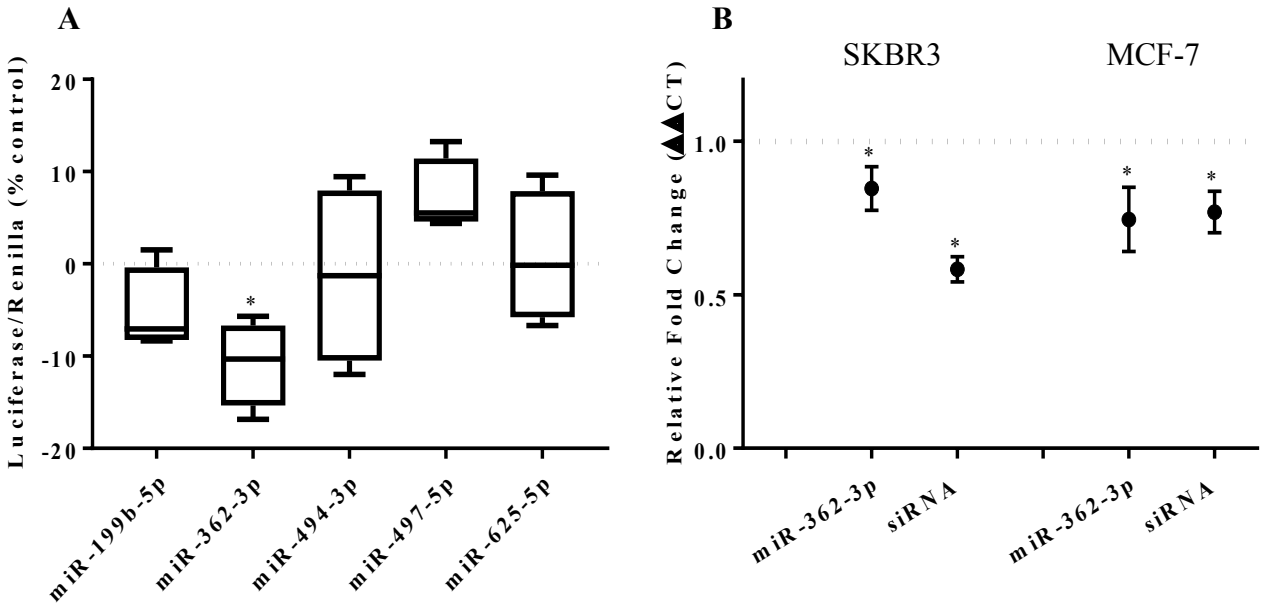

Figure 3:3. (A) Luciferase assay screening of the five putative *KCNH2*-regulating miRNAs. Only miR-362-3p significantly reduced *KCNH2* 3' UTR activity (10% ± 2.3, $P < 0.001$). (B) The effect of miR-362-3p on *KCNH2* expression in SK-BR-3 and MCF-7 cells. Both miR-362-3p and the positive control significantly decreased *KCNH2* mRNA in both cell lines (SK-BR-3: 15.9%, $P < 0.001$ and 42.3%, $P = 0.01$; MCF-7: 25.7%, $P = 0.02$ and 23.7%, $P = 0.03$). Experiments were performed as biological triplicates; error bars depict standard error of means; asterisks denote significance.

3.1.5 Effect of miR-362-3p on hERG protein expression

Relative to GAPDH, miR-362-3p decreased immature endogenous hERG (0.18 ± 0.03 to 0.08 ± 0.01, $P = 0.038$, n=3) by an average of 47%, and mature (i.e. fully glycosylated) endogenous hERG (0.16 ± 0.03 to 0.08 ± 0.01, $P = 0.0369$, n=3) by an average of 51%, as shown in Figure 4A and 4B.

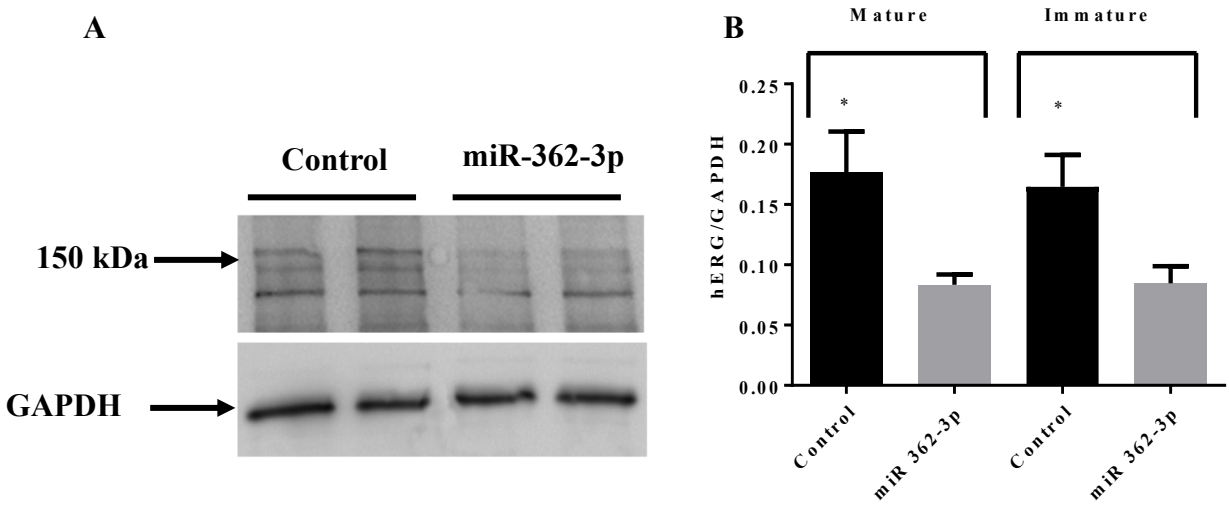

Figure 3:4: (A) Representative protein immunoblots of mature and immature hERG following transfection with miR-362-3p or negative control in SK-BR-3 cells. (B) Mature and immature hERG protein expression was decreased following miR-362-3p expression in SK-BR-3 cells. Experiments were performed as biological triplicates; error bars depict standard error of means; asterisks denote significance.

3.1.6 miR-362-3p decreases cell proliferation in breast cancer cell lines

The role of miR-362-3p in cell proliferation was explored by performing MTS assays in both SK-BR-3 and MCF-7 cancer cells. The assay was performed 48 hours following transfection with a miR-362-3p mimic or negative control. As shown in Figure 3.5, miR-362-3p significantly decreased proliferation of SK-BR-3 cells (23% ± 8.68, $P = 0.014$, n = 3) when compared with control wells. A similar effect was observed in MCF-7 cells (11.7% ± 1.0, $P < 0.001$, n = 3).

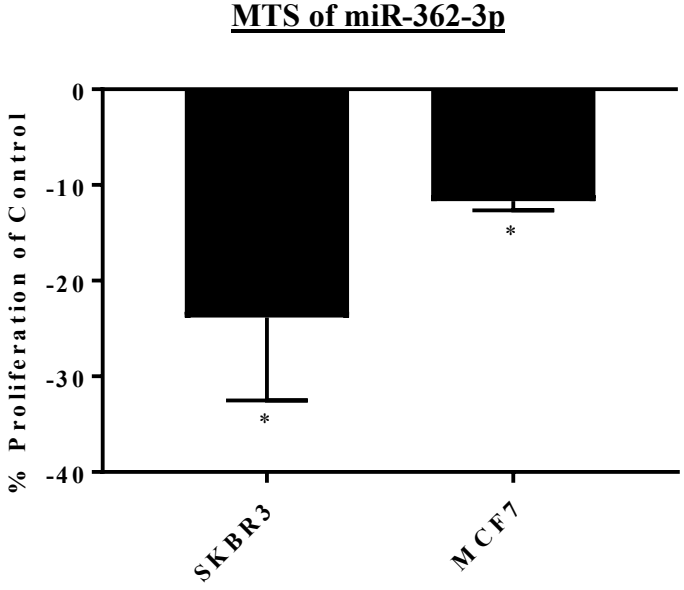

Figure 3:5. Effect of miR-362-3p on proliferation of SK-BR-3 and MCF-7 cells. Proliferation was significantly reduced in transfected cells when compared to negative controls. Experiments were performed as biological triplicates; error bars depict standard error of means; asterisks denote significance.

3.1.7 miR-362-3p and *KCNH2* siRNA significantly increased the proportion of MCF-7 breast cancer cells in G0/G1 phase

To elucidate the effect of miR-362-3p on the cell cycle, the effects of miR-362-3p on SK-BR-3 and MCF-7 cells were assessed. miR-362-3p did not significantly increase the accumulation of cells in G0/G1 phase in SK-BR-3 cells with an average increase of 5.8% (from 59.6% ± 0.12 to 63.0 ± 0.74, $P = 0.06$, n = 3) when compared to control group. However, *KCNH2* siRNA decreased the accumulation of cells in G0/G1 phase in SK-BR-3 cells by 5.13% (from 59.6% ± 0.12 to 56.3 ± 0.73, $P = 0.006$, n = 3) as displayed in Figure 3.6A. On the other hand, miR-362-3p significantly increased the accumulation of cells in G0/G1 phase in MCF-7 cells by 11.7% (from 51.1% ± 0.64 to 57.1 ± 0.96, $P = 0.002$, n = 3) when compared to control. Additionally, siRNA *KCNH2* behaved similar to miR-362-3p, in which *KCNH2* siRNA increased cells count in G0/G1 phase by 10% (from 51.1% ± 0.64 to 56.8 ± 0.96, $P < 0.001$, n = 3) (Figure 3.6B).

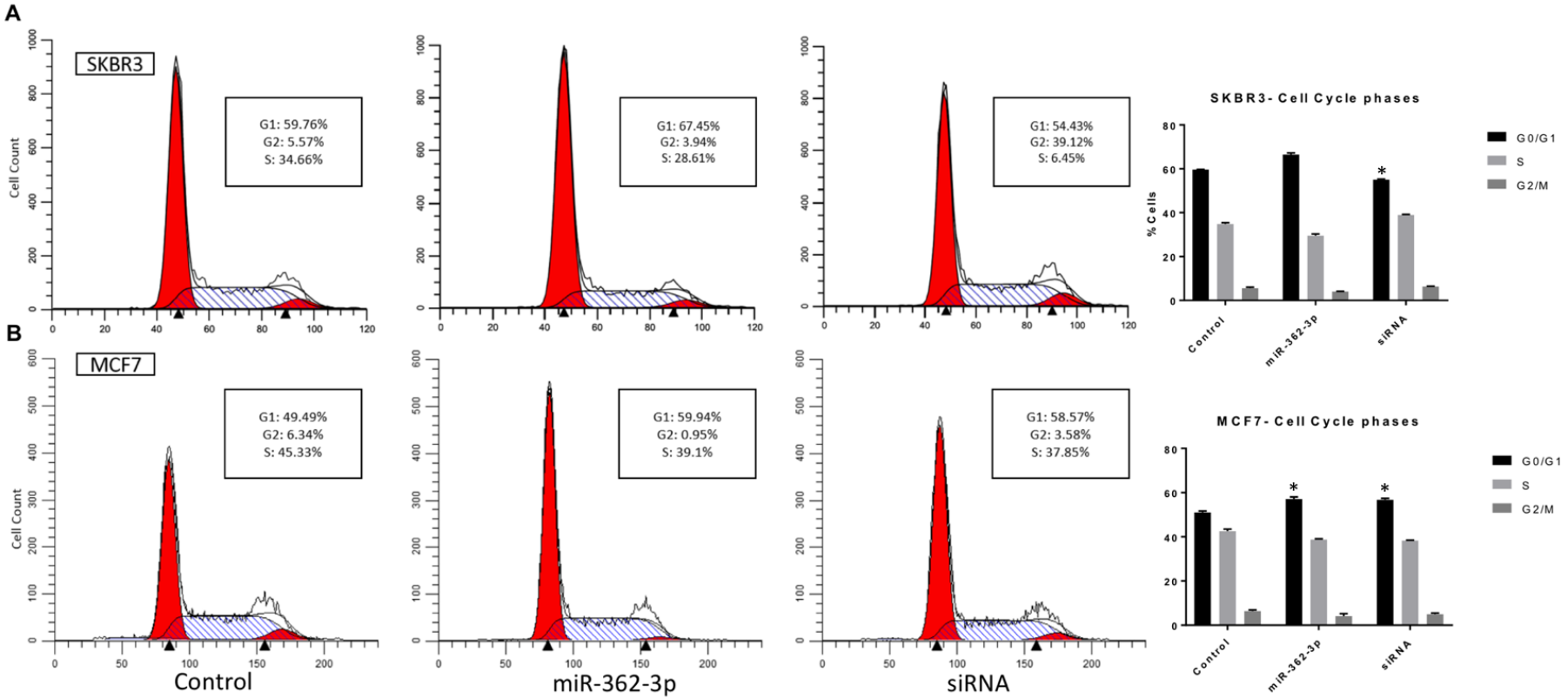

Figure 3:6. Effects of miR-362-3p on cell cycle in SK-BR-3 (A) and MCF-7 (B) cells 48 hours' post-transfection. Experiments were performed as biological triplicates with error bars depicting standard error of means. asterisks denote significance.

3.2 SPECIFIC AIM II

In specific Aim I, miR-362-3p was identified as a regulator of hERG expression and function in cultured breast cancer cells. In addition, our laboratory has previously shown that miR-362-3p is expressed in cardiac tissue and up-regulated in cardiac tissue in patients with heart failure. Therefore, the objective of Specific Aim II was to *investigate the contribution of miR-362-3p to drug-associated* QT_C *interval lengthening in heart failure.*

The hypothesis tested was that miR-362-3p predicts patient sensitivity to drug-induced QTc interval lengthening in patients with heart failure. To test this hypothesis, a population PKPD model was developed from a clinical study to determine the influence of several covariates, including miR-362-3p expression and heart failure status, on drug-associated QTc interval lengthening in heart failure patients.

3.2.1 Participant demographics and characteristics

A total of 22 patients met the study inclusion and exclusion criteria and were enrolled in the three groups (HFpEF n=10, HFrEF n=2, and control n=10). A total of 1440 ibutilide concentrations and QT interval observations were collected from subjects who completed the study (n = 22) and included in the final analysis. The characteristics of the study patients are summarized in Table 3.2.

Table 3.2. Study population characteristics.

Characteristics	HFrEF (n=2)	HFpEF (n=10)	Control (n=10)
Males	1 (50)	3 (30)	3 (30)
White	1 (50)	7 (70)	8 (80)
African American	1 (50)	3 (30)	2 (20)
Age (years)	67 ± 1	69 ± 8	67 ± 9
Body Weight (Kg)	87.3 ± 3	89.7 ± 13	82.2 ± 12
Ibutilide dose (mg)	0.26 ± 0.01	0.27 ± 0.04	0.25 ± 0.04
Concurrent diseases			
- Hypertension	2 (100)	8 (80)	6 (60)
- Coronary artery disease	2 (100)	3 (30)	1 (10)
- Diabetes mellitus	1 (50)	5 (50)	2 (20)
- Hyperlipidemia	2 (100)	5 (50)	6 (60)
Concomitant medications			
- ACE inhibitors/ARBs	2 (100)	7 (70)	3 (30)
- Loop diuretics	2 (100)	7 (70)	2 (20)
- β-blockers	2 (100)	8 (80)	2 (20)
- Statins	2 (100)	5 (50)	4 (40)

Data presented as n (%) or mean ± SD.
HFpEF = heart failure with preserved ejection fraction, HFrEF = heart failure with reduced ejection fraction, ACE = angiotensin-converting enzyme, ARB = angiotensin receptor blocker.

3.2.2 Population PK model

A structural pharmacokinetic model was developed to describe the disposition of ibutilide following IV infusion (Figure 3.7). Ibutilide disposition was best described by a 3-compartment model with first-order elimination from the central compartment. Compared to a 2-compartment model, the 3-compartment model AIC was decreased by 63 (-1210 vs -1147). Its residual error was best described as a proportional residual error model, as other residual error models did not improve model performance (ΔOFV < 3.84). Therefore, a 3-compartment model with first order elimination and proportional residual error was selected as the base structural model. Population parameter estimates for the base model were: clearance (CL) = 240 L/hr, volume distribution of central compartment (V_C) = 40.3 L, volume distribution of peripheral compartment 1 (V_{P1}) = 78.5 L, and volume distribution of peripheral compartment 2 (V_{P2}) = 1120 L. Inter-individual and residual variabilities are summarized in Table 3.3.

To explore all covariate relationships, each covariate was first tested independently as shown in Table 3.4. None of the covariates tested were found to have a significant impact on any of the PK parameters. Therefore, the base structural model was determined to be the final PK model. GOF diagnostic plots for the final model comparing individual and population predictions against measured concentrations are shown in Figure 3.8. The weighted residuals were approximately normally distributed and displayed an even distribution around zero and mostly within two units of the null ordinate. All individual plots for the final PK model are illustrated in Figure 3.9.

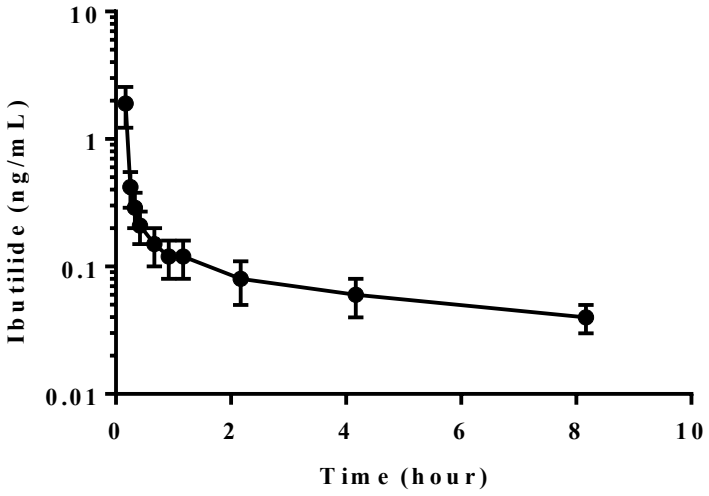

Figure 3:7. Ibutilide serum concentration over time for all patients included in the analysis (n=22). Data presented with mean ± SD.

Table 3.3. Final model and bootstrap parameter estimates for the population pharmacokinetic model of ibutilide.

Parameter	Population Estimates	Bootstrap Estimates (95 CI%)
CL, L/hr	240	242 (210, 276)
CL_{ic1}, L/hr	227	220 (179, 270)
CL_{ic2}, L/hr	407	414 (366, 467)
V_c, L	40.3	
V_{P1}, L	78.5	
V_{P2}, L	1120	1112 (946, 1300)
ω Cl %	31.6	30.9 (22.1, 39.7)
ω Cl_{ic1} %	34.8	31.6 (10.2, 47.8)
ω Cl_{ic2} %	19.5	18.2 (0.7, 24.5)
ω Vc %	10	
ω V_{P1} %	47.9	
ω V_{P2} %	36.7	34.8 (20.5, 45.1)
σ PROP %	16.1	16.2 (14.3, 18.1)

CL = systemic clearance, CL_{ic1} = intercompartmental clearance 1, CL_{ic2} = intercompartmental clearance 2, V_C = volume distribution of central compartment, V_{P1} = volume distribution of peripheral compartment 1, V_{P2}= volume distribution of peripheral compartment 2, ω = inter-individual variability (omega), σ = residual variability (sigma), PROP = proportional, CI = confidence interval.

Table 3.4. Summary of PK covariate model analysis.

PK model	OFV	Δ OFV	P-value
Base model	-1262		
Base model + WT on CL	-1263	-1	ns
Base model + WT on Vc	-1244	18	ns
Base model + WT on Vp_1	-1263	-1	ns
Base model + WT on Vp_2	-1264	-2	ns
Base model + AGE on CL	-1264	-2	ns
Base model + SEX on CL	-1258	4	ns
Base model + RACE on CL	-1263	-1	ns
Base model + HF on CL	-1264	-2	ns

ΔOFV is the difference in objective function values between base and covariate model. CL = systemic clearance, V_C = volume distribution of central compartment, V_{P1} = volume distribution of peripheral compartment 1, V_{P2} = volume distribution of peripheral compartment 2, WT = weight, HF = heart failure, ns = not significant.

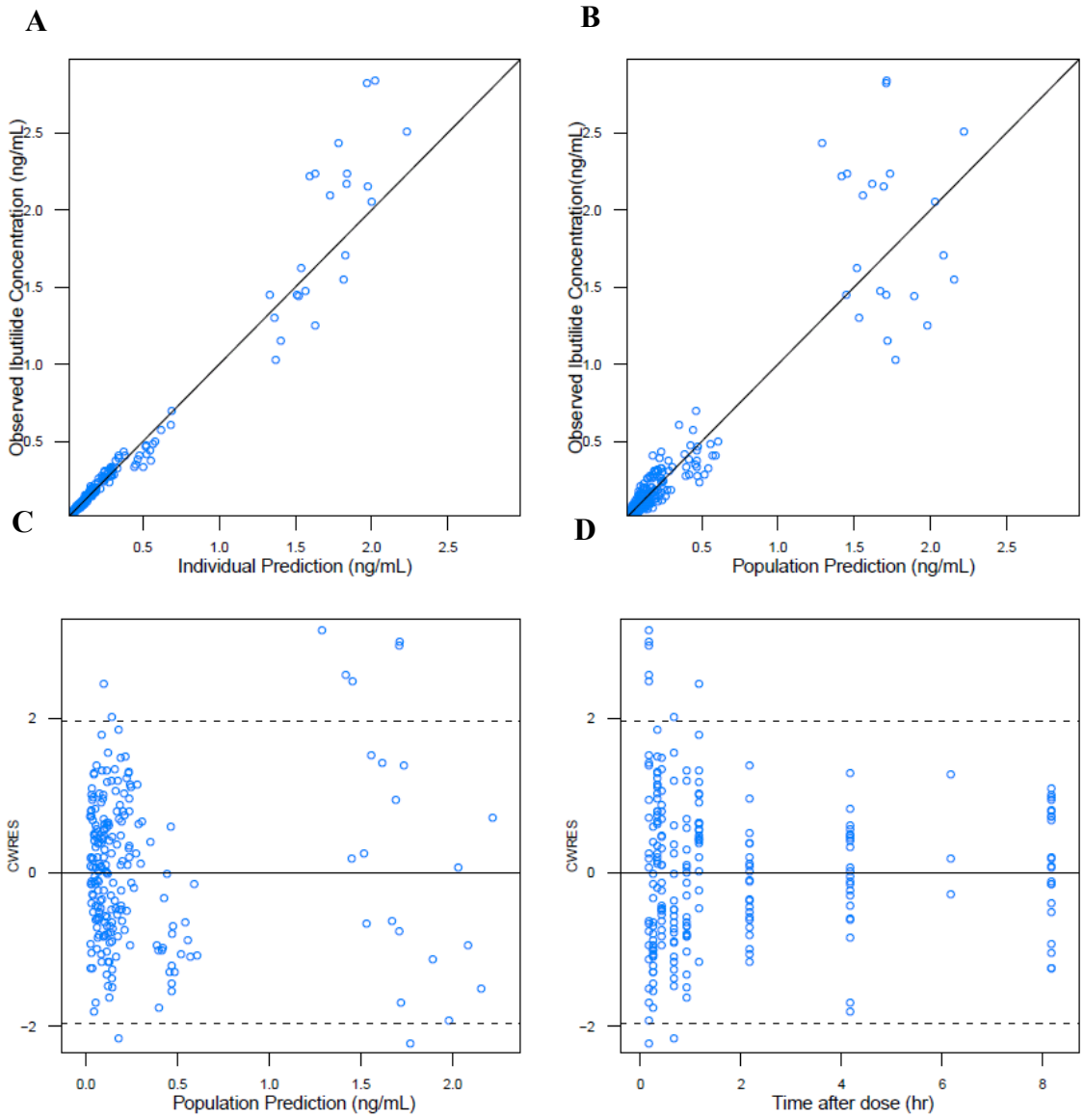

Figure 3:8. Goodness of fit for the final PK model. (A) Observed concentration vs. individual predicted concentration. (B) Observed concentration vs. population predicted concentration. (C) Conditional weighted residuals (CWRES) vs. population predicted concentration. (D) CWRES vs. time (hour)

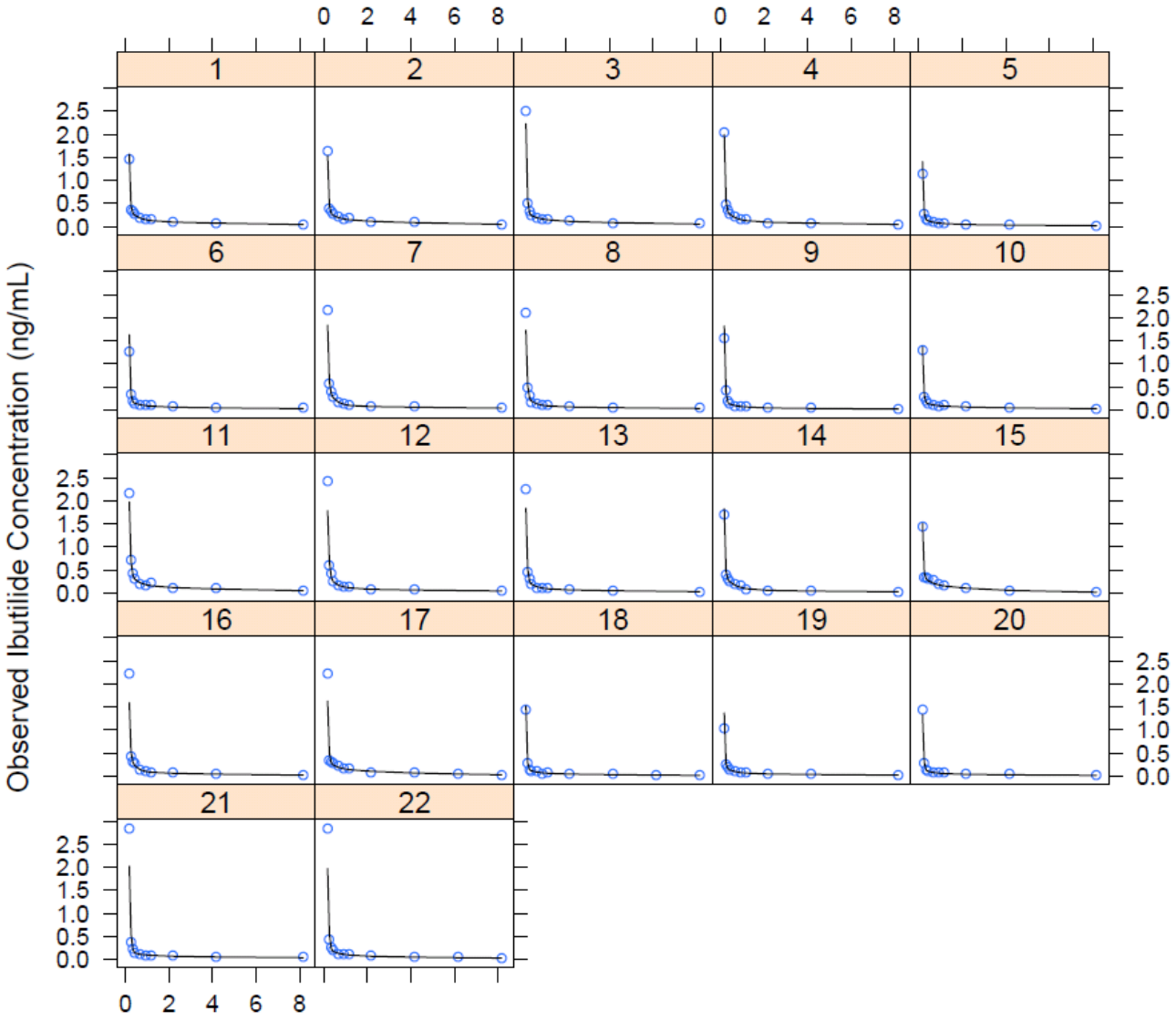

Figure 3:9. Individual GOF plots from the final PK model. Open blue circles are observed serum concentrations. Solid lines are individual predicted drug concentrations.

3.2.4 PK final model evaluation

The predictive performance of the model was assessed using VPCs that were generated with the final PK model. Model predictive performance was determined to be adequate as most observed data points were included in the 90% prediction interval (5^{th}-95^{th} percentiles) of the model (Figure 3.10). Additionally, the final population PK parameter estimates for both fixed-effect and random-effect parameters were in very close agreement with the corresponding median estimates derived from bootstrapping, indicating model robustness and precision of the final parameter estimates (Table 3.3).

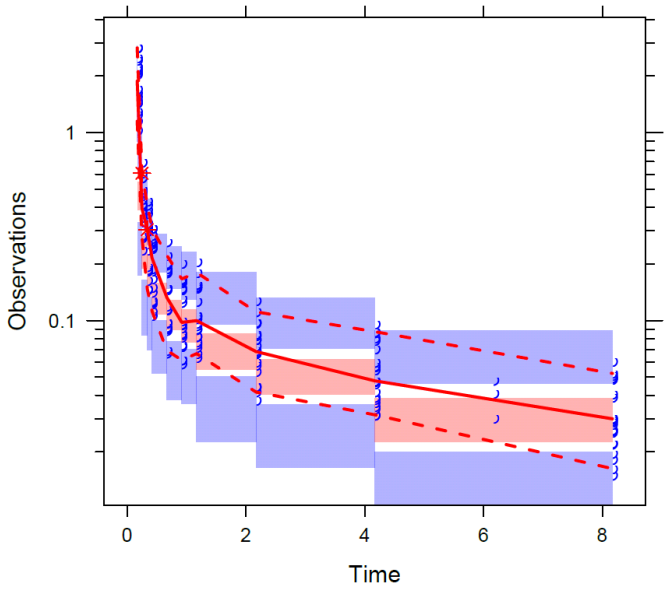

Figure 3:10. Visual predictive checks (VPCs) for the final PK model. The figure illustrates the relationship of observed ibutilide serum concentration (ng/mL) with time (hour). Observed serum concentrations are represented by open blue circles. The solid red line represents the median observed plasma concentration while the semitransparent red field represents the corresponding predicted 95% confidence interval for the simulated ibutilide concentration median. The dashed red lines represent the 5^{th} and 95^{th} percentiles, while the semitransparent blue field represents the 95% confidence interval for the corresponding predicted percentiles.

3.2.5 Population PKPD model

The PD dataset consisted of 176 $\Delta\Delta QT_F$ observations from 22 subjects. The initial PD model structure was determined based on $\Delta\Delta QT_F$-ibutilide concentration exploratory plots. The $\Delta\Delta QT_F$-ibutilide concentration relationship demonstrated a counterclockwise hysteresis loop in most patients suggesting a delay effect as illustrated in the representative plots in Figure 3.11.

First, the concentration-response relationship was characterized by testing several models with or without an intercept term (α), including linear, E_{max}, and sigmoid models. Both direct and effect compartment models were evaluated, with the effect compartment model best describing the delay observed between serum ibutilide concentration and $\Delta\Delta QT_F$ intervals. According to changes in AIC and improved GOF plots, the lengthening of $\Delta\Delta QT_F$ interval following ibutilide administration was best explained by an E_{max} model with intercept and an effect compartment, which was therefore utilized as the structural base model. An intercept term was introduced to the model to enhance stability by permitting prediction of negative $\Delta\Delta QT_F$ observations. The model is schematically depicted in Figure 3.12. GOF plots for the base model are displayed in Figure 3.13.

The residual error variability was best described by an additive error model. In the structural base model, the final parameters for E_{max} and EC_{50} were 44.1 ms and 0.065 ng/mL, respectively. Other estimated parameters along with Inter-individual and residual variabilities are summarized in Table 3.5.

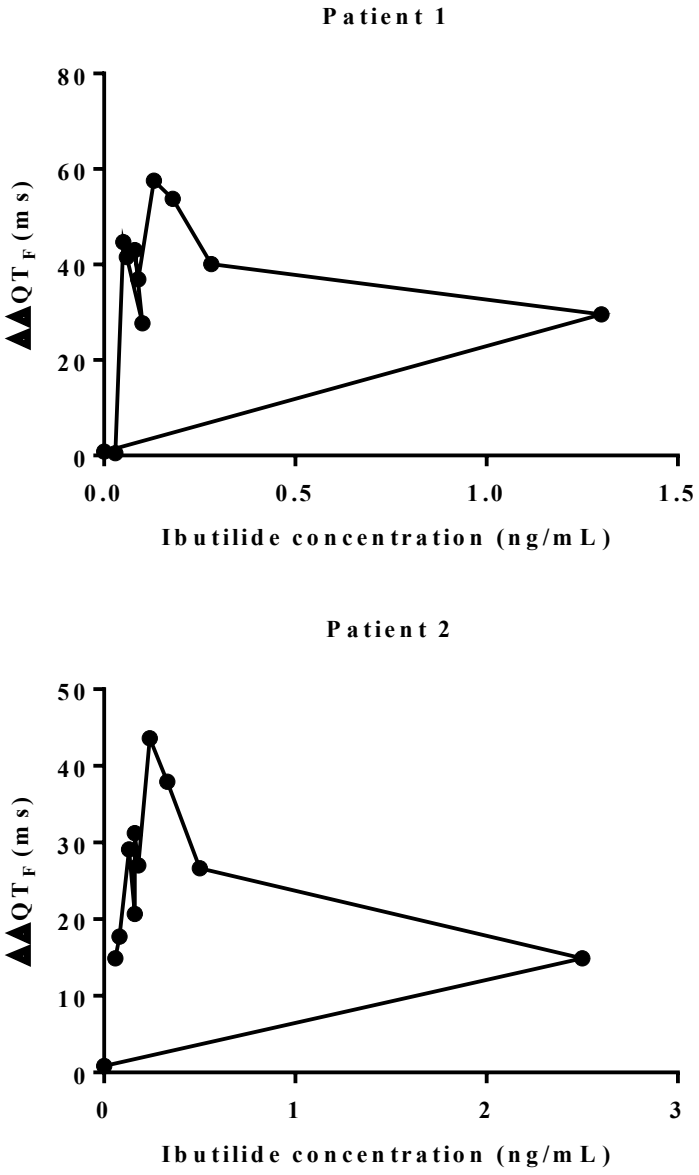

Figure 3:11. The $\Delta\Delta QT_F$-ibutilide serum concentration relationship derived from observed data for 2 patients. The $\Delta\Delta QT_F$-ibutilide serum concentration relationship in both patients demonstrated a hysteresis loop, suggesting a delay effect between response and ibutilide concertation.

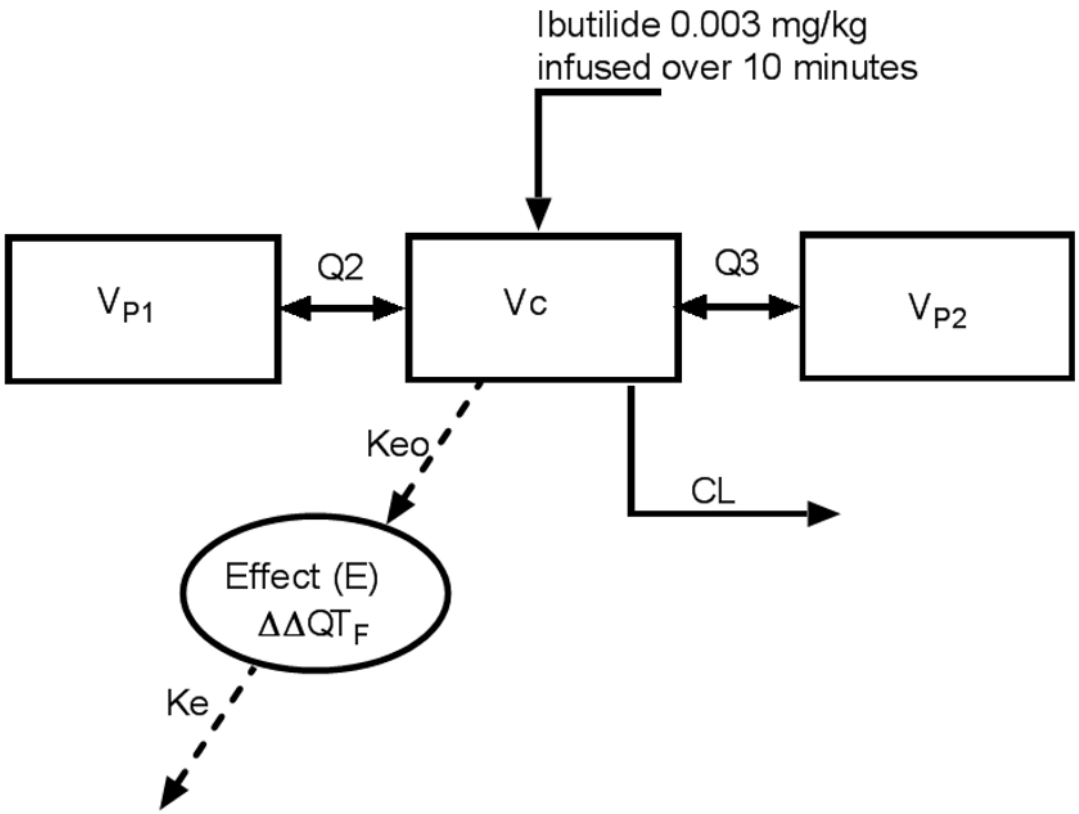

Figure 3:12. Schematic for the structural PKPD model. CL = systemic clearance, V_C = volume distribution of the central compartment, V_{P1} = volume distribution of peripheral compartment 1, V_{P2} = volume distribution of peripheral compartment 2, Q2 = intercompartment clearance for compartment 2, Q3 = intercompartment clearance for compartment 3, K_{eo} = effect rate constant, K_e = hypothetical elimination rate constant.

Table 3.5. Summary of the estimated population PKPD parameters from both base and covariate model.

Parameter	Base Model	Covariate Model	
	Population Estimates	Population Estimates	Bootstrap Estimates (95 CI%)
OFV		1309	
E_{max} (ms)	44.1	35.6	36.2 (29.4, 43.6)
EC_{50} (ng/mL)	0.06	0.15*	0.15 (0.11, 0.25)
		0.17**	0.168 (0.1, 0.2)
A (ms)	-3.7	-4.33	-4.3 (-6.8, -1.6)
KeO (hr^-)	2.2	5.36	4.9 (2.5, 8.7)
Ke (hr^-)	8.1	8.5	8.1 (6.5, 10.3)
HF on E_{max}	-	1.39	1.42 (1.1, 1.9)
miR-362-3p on EC_{50}	-	-0.09	-0.07 (-0.14, 0.01)
ω E_{max} %	30.8	26.2	25.7 (5.1, 4.74)
ω EC_{50} %	32.4	26.4	
σ ADD (ms)	7.9	7.87	7.8 (6.9, 8.8)

E_{max} = maximum effect of ibutilide on QT interval length, EC_{50} = serum ibutilide concentration required to achieve 50% of the maximum effect on $\Delta\Delta QT_F$, α = intercept, KeO = effect rate constant, Ke = elimination rate constant, ω = inter-individual variability (omega), σ = residual variability (sigma), ADD = additive.
* EC_{50} for patients without miR-362-3p expression data.
** EC_{50} for patients with miR-362-3p expression data.

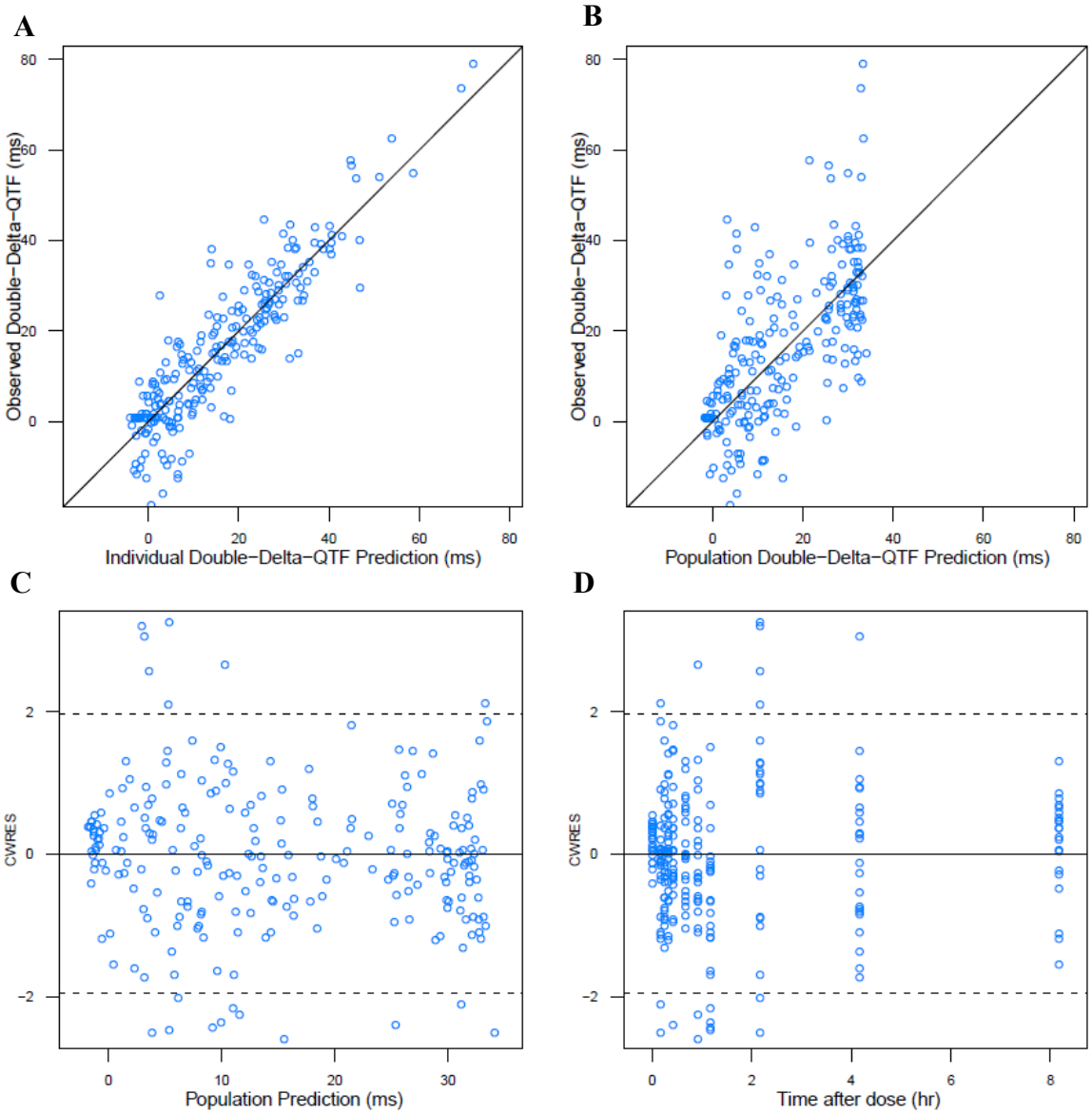

Figure 3:13. Validation of the structural PKPD model. (A) Observed ΔΔQTF vs. individual predicted ΔΔQTF. (B) Observed ΔΔQTF vs. population predicted ΔΔQTF. (C) Conditional weighted residuals (CWRES) vs. population predicted ΔΔQTF. (D) CWRES vs. time (hour).

3.2.6 Covariate PKPD model

Several covariates were evaluated as potential predictors of ibutilide-associated $\Delta\Delta QT_F$ changes. Tested covariates included miR-362-3p expression, age, sex, race, weight, and HFrEF or HFpEF. miR-362-3p expression data was collected from 12 patients. The miR-362-3p expression-time profile for the three groups are illustrated in figures 3.14 and 3.15. The miR-362-3p and $\Delta\Delta QT_F$ relationship was further explored and characterized in each group as demonstrated in Figure 3.16.

First, to explore all covariate relationships and their impact on the performance of the PKPD model, each covariate was first tested independently (Table 3.6). Of the tested covariates, both HF status (either HFrEF or HFpEF) and miR-362-3p expression significantly decreased the OFV by > 3.84 (P <0.05). Due to model complexity and the inability to pursue covariate model building while testing HFrEF and HFpEF as independent covariates, these two groups were combined into one covariate (HF status) for subsequent analysis. Next, the final model with significant covariates were built through the forward addition and backward elimination approach, resulting in HF status on E_{max} and miR-362-3p expression on EC_{50} as significant contributors to ibutilide-induced changes in $\Delta\Delta QT_F$.

Individual and population predictions were improved in the final model over the base model, as displayed in Figure 3.17. The weighted residuals were nearly normally distributed in the final model, displaying an even distribution around zero and mostly within two units of the null ordinate.

Overall performance of the final model was better than the base model, and the incorporated covariates explained large portions of the variability in the population predictions. Between base and final models, the ΔOFV was -14 (P < 0.01). All individual plots for the final

PKPD model are shown in Figure 3.18. In the final PKPD model, the unexplained interpatient variability decreased from 30.9% to 26.2% for E_{max}, and 32.4% to 26.5% for EC_{50}. The mean individuals estimated E_{max} was significantly higher in HFrEF or HFpEF patients when compared to matched control, with P <0.0001, and P <0.05 respectively (Figure 3.19) while EC_{50} was negatively correlated with miR-362-3p expression, with P value < 0.0001 and R^2 of 0.93 (Figure 3.20). Figure 3.21 displays representative plot of $\Delta\Delta QT_F$ vs time plot in which incorporated covariates improved PKPD model fitting.

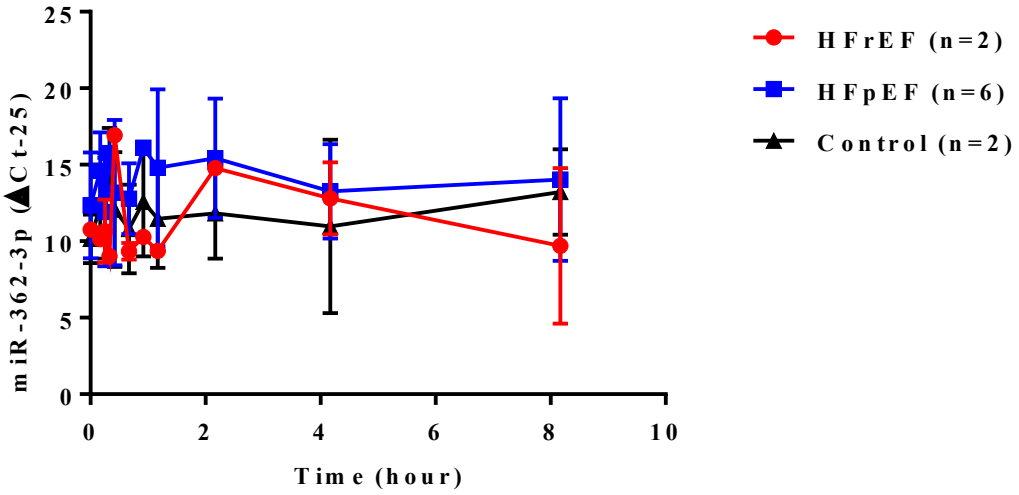

Figure 3:14. miR-362-3p expression-time profile (Over 8 hours) for all patients included in the analysis.

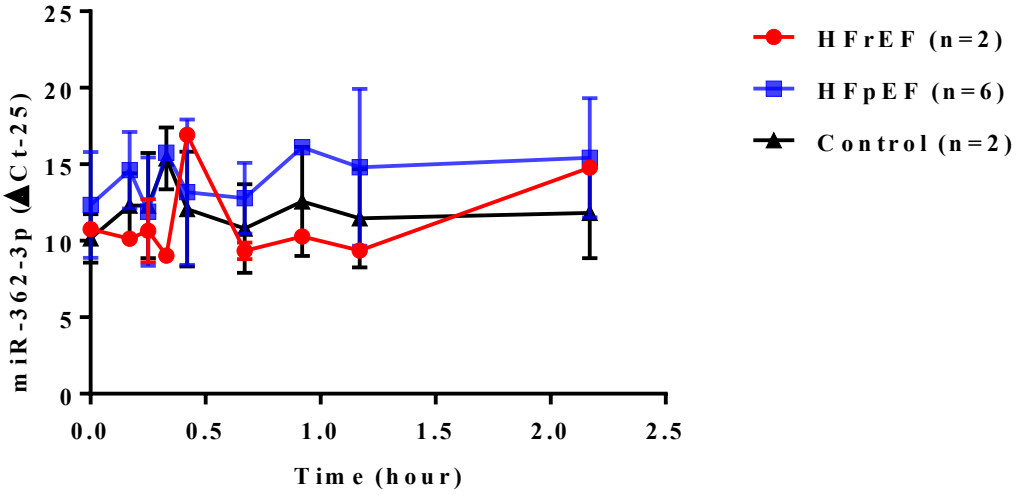

Figure 3:15. miR-362-3p expression-time profile (Over 2 hours) for all patients included in the analysis.

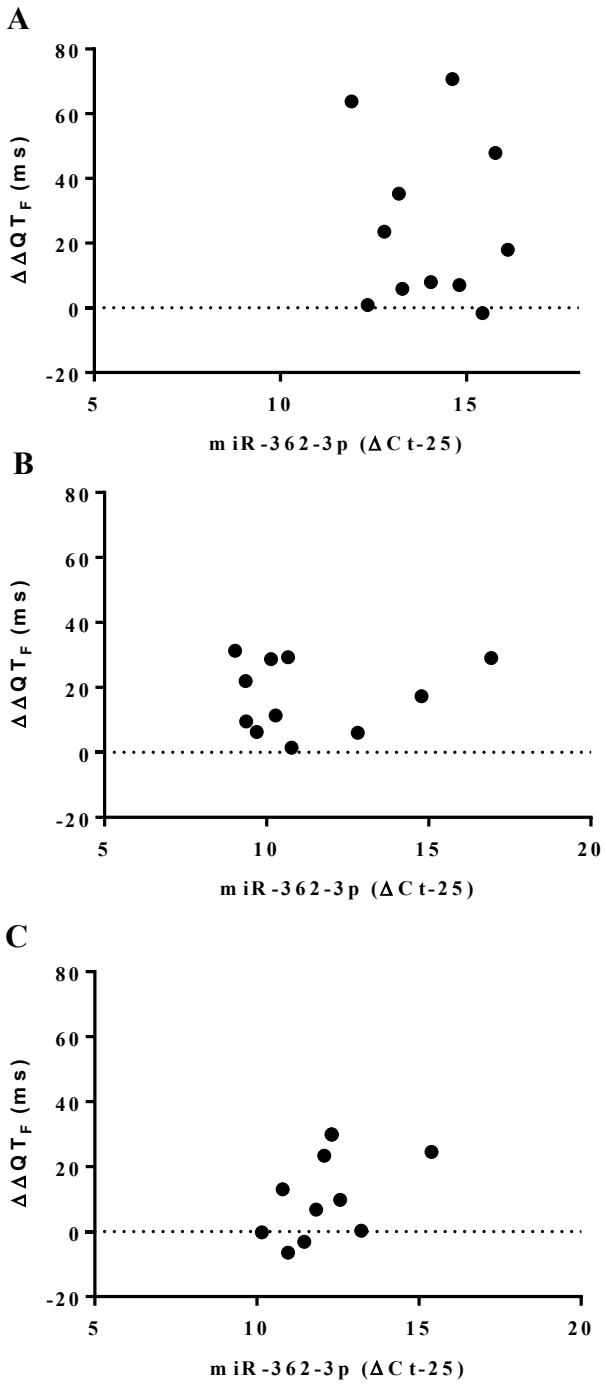

Figure 3:16. $\Delta\Delta QT_F$-miR-362-3p serum expression relationship for (A) HFrEF patients (n=2), (B) HFpEF patients (n=10), (C) and match control (n=10). Data presented as mean.

Table 3.6. Summary of PD covariate model analysis.

PD model	OFV	ΔΔ OFV	P-value
Base model	1323.9		
Base model + HF on E_{max}	1319.8	-4.1	<0.05
Base model + HF on EC_{50}	1314.4	-9.5	<0.05
Base model + MIR on E_{max}	1317.8	-6.1	<0.05
Base model + MIR on EC_{50}	1313.9	-9.9	<0.05
Base model + AGE on E_{max}	1322.6	-1.2	ns
Base model + AGE on EC_{50}	1320.5	-3.3	ns
Base model + SEX on E_{max}	1334.4	10.6	ns
Base model + SEX on EC_{50}	1323.7	-0.1	ns
Base model + RACE on E_{max}	1323.7	-0.2	ns
Base model + RACE on EC_{50}	1323.7	-0.13	ns
Base model + MIR + HF on EC_{50}	1311.2	-2.7	ns
Base model + MIR on EC_{50} & E_{max}	1313.9	-0.02	ns
Base model + MIR on EC_{50} + HF on E_{max}	1309.9	-4.03	<0.05

ΔOFV is the difference in objective function values between base and covariate model. HF = heart failure, MIR = miRNA-362-2p, E_{max} = maximum effect of ibutilide on $\Delta\Delta QT_F$, EC_{50} = serum ibutilide concentration required to achieve 50% of the maximum effect on QT_F, ns= not significant.

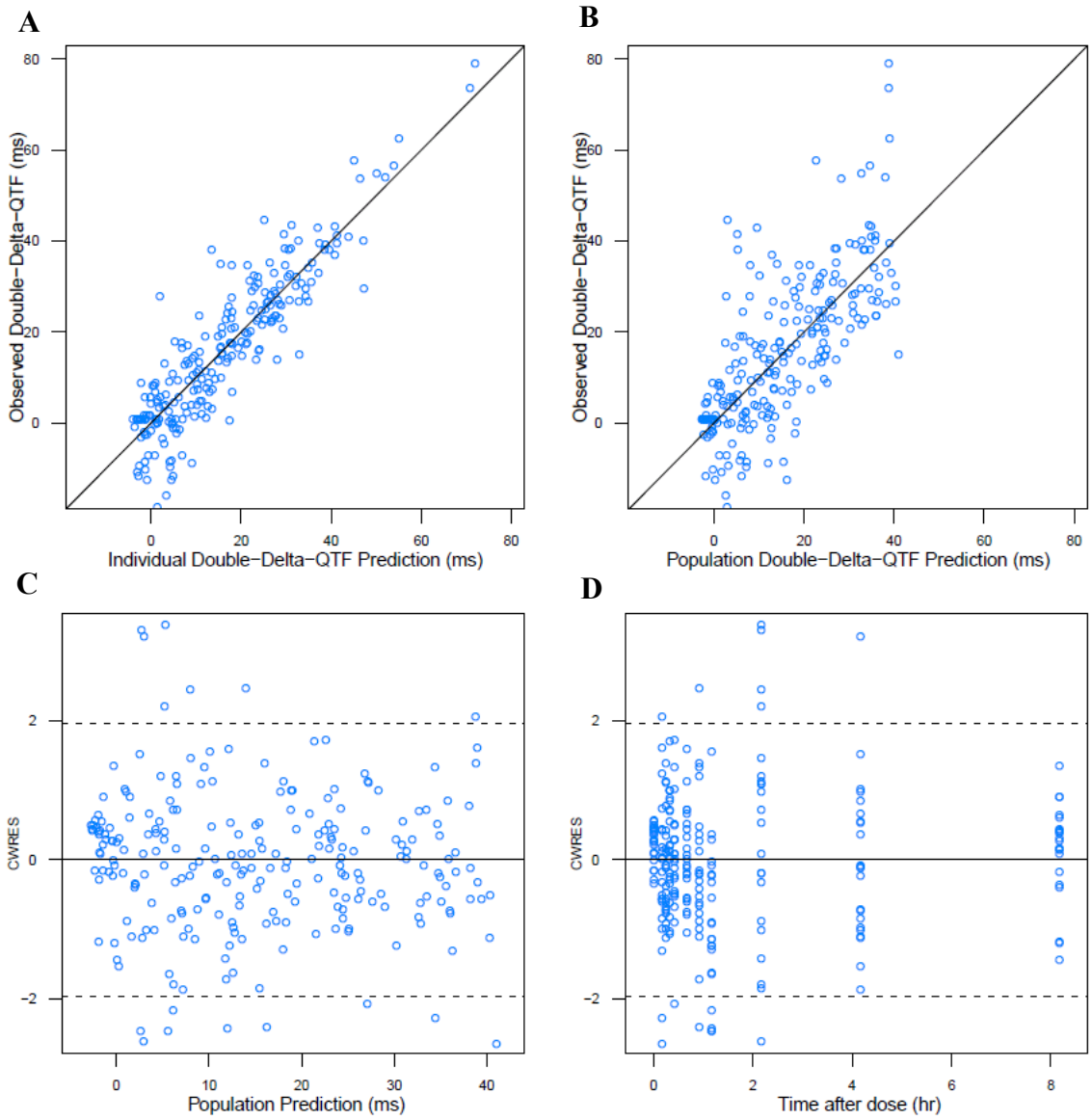

Figure 3:17. Final PKPD model validation. (A) Observed $\Delta\Delta QT_F$ vs. individual predicted $\Delta\Delta QT_F$. (B) Observed $\Delta\Delta QT_F$ vs. population predicted $\Delta\Delta QT_F$. (C) Conditional weighted residuals (CWRES) vs. population predicted $\Delta\Delta QT_F$. (D) CWRES vs. time (hour).

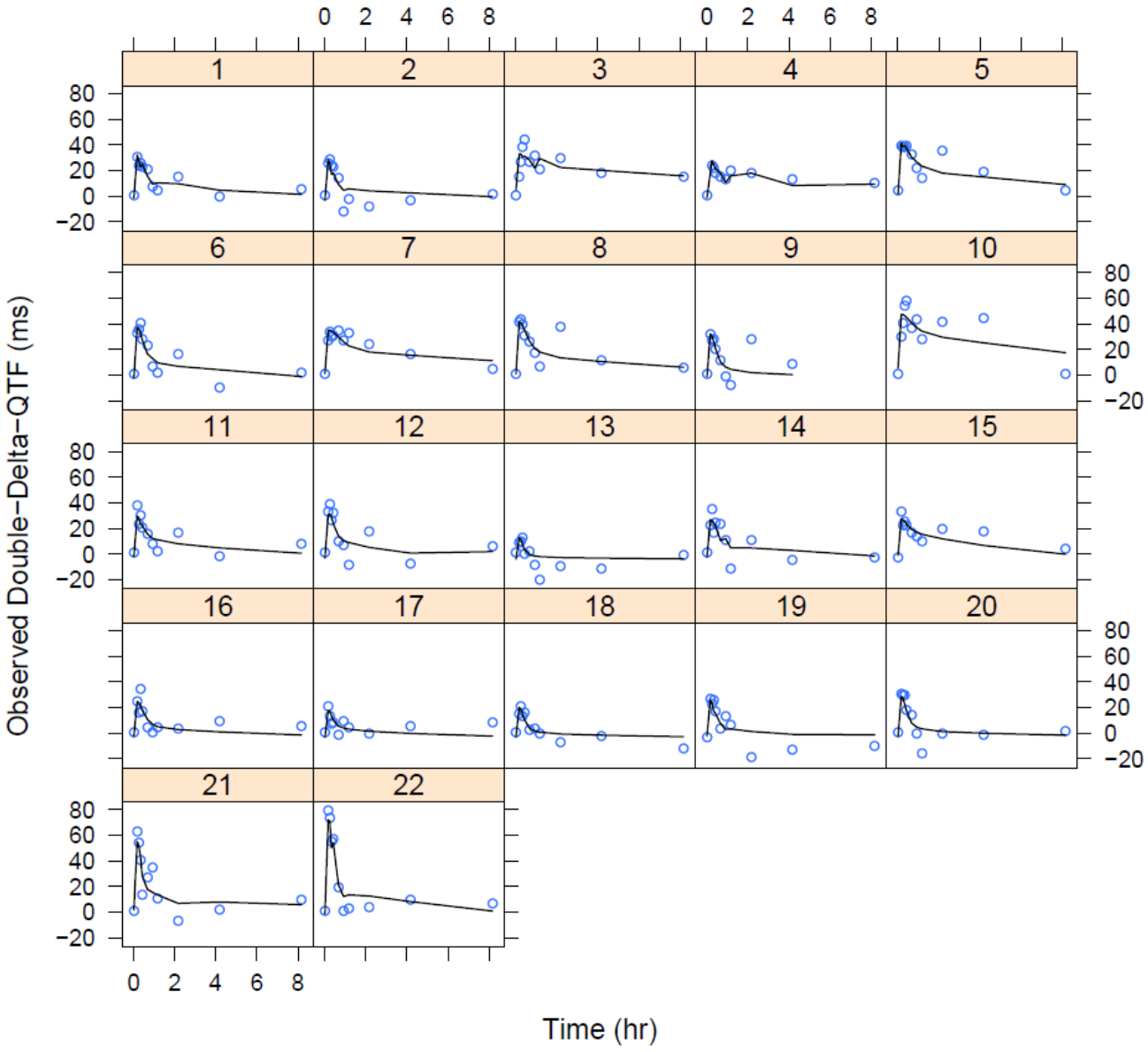

Figure 3:18. Individual GOF plots for the final PKPD model. Open blue circles are observed $\Delta\Delta QT_F$. Solid lines are individual predicted drug concentrations.

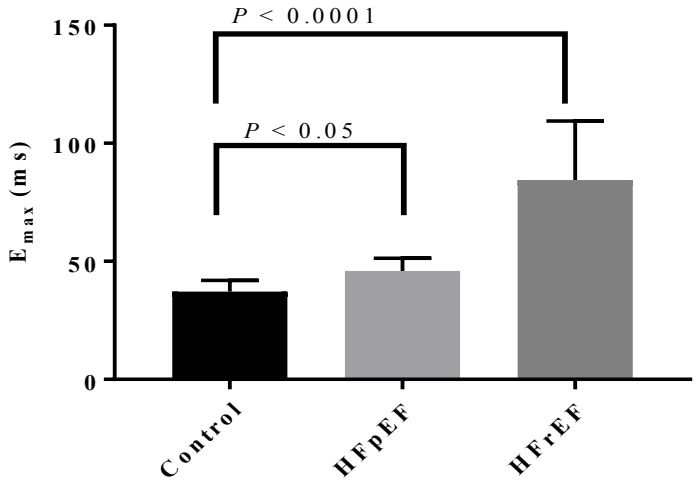

Figure 3:19. Representative ibutilide individual E_{max} for patients with or without HF. Mean individual E_{max} was significantly higher in patients with either HFrEF or HFpEF when compared to matched control group.

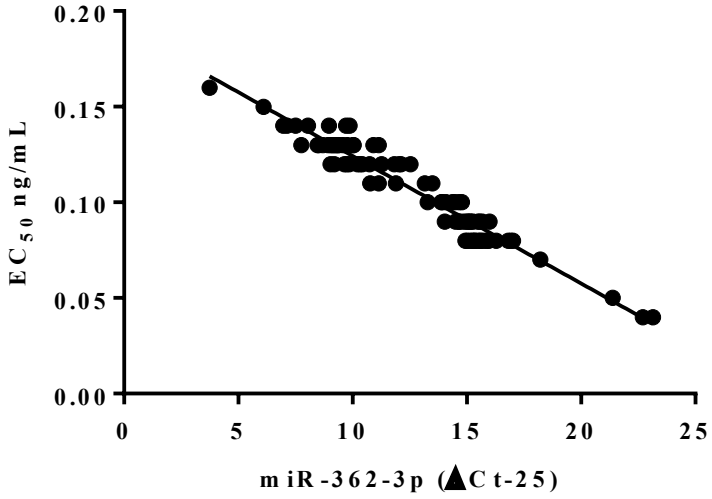

Figure 3:20. Representative ibutilide EC_{50} individual estimated concentrations versus miR-362-3p expression (ΔCT-25). The solid line represents the best-fit line. The correlation is negative ($P < 0.0001$ and $R^2=0.93$), in which higher expression of miR-362-3p is associated with lower EC_{50} values.

A

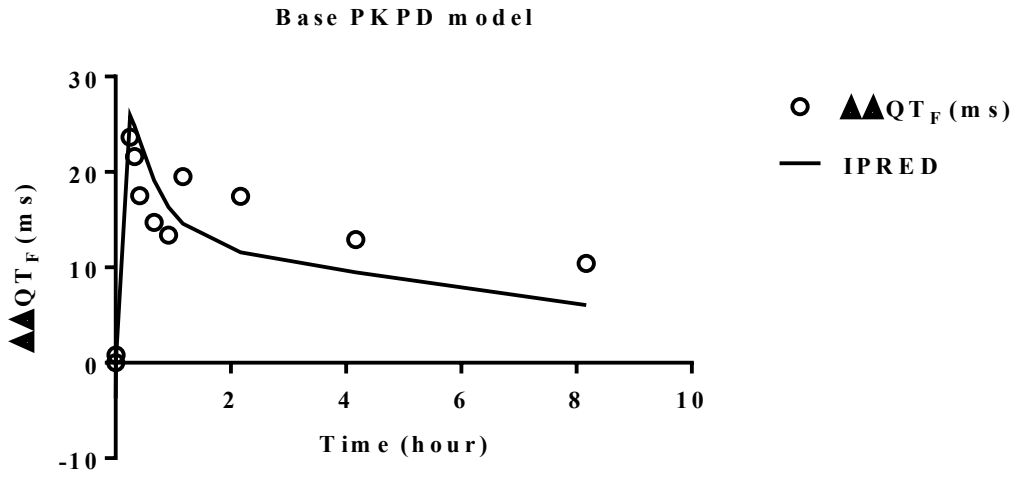

B

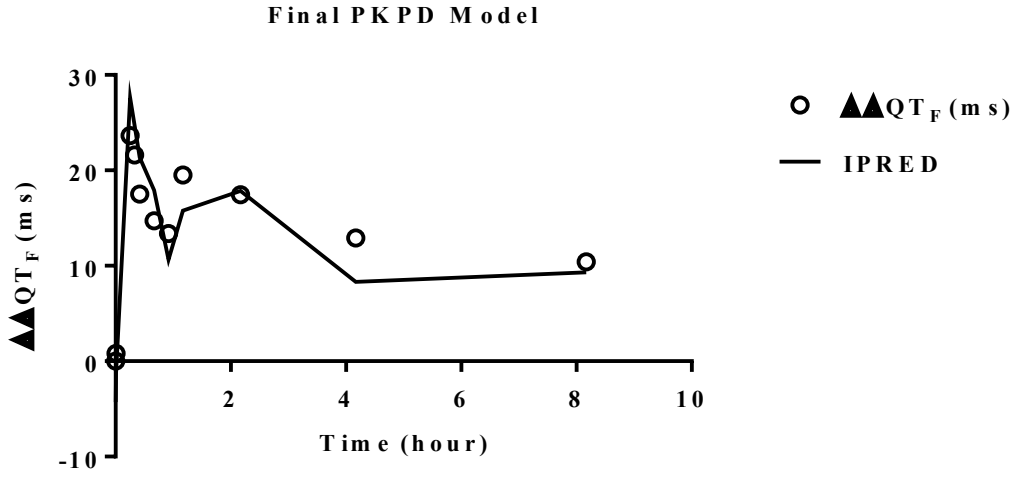

Figure 3:21. Representative individual PKPD model fit before (A) and after (B) significant covariates were incorporated. Heart failure (HFrEF or HFpEF) on E_{max} and miR-362-3p expression on EC_{50} improved model fitting.

3.2.7 PKPD final model evaluation

Predictive performance of the models is evident in the VPCs, in which most observed data points were included in the 90% prediction interval (5^{th}-95^{th} percentiles), as shown in Figure 3.22. Final PD parameter estimates for both fixed-effect and random-effect parameters were comparable to the median parameter estimates obtained from bootstrapping and fell within the 95% Cl, indicating precision and stability of the final parameter estimates (Table 3.5). In addition, all parameters were normally distributed, confirming the assumption of symmetry for model building.

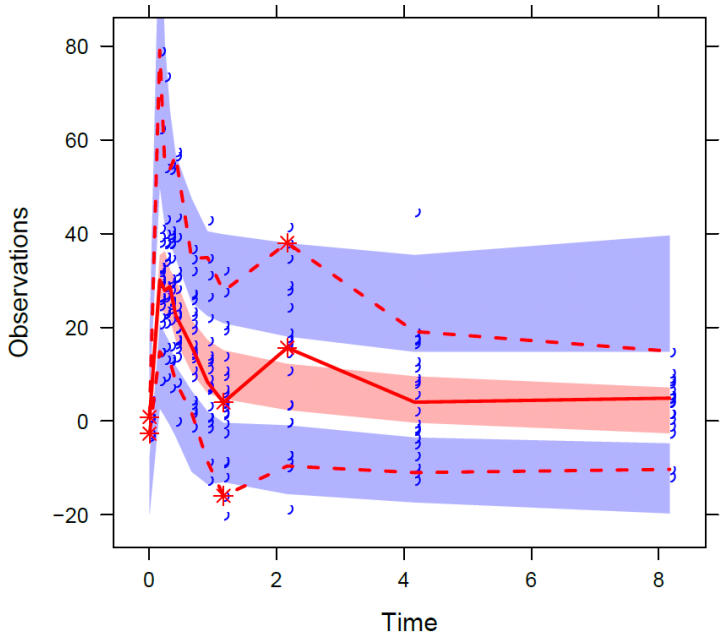

Figure 3:22. Visual predictive checks (VPCs) for the PKPD model. The figure illustrates the relationship of $\Delta\Delta QT_F$ (ms) with time (hour). Observed $\Delta\Delta QT_F$ values are represented by blue open circles. The solid red line represents the median $\Delta\Delta QT_F$ while the semitransparent red field represents the corresponding predicted 95% confidence interval for the simulated median. Dashed red lines represent the 5^{th} and 95^{th} percentiles while the semitransparent blue field represents the 95% confidence interval for the corresponding predicted percentiles.

3.2.8 Population PKPD simulations

Monte Carlo simulations were performed using the PKPD covariate model (n=1000 per miR-362-3p expression group) to evaluate the effect of miR-362-3p on ibutilide EC_{50}. Three groups of subjects with different levels of miR-362-3p expression were included as follows: high expression (miR-362-3p ΔCT-25 = 25), medium expression (miR-362-3p ΔCT-25 =15), and low expression (miR-362-3p ΔCT-25 =1). Each subject's miR-362-3p expression level remained consistent across all time points (0, end of infusion, and at 5, 10, 15, 20, 30, and 45 minutes and 1, 2, 4, 6, 8, and 12 hours following infusion). Simulations revealed that ibutilide EC_{50} differed significantly between the three groups ($P < 0.001$), as displayed in Figure 3.23. Subjects with high expression of miR-362-3p demonstrated a lower ibutilide EC_{50} compared to those in either the medium or low expression groups.

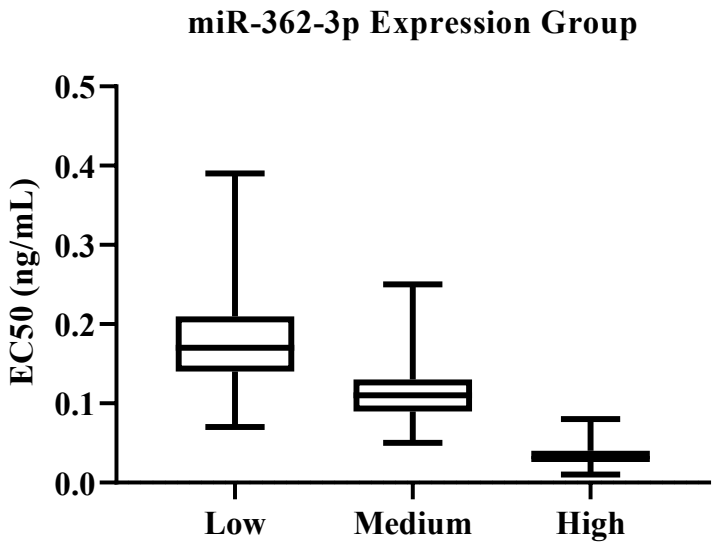

Figure 3:23. Simulation results for the effect of low, medium, and high miR-362-3p serum expression of on ibutilide EC_{50} ($P < 0.001$).

3.3 SPECIFIC AIM III

Specific Aims I and II demonstrated that miR-362-3p regulates hERG-related current, along with the potential role for serum expression to predict patient sensitivity to ibutilide-induced QT interval lengthening. These findings suggest a potential role for miRNAs in regulating hERG expression and function. While hERG is a direct target of miR-362-3p, several miRNAs commonly regulategene expression. Therefore, the objective of Specific Aim 3 was to develop *a comprehensive screening bioassay to identify miRNAs that potentially regulate KCNH2 expression and function during pathophysiological consequences of HF. The bioassay utilized hiPS-CMs that were exposed to classical consequences of heart failure; including βAR stimulation or activated CaMKII overexpression*.

3.3.1 High-throughput screening strategy identified 16 binding sites potentially regulated by miRNAs in hiPS-CMs cells

Using bioinformatic tools, 327 target predicted miRNA target sequences were identified in the *KCNH2* 3'UTR, which are predicted to be regulated by miRNAs. Of those sites, eight were significantly downregulated in the CAMKII group (P <0.05, log fold change between -0.29 and -1.07), and six were significantly downregulated in the sustained βAR stimulation group (P <0.05, log fold change between -0.29 and -0.72). Two binding sites were significantly reduced in both treated groups (P < 0.05, log fold change between -0.38 and -0.61). These 16 putative regulatory sites were predicted to be bound by 31 miRNAs (Table 3.7).

Table 3.7. Summary of HT-bioassay identified binding sites significantly downregulated in hiPS-CMs treated cells.

Binding sites	Fold change	P Value	Putative miRNAs
CAMKII group			
GCCGCTCCCCTTGGAGGCCCTGCTCAGGAGGCCCT	-0.59	0.01	miR-378a-5p miR-1200* miR-3653-5p*
GGCTCGGACCCGGGCAGTTAGTGGGGCTGCCCAGT	-0.40	0.01	miR-4690-3p
TGCTCAGGAGGCCCTGACCGTGGAAGGGGAGAGGA	-0.8	0.02	miR-4512
TGCTCAGGAGGCCCTGACCGTGGAAGGGGAGAGGA	-0.38	0.02	miR-3127-3p miR-6756-3p
GGCCATGTGGTTCCCTGCAGCCTCATGCCTGGCCC	-0.66	0.03	miR-3622b-5p
CATTAGCTGGTCTAACTGCCCGGAGGCACCCGGCC	-1.07	0.04	miR-7843-5p
AGGGATCAAGGCGCTGCTGGGCCGCTCCCCTTGGA	-0.29	0.04	miR-920 miR-6090 miR-1343-5p miR-939-5p
ACTGCCCGGAGGCACCCGGCCCTGGGCCTTAGGCA	-0.39	0.05	miR-4747-3p

Table 3.7 continued

ISO treated group			
GAACTCGAAAGCACAGCTCCTCCCCCAGCCCTTGG	-0.68	<0.001	miR-5589-5p* miR-5787 miR-4505
AACTCGAAAGCACAGCTCCTCCCCCAGCCCTTGGG	-0.59	0.01	miR-5787 miR-5001-5p miR-4498 miR-762 miR-4492
GGAACTCGAAAGCACAGCTCCTCCCCCAGCCCTTG	-0.57	0.01	miR-4731-5p
CATGCCTGGCCCCTTGACACATCCAAAGCAAAGGG	-0.50	0.02	miR-1251-3p
GCATGTGGTTCATTCTAGCATTTCTGTTCTGTGCT	-0.29	0.04	miR-4773
GCAGTAGAGGAAGAAATGCTAGCCTGGAAGCTCGG	-0.72	0.04	miR-3180-5p
Downregulated in both groups			
ACTCGAAAGCACAGCTCCTCCCCCAGCCCTTGGGA	-0.53 (CAMKII) -0.62 (ISO)	0.01 <0.001	miR-6085 miR-4446-3p
AGGAACTCGAAAGCACAGCTCCTCCCCCAGCCCTT	-0.38 (CAMKII) -0.38 (ISO)	0.04 0.04	miR-4665-5p* miR-7109-5p* miR-637*

*miRNAs selected for HT-bioassay validations.

3.3.2 Luciferase assay screening of miRNAs identified from the HT-bioassay

Of those 31 miRNAs, seven were selected for subsequent validation analysis: miR-637, miR-1200, miR-3653-5p, miR-4665-5p, miR-5589-5p, miR-7109-5p, and miR-7843. From the CAMKII group, miR-7843, miR-1200, and miR-3653 were selected since their corresponding sites demonstrated the lowest *P* value ($P = 0.01$) and highest fold changes (log fold change = -0.59) among all miRNAs in this group. From the ISO group, miR-5589-5p was selected since the corresponding binding site demonstrated the lowest *P* value ($P < 0.001$) and the highest fold change (log fold change = -0.68) among all miRNAs. Lastly, miR-4665-5p, miR-7109-5p, and miR-637 were selected due to their presence in both groups ($P = 0.04$, log fold change between -0.38).

These seven miRNAs were quantitatively screened for *KCNH2* 3′UTR activity using luciferase assays (n = 3 per group). None were found to significantly reduce *KCNH2* 3'UTR activity (Figure 3.24).

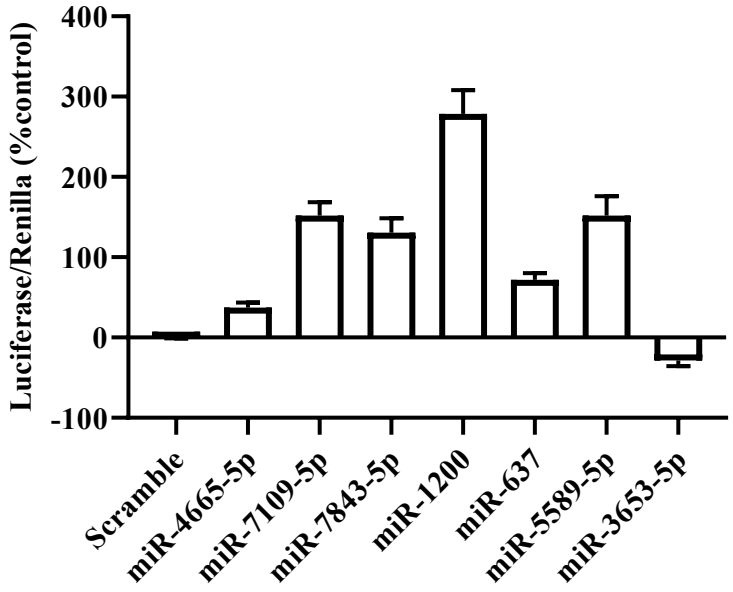

Figure 3:24. Screening of HT-bioassay-identified miRNAs with luciferase assays. A *KCNH2* 3′UTR reporter clone was co-transfected with a control reporter plasmid (renilla) and MISSION miRNA mimics of the selected miRNAs or negative control into a human adenocarcinoma cell line (SK-BR-3); n=3 per group. None of the seven miRNAs significantly reduced *KCNH2* 3' UTR activity.

3.3.3 Three selected miRNAs attenuate I_{kr} in HEK293-hERG cells

While most of the identified miRNAs failed to reduce *KCNH2* 3' UTR activity in luciferase assays, three of these miRNAs (miR-637, miR-1200, miR-3653-5p) were screened further for their effects on I_{kr} current in HEK293-hERG. Current-voltage relationships for I_{kr} current were recorded 48 hours post-transfection in cells transfected with miRNA mimics and in control cells. At 48 hours post transfection, there were significant differences in mean peak tail currents between groups over the voltage range -100 to +40 mV (P <0.05), as shown in Figure 3.25.

The voltage-dependence of hERG channel activation was assessed by analyzing tail currents from the activation protocol. From a holding potential of -60 mV, cells were depolarized

using a series of depolarizing pulses between -50 and +60 mV for one second to activate hERG channels. The cells were then stepped back to a repolarizing voltage of -50 mV to allow recovery from inactivation for tail current measurement. Representative I_{kr} current traces recorded using this voltage protocol from HEK293-hERG are in shown in Figure 3.25A&D. In cells transfected with a positive control (miR-362-3p) and *KCNH2* siRNA, I_{kr} current was attenuated (Figure 3.25B). Corrected tail current (tail current amplitude normalized to the maximum peak tail current amplitude) was used to construct the activation curve shown in Figure 3.25E. At 48 hours post-transfection, the three selected miRNAs significantly reduced hERG activation currents (P <0.05). The ability of the tested miRNAs to reduce I_{kr} current indicates that the novel high-throughput bioassay was more accurate at identifying miRNAs with regulatory effects than the commonly-used luciferase assays.

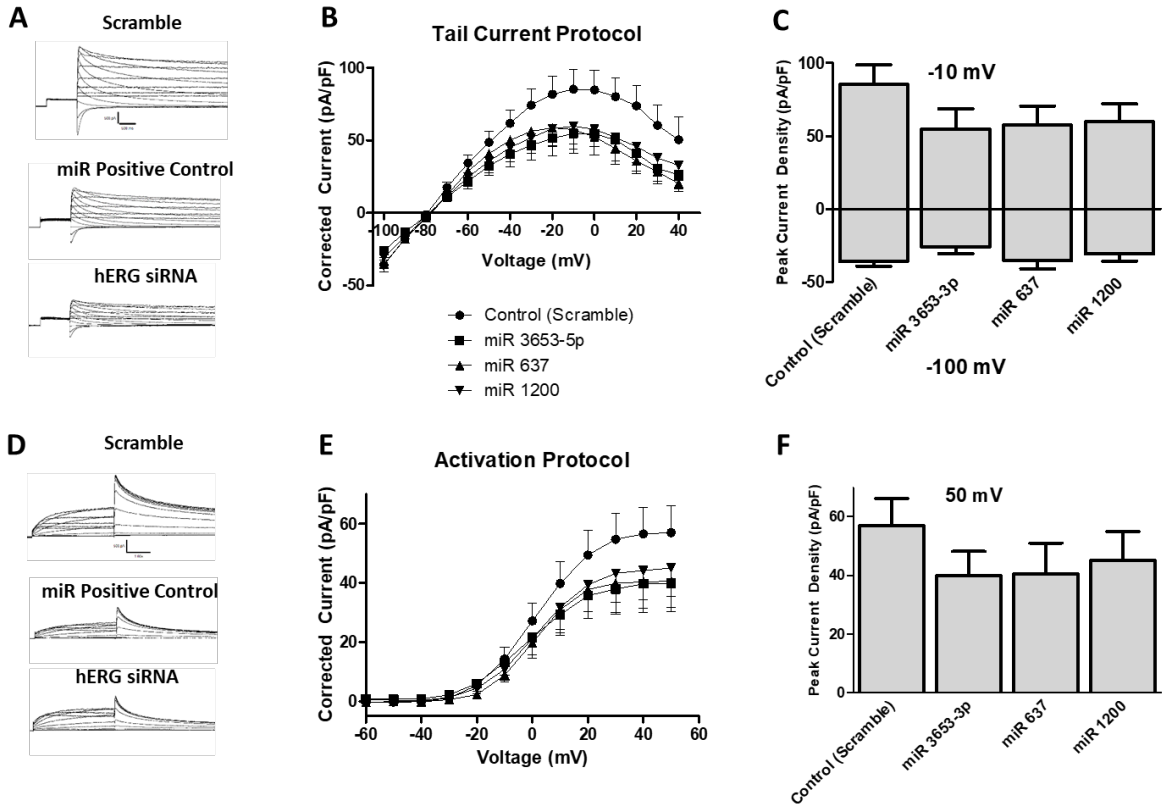

Figure 3:25. (A) Representative traces of KCNH2 tail currents following transfection with scrambled, positive control, or *KCNH2* siRNA. (B) Current-Voltage (I-V) plot showing the three selected miRNAs significantly reduced KCNH2 tail currents. (C) Maximum peak activation current. (D) Representative traces of KCNH2 activation currents following transfection with scrambled, positive control, or *KCNH2* siRNA. (E) Current-Voltage (I-V) plot showing the three selected miRNAs significantly reduced KCNH2 activation currents. (F) Maximum activation current.

3.3.4 Association between expression of HT-bioassay identified miRNAs and maximum QT_F interval ($maxQT_F$)

After assessment of the HT-bioassay with the patch clamp technique, the expression of HT-bioassay miRNAs was examined in the serum of a total of 12 patients from the clinical trial described in Specific Aim 2. The patients demographics are described in Table 3.8. A total of 14 serum samples were collected from the patients at baseline (nine samples), one hour (one sample) and four hours (four samples) following ibutilide administration and included in the correlation analysis. QT intervals were measured at each timepoint. Of the 31 HT-bioassay-identified miRNAs (Table 3.7), six were found to be expressed in patients: miR-378a-5p, miR-939-5p, miR-4446-3p, miR-4665-5p, miR-4690-3p, and miR-5589.

Correlation analysis was performed to assess the potential association between expressed miRNAs and corresponding max QTc interval lengthening. Of the six expressed miRNAs, only miR-4665-5p was significantly associated with max QTc interval ($P = 0.0379$) (Figure 3.26).

Table 3.8. Study population characteristics.

Characteristics	HFrEF (n=2)	HFpEF (n=6)	Control (n=4)
Males	1 (50)	1 (17)	1 (25)
White	1 (50)	5 (83)	3 (75)
African American	1 (50)	1 (17)	1 (25)
Age (years)	64 ± 1	66 ± 9	61 ± 9
Body Weight (Kg)	87.3 ± 3	92 ± 13	85 ± 16
Ibutilide dose (mg)	0.26 ± 0.01	0.28 ± 0.04	0.26 ± 0.04
Concurrent diseases			
- Hypertension	2 (100)	2 (33)	2 (50)
- Coronary artery disease	2 (100)	2 (33)	1 (25)
- Diabetes mellitus	1 (50)	4 (67)	1 (25)
- Hyperlipidemia	2 (100)	4 (67)	2 (50)
Concomitant medications			
- ACE inhibitors/ARBs	2 (100)	4 (67)	2 (50)
- Loop diuretics	2 (100)	5 (83)	1 (25)
- β-blockers	2 (100)	5 (83)	0 (0)
- Statins	2 (100)	4 (67)	2 (50)

Data presented as n (%) or mean ± SD.
HFpEF = heart failure with preserved ejection fraction, HFrEF = heart failure with reduced ejection fraction, ACE = angiotensin-converting enzyme, ARB = angiotensin receptor blocker.

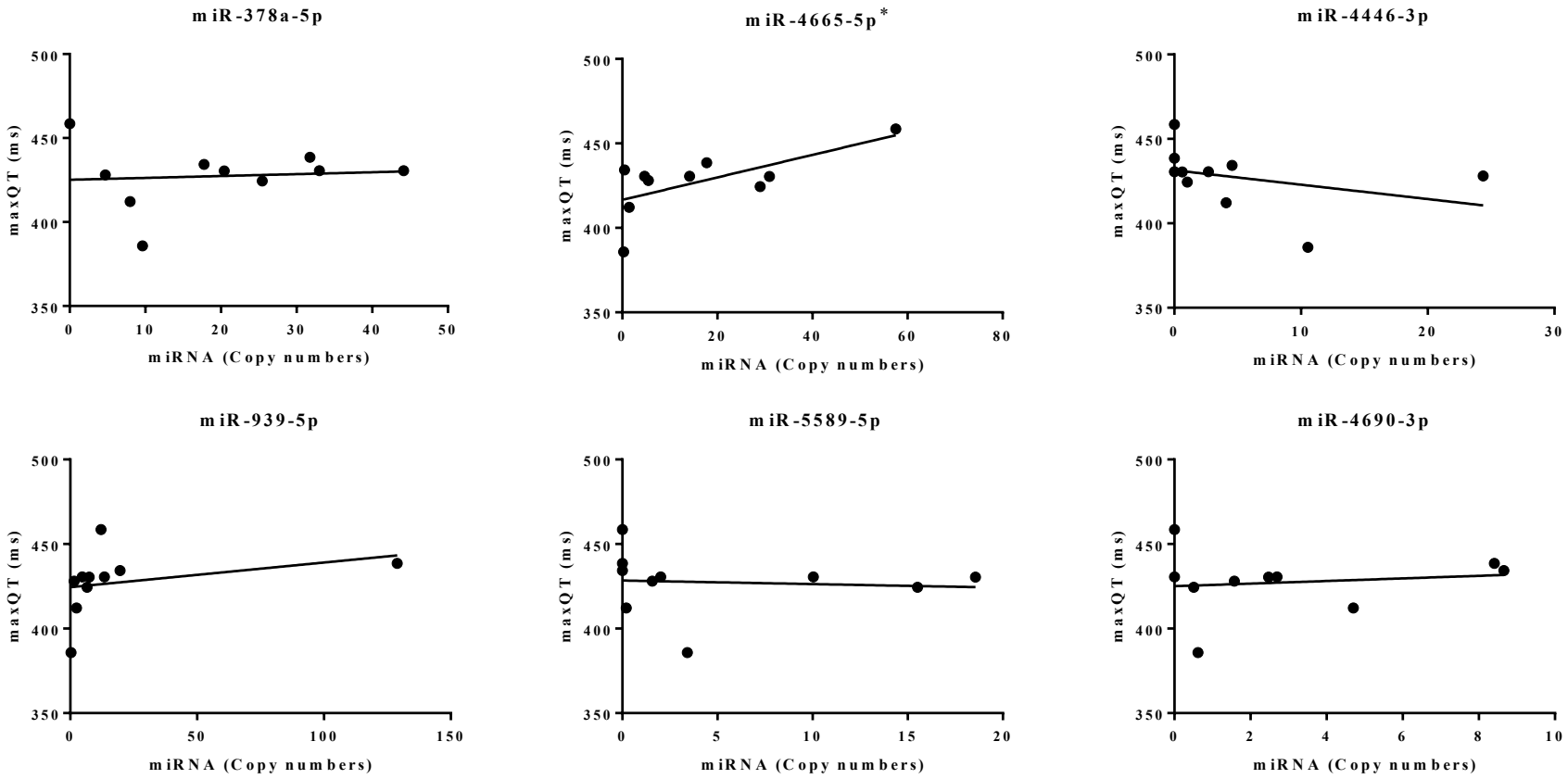

Figure 3:26. Correlation between expression of HT-bioassay-identified miRNAs in patients and maximum QTc interval. Expression of miR-4665-5p was significantly correlated with maximum QTc interval.

CHAPTER 4. DISCUSSION AND SUMMARY

4.1 miRNAs regulate hERG in cancer cells

The first Specific Aim identified the miRNAs that potentially regulate hERG expression and function in cultured breast cancer cells. Breast cancer is the second leading cause of all cancer-related deaths and the most common cancer among females worldwide (Becker 2015). The *KCNH2* gene is expressed in certain cancers including colorectal cancer, glioma, breast cancer, and leukemia, and has been associated with cancer development and progression (Asher, et al. 2010; Babcock and Li 2013; Glassmeier, et al. 2012; Gong, et al. 2010; Li, et al. 2007; Masi, et al. 2005; Shao, et al. 2008; Shao, et al. 2005; Thomas, et al. 2003). In these cancers, inhibition of the hERG potassium channel has been shown to impair cell proliferation and the invasiveness of tumor cells. This work identified miR-362-3p as a potential regulator of hERG expression and function in breast cancer cells.

The expression and role of miR-362-3p has been investigated in several types of cancer (Christensen, et al. 2013; Kang, et al. 2016; Li, et al. 2017; Shen, et al. 2015; Wang, et al. 2018a; Wang, et al. 2018b; Zhang, et al. 2015; Zou, et al. 2016). In colorectal cancer, miR-362-3p expression has been negatively correlated with the risk of tumor progression, and increasing its expression inhibits cell proliferation through the regulation of multiple related cancer genes (Christensen, et al. 2013). For example, the potential tumor suppressors *E2F1*, *USF2*, and *PTPN1* were identified as direct targets of miR-362-3p in colorectal cancer (Christensen, et al. 2013). Additionally, Kang et al. reported that miR-362-3p is a tumor suppressor in human breast cancer; its downregulation promotes tumor progression (Kang, et al. 2016). The oncogene

MCM5 was identified as a direct target of miR-362-3p in cervical adenocarcinoma (Wang, et al. 2018a). Thus, miR-362-3p targets oncogenes to exert beneficial effects.

In addition, miR-362-3p may regulate tumor suppressors in various cancers. For example, in hepatocellular carcinoma, miR-362-3p was found to contribute to hepatic malignancy by directly targeting the *Tob2* gene (Shen, et al. 2015). The *Tob2* gene has been implicated to regulate cell cycle and tumorigenesis as an anti-proliferative protein. A direct target of miR-362-3p in gastric cancer is the metastasis suppressor CD82, which is known to regulate epithelial-to-mesenchymal cell transition (EMT) (Zhang, et al. 2015). Consequently, anti-miR-362-3p inhibited the migration and invasion of gastric cancer. Thus, despite the evidence that miR-362-3p expression is associated with improved cancer outcomes, it may also possess counteractive oncogene activity via targeting *Tob2* or *CD82*.

Previous work has supported an oncogenic effect for hERG in breast cancer, with hERG channel inhibition inducing apoptosis and reducing cancer cell growth in MCF-7 cells (Roy, et al. 2008). Our results demonstrate that miR-362-3p inhibits both *KCNH2* mRNA and hERG protein expression in breast cancer cells that endogenously express hERG channels. miR-362-3p reduced hERG-related current and demonstrated anti-proliferative effects. This is in agreement with previous work demonstrating that miR-362-3p inhibits p130Cas expression in human breast cancer (Kang, et al. 2016). p130Cas has been implicated as an important regulator of cellular signaling, and its overexpression in breast cancer is associated with poor prognosis. Together, hERG and p130Cas might be involved in mediating the downstream effects of miR-362-3p.

hERG channels have also been implicated as being involved in different phases of cell cycle progression (Staudacher, et al. 2014). Therefore, we performed a cell cycle assay to explore this possible mechanism for regulation of breast cancer progression by miR-362-3p.

Indeed, transfection of breast cancer cells (MCF-7) with either miR-362-3p or *KCNH2* siRNA increased the proportion of cells in the G1 phase (Staudacher, et al. 2014). These findings are similar to previous studies in glioblastoma, where hERG inhibitors cause significant arrest of cancer cells in the G1 phase. However, there was no significant change in SK-BR-3 cells transfected with *KCNH2* siRNA when compared with control cells, indicating that the beneficial effects of miR-362-3p in these cells is most likely independent of cell cycle regulation.

There are two prevailing explanations for the distinct effects of miR-362-3p and *KCNH2* siRNA in MCF-7 and SK-BR-3 cells. First, MCF-7 and SK-BR-3 cells are genetically different; thus, distinct tumorigenic pathways drive their proliferation and invasion. Secondly, the primary evidence for hERG being involved in cell cycle regulation is from neuroblastoma and colorectal cancer (Christensen, et al. 2013; Staudacher, et al. 2014). The actual involvement of hERG channels in cell cycle regulation in breast cancer cells has not been investigated. Therefore, the modest effect of miR-362-3p on cell cycle distribution observed in this work might indicate that hERG channels exert their effects in breast cancer cells independent of cell cycle regulation.

4.2 The contribution of miR-362-3p to ibutilide-induced QT-interval lengthening

The ability of miR-362-3p to regulate *KCNH2* in breast cancer cells suggests a potential role for this miRNA in regulation of hERG function. In the present study, we utilized population PKPD modeling to investigate the contribution of miR-362-3p to drug-induced QT prolongation in patients administered ibutilide, known to prolong the QTc interval.

A population PKPD model was developed to characterize the relationship between ibutilide concentration and $\Delta\Delta QT_F$ changes and to determine the contribution of miR-362-3p expression and other potential covariates to variability in ibutilide-induced QT interval lengthening.

Pharmacokinetic and expression data were collected from a prospective, parallel-group comparative study during which a total of 22 patients received subtherapeutic doses (0.003 mg/kg) of ibutilide. This population PKPD model established that only HF (HFrEF or HFpEF) status is a significant predictor of maximum ibutilide-induced $\Delta\Delta QT_F$ interval lengthening, while miR-362-3p expression is a significant predictor of the ibutilide concentration required to produce 50% of maximum ibutilide-induced $\Delta\Delta QT_F$ interval lengthening.

The results showed that the combination of patients with either HFrEF or HFpEF had a greater degree of ibutilide-induced $\Delta\Delta QT_F$ interval lengthening, with a mean E_{max} increased by 39% compared to non-HF patients Thus, HF patients had a higher sensitivity to ibutilide-induced QT interval lengthening. In patients with acute decompensated HF or chronic severe HF, low cardiac output results in reduced hepatic blood flow; therefore, the pharmacokinetics of some high-extraction drugs might be altered (Benowitz and Meister 1976; Ogawa, et al. 2013). In particular, the clearance of high-extraction drugs approximates liver blood flow. One such drug is lidocaine, for which clearance is substantially decreased in HF, leading to increased exposure and subsequent increased risk of toxicity (Thomson, et al. 1973; Zito and Reid 1978). Although ibutilide is a high-extraction drug, in this study its pharmacokinetics were not altered by HF, suggesting that the observed significant increase in mean E_{max} is not related to ibutilide disposition in this population.

Patients with HF are at increased risk for drug-induced TdP, which is associated with a prolonged QT interval (Li and Ramos 2017; Tisdale 2016; Yap and Camm 2003). An increase in QT_c of 60 ms is generally considered a major determinant of the risk of drug-induced TdP. The findings of the present study are in agreement with those of a multicenter prospective study in which 6 patients with heart failure with reduced ejection fraction (HFrEF) and 9 matched control received 1 mg ibutilide intravenously (Tisdale, et al. 2012). They observed that median area under

the effect curve (AUEC) for QT_F vs. time was significantly larger in patients with HF while EC_{50} was lower, indicating that patients with HF have enhanced sensitivity to drug-induced QT interval lengthening.

The effect of miR-362-3p on ibutilide-induced $\Delta\Delta QT_F$ changes was also evaluated as a potential covariate. Indeed, miR-362-3p expression was identified as a predictor of ibutilide EC_{50}; specifically, they are negatively correlated, as patients with higher expression of miR-362-3p demonstrated a lower EC_{50}. This finding is supported by data presented in Aim 1, in which miR-362-3p reduced hERG expression in cultured cancer cells, suggesting hERG regulation may mediate the involvement of miR-362-3p in ibutilide-induced QT interval lengthening. However, the exact mechanism underlying the association between miR-362-3p expression and ibutilide remains unclear. One potential explanation is reduction of expressed channels due to high miR-362-3p expression, leading to fewer available targets for ibutilide and subsequently intensifying its effect. However, the effect of miR-362-3p on hERG channels is not immediate, as hERG turnover has a half-life of 8 to12 hours. Therefore, it would not be possible for miR-362-3p to instantly influence drug-associated QT interval lengthening through hERG downregulation. Another possible explanation is that the observed change in miR-362-3p expression might be mainly driven by ibutilide-associated QT changes; subsequently, the effect of miR-362-3p on QT interval lengthening could be evaluated more precisely several hours (>12 hours) following ibutilide administration, which was not the case in this study. A third explanation is that ibutilide might have a potential involvement in regulation of miR-362-3p expression. Recent studies have revealed that several drugs might be associated with alteration of miRNA expression (Rodrigues, et al. 2011). Rodrigues et al. investigated the influence of 19 drugs on the expression of ten different miRNAs in four different cell lines, and found that all ten miRNAs were differentially

expressed, depending on the administered drugs. Therefore, miR-362-3p expression might have been altered following ibutilide administration. Lastly, the observed change in ibutilide response could be attributed to either a significant increase in releasing cellular miRNAs to circulation or a significant elimination of miRNAs from circulation, resulting in alteration to levels of circulating miR-362-3p. The mechanisms underlining the release of miRNAs to circulation and their elimination from circulation have not been fully elucidated. Therefore, further studies are needed to understand the association between miR-362-3p serum expression and QT interval changes. Further investigation of this association would provide insight into the precise role and contribution of miR-362-3p in ibutilide-induced QT interval lengthening.

Few studies have examined the regulation of hERG by miRNAs. Wang et al. identified miR-17-5p as a regulator of hERG trafficking in neonatal rat ventricular myocytes (Wang, et al. 2013). Specifically, they found that miR-17-5p targeted multiple ER chaperones, and its upregulation interrupted hERG trafficking, which resulted in reduction of I_{kr} current. In addition, *KCNH2* has been identified as a direct target of miR-96 and miR-493. The expression of miR-96 is downregulated in pancreatic cancer tissues, and its ectopic expression reduces hERG expression, which subsequently inhibits the proliferation, migration, and invasion of pancreatic cancer cells (Feng, et al. 2014). Similarly, Zhi et al. demonstrated that miR-493 acts as a tumor suppressor by reducing hERG expression, leading to inhibition of malignant behavior in pancreatic cancer (Zhi, et al. 2017).

Endogenous expression of miRNAs has additionally been assessed in healthy and failing human hearts through deep sequencing and bioinformatics tools (Leptidis, et al. 2013). Over 250 miRNAs were differently expressed in failing hearts when compared with controls; among these, miR-362-3p was found to be highly expressed in patients with refractory end-stage heart failure.

4.3 Global miRNA involvement in regulation of *KCNH2* in hiPS-CM cells

While it is evident that patients with HF are at higher risk of drug-induced QT prolongation, the underlying mechanism remains unclear. The data presented in Aim 1 and 2 indicate a potential involvement of miR-362-3p in drug-induced QT prolongation. In addition, previous evidence indicates that miR-362-3p expression is altered in patients with HF (Leptidis, et al. 2013). Overall, mounting evidence suggests that miRNA in general are aberrantly expressed in HF (Vegter, et al. 2016; Wong, et al. 2016). While *KCNH2* is a direct target of miR-362-3p, it is potentially regulated by a set of miRNAs, especially others aberrantly expressed in HF. Several pieces of evidence demonstrate that most genes are under miRNA regulatory control (Catalanotto, et al. 2016). Initially, miRNA studies focused on the mapping of one individual miRNA to one novel mRNA target. However, multiple miRNAs can modulate the expression of a single gene (Selbach, et al. 2008). This was first experimentally confirmed by Wu et al. with the identification of 28 miRNAs that suppress the expression of cyclin-dependent kinase inhibitor 1A (*CDKN1A*), also known as p21aCip1/Waf1, by directly binding its 3' UTR (Wu, et al. 2010). Therefore, a large-scale high-throughput bioassay was developed to identify all miRNAs, in addition to miR-362-3p, potentially involved in regulating *KCNH2* expression and function in hiPS-CM during sustained β-adrenergic receptor (βAR) stimulation or overexpression of activated calcium/calmodulin-dependent protein kinase 2 (CaMKII), which are classical consequences of HF.

The developed HT-bioassay identified 31 miRNAs that potentially regulate the expression of *KCNH2*. These 31 miRNAs corresponded to 16 binding sites in the KCNH2 3' UTR, indicating that multiple miRNAs can share common binding sites. Interestingly, miR-362-3p was not identified among these miRNAs. While this result might contradict previous data suggesting upregulation of miR-362-3p in HF, it suggests that miR-362-3p might be regulated independently

of sustained βAR stimulation or the CAMKII signaling pathway. Meanwhile, the molecular systems underlying the progression of HF are very complex, and it is unrealistic to expect an *in vitro* experiment to take into account all pathways altered during HF. In fact, the HT-bioassay findings implicate miRNAs in regulating *KCNH2* through druggable pathways that warrant further investigation.

The HT-bioassay was further validated by testing seven of the 31 identified miRNAs through dual luciferase assays. Surprisingly, none reduced luciferase activity, indicating that luciferase assays might not be sensitive enough to detect or determine the binding of these miRNAs to the *KCNH2* 3' UTR. However, additional validation was performed by assessing hERG-related current density through whole cell electrophysiology using three of those six miRNAs. All three tested miRNA mimics significantly decreased I_{kr} current (P <0.05), suggesting that the HT-bioassay successfully identified miRNAs that potentially regulate hERG protein expression.

The lack of confirmation from the screening of HT-identified miRNAs with the luciferase assay may be attributable to the performance of those assays in SK-BR-3 cells. Several studies have shown that cellular context influences miRNA function, including through differences in expression of mRNA-binding proteins (RBPs) (Zealy, et al. 2017). In conjunction with miRNAs, RBPs play a major role in post-transcriptional gene regulation; for example, which types of RBPs are expressed may determine whether miRISC binds to its target. Therefore, it is possible that impaired miRNA-mRNA interaction in SK-BR-3 cells affected the ability of the tested miRNAs to repress luciferase activity.

Finally, expression of the miRNAs identified by HT-bioassay was examined in patients enrolled in a clinical trial in which genome-wide next generation sequencing was performed on miRNAs extracted from whole blood samples. Of the 31 HT-bioassay miRNAs, only six were

detected in serum samples (n = 12). A possible explanation for why only these six miRNAs were detected is that circulating miRNAs may not fully reflect those expressed in cardiac tissue (Dufresne, et al. 2018). In addition, the hiPS-CM miRNA expression profile might differ from the adult circulating miRNA expression profile. For the six detected miRNAs, a correlation analysis was performed to explore the relationship between their expression levels and ibutilide-induced QT_F interval lengthening. Of the six, only miR-4665-5p was significantly associated with QT_F interval length. It is important to mention that this analysis was performed using very a low sample size; therefore, the absence of significant correlation for the other miRNAs does not necessary imply that there is no relation between their expression and QT_F interval length.

miR-4665-5p has not been thoroughly studied. Slattery et al. suggest a potential contribution of miR-4665-5p to regulating the TGFβ signaling pathway in colon and rectal cancer (Slattery, et al. 2017). The role of miR-4665-5p in cardiac cells has not been investigated; the finding of this work suggests a potential involvement for this miRNA in *KCNH2* regulating that warrant further investigation.

CONCLUSION

In summary, miR-362-3p was identified to regulate hERG, and reduces proliferation of breast cancer cells through a mechanism that may be partially mediated by hERG inhibition. While this effect is modest and may not support the development of miR-362-3p as a therapeutic option in cancer, the role of hERG and its modulation should be assessed as a potential biomarker or further for potential benefit in cancers that overexpress this potential oncogene. Notably, miR-362-3p expression was altered during HF and did account for a significant amount of variability in QT_F prolongation following ibutilide administration. Consistent with findings from Aim 1, high expression of miR-362-3p was associated with a lower ibutilide concentration to produce response, suggesting sensitivity to ibutilide may be increased as a result of hERG inhibition by miR-362-3p. However, several miRNAs commonly regulate the same target protein or ion channel. Therefore, in the interest of obtaining a better perspective on global changes in miRNA expression associated with HF, the HT-bioassay was developed to identify all miRNAs that potentially regulate *KCNH2* during HF. This assay identified 31 other miRNAs predicted to regulate *KCNH2*, of which one (miR-4665-5p) was significantly associated with QT_F prolongation. Therefore, the potential for miR-362-3p and HT-bioassay-identified miRNAs to reduce hERG-related current and influence susceptibility to drug-induced QT interval prolongation warrants further investigation.

BIBLIOGRAPHY

Abbott, G. W., et al.

1999 MiRP1 forms IKr potassium channels with HERG and is associated with cardiac arrhythmia. Cell 97(2):175-87.

Aggarwal, S. K., and R. MacKinnon

1996 Contribution of the S4 segment to gating charge in the Shaker K+ channel. Neuron 16(6):1169-77.

Akbarali, H. I., et al.

1999 Role of HERG-like K(+) currents in opossum esophageal circular smooth muscle. Am J Physiol 277(6):C1284-90.

Anantharam, A., and G. W. Abbott

2005 Does hERG coassemble with a beta subunit? Evidence for roles of MinK and MiRP1. Novartis Found Symp 266:100-12; discussion 112-7, 155-8.

Anaya, Jordan

2016 OncoLnc: linking TCGA survival data to mRNAs, miRNAs, and lncRNAs. PeerJ Computer Science 2.

Anderson, C. L., et al.

2006 Most LQT2 mutations reduce Kv11.1 (hERG) current by a class 2 (trafficking-deficient) mechanism. Circulation 113(3):365-73.

Ardekani, Ali M., and Mozhgan Moslemi Naeini

2010 The Role of MicroRNAs in Human Diseases. Avicenna journal of medical biotechnology 2(4):161-179.

Asher, V., et al.

2010 Eag and HERG potassium channels as novel therapeutic targets in cancer. World J Surg Oncol 8:113.

Babcock, J. J., and M. Li

2013 hERG channel function: beyond long QT. Acta Pharmacol Sin 34(3):329-35.

Bartel, D. P.

2009 MicroRNAs: target recognition and regulatory functions. Cell 136(2):215-33.

Bayes-Genis, A., et al.

2018 Prognostic value of circulating microRNAs on heart failure-related morbidity and mortality in two large diverse cohorts of general heart failure patients. Eur J Heart Fail 20(1):67-75.

Becker, S.

2015 A historic and scientific review of breast cancer: The next global healthcare challenge. Int J Gynaecol Obstet 131 Suppl 1:S36-9.

Benning, C. M., and N. Kyprianou

2002 Quinazoline-derived alpha1-adrenoceptor antagonists induce prostate cancer cell apoptosis via an alpha1-adrenoceptor-independent action. Cancer Res 62(2):597-602.

Benowitz, N. L., and W. Meister

1976 Pharmacokinetics in patients with cardiac failure. Clin Pharmacokinet 1(6):389-405.

Bianchi, L., et al.

1998 herg encodes a K+ current highly conserved in tumors of different histogenesis: a selective advantage for cancer cells? Cancer Res 58(4):815-22.

Binggeli, R., and R. C. Weinstein

1986 Membrane potentials and sodium channels: hypotheses for growth regulation and cancer formation based on changes in sodium channels and gap junctions. J Theor Biol 123(4):377-401.

Broughton, J. P., et al.

2016 Pairing beyond the Seed Supports MicroRNA Targeting Specificity. Mol Cell 64(2):320-333.

Carmeliet, E.

1992 Voltage- and time-dependent block of the delayed K+ current in cardiac myocytes by dofetilide. J Pharmacol Exp Ther 262(2):809-17.

Catalanotto, Caterina, Carlo Cogoni, and Giuseppe Zardo

2016 MicroRNA in Control of Gene Expression: An Overview of Nuclear Functions. International journal of molecular sciences 17(10):1712.

Chendrimada, T. P., et al.

2005 TRBP recruits the Dicer complex to Ago2 for microRNA processing and gene silencing. Nature 436(7051):740-4.

Christensen, L. L., et al.

2013 MiRNA-362-3p induces cell cycle arrest through targeting of E2F1, USF2 and PTPN1 and is associated with recurrence of colorectal cancer. Int J Cancer 133(1):67-78.

Cullen, B. R.

2004 Transcription and processing of human microRNA precursors. Mol Cell 16(6):861-5.

D'Amico, M., L. Gasparoli, and A. Arcangeli

2013 Potassium channels: novel emerging biomarkers and targets for therapy in cancer. Recent Pat Anticancer Drug Discov 8(1):53-65.

Dawson, K., et al.

2013 MicroRNA29: a mechanistic contributor and potential biomarker in atrial fibrillation. Circulation 127(14):1466-75, 1475e1-28.

de Rie, D., et al.

2017 An integrated expression atlas of miRNAs and their promoters in human and mouse. Nat Biotechnol 35(9):872-878.

Denli, A. M., et al.

2004 Processing of primary microRNAs by the Microprocessor complex. Nature 432(7014):231-5.

Drici, M. D., and J. Barhanin

2000 Cardiac K+ channels and drug-acquired long QT syndrome. Therapie 55(1):185-93.

Dueck, Anne, et al.

2012 microRNAs associated with the different human Argonaute proteins. Nucleic acids research 40(19):9850-9862.

Dufresne, S., et al.

2018 A Review of Physical Activity and Circulating miRNA Expression: Implications in Cancer Risk and Progression. Cancer Epidemiol Biomarkers Prev 27(1):11-24.

El-Sherif, N., G. Turitto, and M. Boutjdir

2018 Acquired long QT syndrome and torsade de pointes. Pacing Clin Electrophysiol 41(4):414-421.

Endo, K., et al.

2013 MicroRNA 210 as a biomarker for congestive heart failure. Biol Pharm Bull 36(1):48-54.

Engel, L. W., and N. A. Young

1978 Human breast carcinoma cells in continuous culture: a review. Cancer Res 38(11 Pt 2):4327-39.

Feldman, A., et al.

2017 Analysis of Circulating miR-1, miR-23a, and miR-26a in Atrial Fibrillation Patients Undergoing Coronary Bypass Artery Grafting Surgery. Ann Hum Genet 81(3):99-105.

Feng, J., et al.

2014 HERG1 functions as an oncogene in pancreatic cancer and is downregulated by miR-96. Oncotarget 5(14):5832-44.

Fiore, A., et al.

2013 Characterization of hERG1 channel role in mouse colorectal carcinogenesis. Cancer Med 2(5):583-94.

Glassmeier, G., et al.

2012 Inhibition of HERG1 K+ channel protein expression decreases cell proliferation of human small cell lung cancer cells. Pflugers Arch 463(2):365-76.

Gong, J. H., et al.

2010 HERG K+ channel related chemosensitivity to sparfloxacin in colon cancer cells. Oncol Rep 23(6):1747-56.

Guasti, L., et al.

2005 Expression pattern of the ether-a-go-go-related (ERG) family proteins in the adult mouse central nervous system: evidence for coassembly of different subunits. J Comp Neurol 491(2):157-74.

Ha, M., and V. N. Kim

2014 Regulation of microRNA biogenesis. Nat Rev Mol Cell Biol 15(8):509-24.

Harling, L., et al.

2017 Elevated serum microRNA 483-5p levels may predict patients at risk of post-operative atrial fibrillation. Eur J Cardiothorac Surg 51(1):73-78.

Huffaker, S. J., et al.

2009 A primate-specific, brain isoform of KCNH2 affects cortical physiology, cognition, neuronal repolarization and risk of schizophrenia. Nat Med 15(5):509-18.

Ipe, J., et al.

2018 PASSPORT-seq: A Novel High-Throughput Bioassay to Functionally Test Polymorphisms in Micro-RNA Target Sites. Front Genet 9:219.

Itoh, T., et al.

1998 Genomic organization and mutational analysis of HERG, a gene responsible for familial long QT syndrome. Hum Genet 102(4):435-9.

Jiang, Y., et al.

2002 Crystal structure and mechanism of a calcium-gated potassium channel. Nature 417(6888):515-22.

Kang, H., et al.

2016 Downregulation of microRNA-362-3p and microRNA-329 promotes tumor progression in human breast cancer. Cell Death Differ 23(3):484-95.

Kao, J., et al.

2009 Molecular profiling of breast cancer cell lines defines relevant tumor models and provides a resource for cancer gene discovery. PLoS One 4(7):e6146.

Lastraioli, E., et al.

2004 herg1 gene and HERG1 protein are overexpressed in colorectal cancers and regulate cell invasion of tumor cells. Cancer Res 64(2):606-11.

Lastraioli, E., et al.

2015 hERG1 Potassium Channels: Novel Biomarkers in Human Solid Cancers. Biomed Res Int 2015:896432.

Lee, H. C., et al.

2011 Single point mutation of microRNA may cause butterfly effect on alteration of global gene expression. Biochem Biophys Res Commun 404(4):1065-9.

Lee, R. C., R. L. Feinbaum, and V. Ambros

1993 The C. elegans heterochronic gene lin-4 encodes small RNAs with antisense complementarity to lin-14. Cell 75(5):843-54.

Lees-Miller, J. P., et al.

1997 Electrophysiological characterization of an alternatively processed ERG K+ channel in mouse and human hearts. Circ Res 81(5):719-26.

Leptidis, S., et al.

2013 A deep sequencing approach to uncover the miRNOME in the human heart. PLoS One 8(2):e57800.

Li, C., et al.

2014 MicroRNA-328 as a regulator of cardiac hypertrophy. Int J Cardiol 173(2):268-76.

Li, H., et al.

2007 Expression and functional role of HERG1, K+ channels in leukemic cells and leukemic stem cells. J Huazhong Univ Sci Technolog Med Sci 27(3):257-60.

Li, M., et al.

2017 MiR-362-3p inhibits the proliferation and migration of vascular smooth muscle cells in atherosclerosis by targeting ADAMTS1. Biochem Biophys Res Commun 493(1):270-276.

Li, Matthew, and Liz G. Ramos

2017 Drug-Induced QT Prolongation And Torsades de Pointes. P & T : a peer-reviewed journal for formulary management 42(7):473-477.

Liman, E. R., et al.

1991 Voltage-sensing residues in the S4 region of a mammalian K+ channel. Nature 353(6346):752-6.

Liu, M., and A. Grigoriev

2004 Protein domains correlate strongly with exons in multiple eukaryotic genomes--evidence of exon shuffling? Trends Genet 20(9):399-403.

Livak, K. J., and T. D. Schmittgen

2001 Analysis of relative gene expression data using real-time quantitative PCR and the 2(-Delta Delta C(T)) Method. Methods 25(4):402-8.

London, B., et al.

1997 Two isoforms of the mouse ether-a-go-go-related gene coassemble to form channels with properties similar to the rapidly activating component of the cardiac delayed rectifier K+ current. Circ Res 81(5):870-8.

Masi, A., et al.

2005 hERG1 channels are overexpressed in glioblastoma multiforme and modulate VEGF secretion in glioblastoma cell lines. Br J Cancer 93(7):781-92.

McDonald, T. V., et al.

1997 A minK-HERG complex regulates the cardiac potassium current I(Kr). Nature 388(6639):289-92.

Meister, G., and T. Tuschl

2004 Mechanisms of gene silencing by double-stranded RNA. Nature 431(7006):343-9.

Morais Cabral, J. H., et al.

1998 Crystal structure and functional analysis of the HERG potassium channel N terminus: a eukaryotic PAS domain. Cell 95(5):649-55.

Morishima, M., et al.

2016 Atrial Fibrillation-Mediated Upregulation of miR-30d Regulates Myocardial Electrical Remodeling of the G-Protein-Gated K(+) Channel, IK.ACh. Circ J 80(6):1346-55.

Nishi, H., et al.

2013 Impact of microRNA expression in human atrial tissue in patients with atrial fibrillation undergoing cardiac surgery. PLoS One 8(9):e73397.

O'Brien, J., et al.

2018 Overview of MicroRNA Biogenesis, Mechanisms of Actions, and Circulation. Front Endocrinol (Lausanne) 9:402.

Ogawa, R., J. M. Stachnik, and H. Echizen

2013 Clinical pharmacokinetics of drugs in patients with heart failure: an update (part 1, drugs administered intravenously). Clin Pharmacokinet 52(3):169-85.

Orom, U. A., F. C. Nielsen, and A. H. Lund

2008 MicroRNA-10a binds the 5'UTR of ribosomal protein mRNAs and enhances their translation. Mol Cell 30(4):460-71.

Ovchinnikova, E. S., et al.

2016 Signature of circulating microRNAs in patients with acute heart failure. Eur J Heart Fail 18(4):414-23.

Perron, M. P., and P. Provost

2008 Protein interactions and complexes in human microRNA biogenesis and function. Front Biosci 13:2537-47.

Piper, D. R., et al.

2005 Regional specificity of human ether-a'-go-go-related gene channel activation and inactivation gating. J Biol Chem 280(8):7206-17.

Pointer, K. B., et al.

2017 Administration of Non-Torsadogenic human Ether-a-go-go-Related Gene Inhibitors Is Associated with Better Survival for High hERG-Expressing Glioblastoma Patients. Clin Cancer Res 23(1):73-80.

Roden, Dan M., and Prakash C. Viswanathan

2005 Genetics of acquired long QT syndrome. The Journal of clinical investigation 115(8):2025-2032.

Rodrigues, A. C., et al.

2011 MicroRNA expression is differentially altered by xenobiotic drugs in different human cell lines. Biopharm Drug Dispos 32(6):355-67.

Romaine, S. P., et al.

2015 MicroRNAs in cardiovascular disease: an introduction for clinicians. Heart 101(12):921-8.

Rosati, B., et al.

2000 Glucose- and arginine-induced insulin secretion by human pancreatic beta-cells: the role of HERG K(+) channels in firing and release. Faseb j 14(15):2601-10.

Roy, J., et al.

2008 Pharmacological separation of hEAG and hERG K+ channel function in the human mammary carcinoma cell line MCF-7. Oncol Rep 19(6):1511-6.

Sanguinetti, M. C., et al.

1995 A mechanistic link between an inherited and an acquired cardiac arrhythmia: HERG encodes the IKr potassium channel. Cell 81(2):299-307.

Sanguinetti, M. C., and M. Tristani-Firouzi

2006 hERG potassium channels and cardiac arrhythmia. Nature 440(7083):463-9.

Selbach, Matthias, et al.

2008 Widespread changes in protein synthesis induced by microRNAs. Nature 455:58.

Shao, X. D., et al.

2008 Expression and significance of HERG protein in gastric cancer. Cancer Biol Ther 7(1):45-50.

Shao, X. D., et al.

2005 The potent inhibitory effects of cisapride, a specific blocker for human ether-a-go-go-related gene (HERG) channel, on gastric cancer cells. Cancer Biol Ther 4(3):295-301.

Shapovalov, G., et al.

2011 TRP channels in cell survival and cell death in normal and transformed cells. Cell Calcium 50(3):295-302.

Shen, H., et al.

2015 Upregulation of miR-362-3p Modulates Proliferation and Anchorage-Independent Growth by Directly Targeting Tob2 in Hepatocellular Carcinoma. J Cell Biochem 116(8):1563-73.

Slattery, Martha L., et al.

2017 Genetic variants in the TGFβ-signaling pathway influence expression of miRNAs in colon and rectal normal mucosa and tumor tissue. Oncotarget 8(10):16765-16783.

Smith, G. A., et al.

2002 Functional up-regulation of HERG K+ channels in neoplastic hematopoietic cells. J Biol Chem 277(21):18528-34.

Smith, J. L., et al.

2016 Molecular pathogenesis of long QT syndrome type 2. J Arrhythm 32(5):373-380.

Smith, P. L., T. Baukrowitz, and G. Yellen

1996 The inward rectification mechanism of the HERG cardiac potassium channel. Nature 379(6568):833-6.

Soule, H. D., et al.

1973 A human cell line from a pleural effusion derived from a breast carcinoma. J Natl Cancer Inst 51(5):1409-16.

Staudacher, I., et al.

2014 HERG K+ channel-dependent apoptosis and cell cycle arrest in human glioblastoma cells. PLoS One 9(2):e88164.

Sticht, Carsten, et al.

2018 miRWalk: An online resource for prediction of microRNA binding sites. PloS one 13(10):e0206239-e0206239.

Subbiah, R. N., et al.

2004 Molecular basis of slow activation of the human ether-a-go-go related gene potassium channel. J Physiol 558(Pt 2):417-31.

Sygitowicz, G., et al.

2015 Circulating microribonucleic acids miR-1, miR-21 and miR-208a in patients with symptomatic heart failure: Preliminary results. Arch Cardiovasc Dis 108(12):634-42.

Tanzer, A., and P. F. Stadler

2004 Molecular evolution of a microRNA cluster. J Mol Biol 339(2):327-35.

Thomas, D., et al.

2003 Inhibition of cloned HERG potassium channels by the antiestrogen tamoxifen. Naunyn Schmiedebergs Arch Pharmacol 368(1):41-8.

Thomson, P. D., et al.

1973 Lidocaine pharmacokinetics in advanced heart failure, liver disease, and renal failure in humans. Ann Intern Med 78(4):499-508.

Tisdale, J. E.

2016 Drug-induced QT interval prolongation and torsades de pointes: Role of the pharmacist in risk assessment, prevention and management. Can Pharm J (Ott) 149(3):139-52.

Tisdale, J. E., et al.

2012 Enhanced sensitivity to drug-induced QT interval lengthening in patients with heart failure due to left ventricular systolic dysfunction. J Clin Pharmacol 52(9):1296-305.

Tristani-Firouzi, M., J. Chen, and M. C. Sanguinetti

2002 Interactions between S4-S5 linker and S6 transmembrane domain modulate gating of HERG K+ channels. J Biol Chem 277(21):18994-9000.

Vandenberg, J. I., et al.

2012 hERG K(+) channels: structure, function, and clinical significance. Physiol Rev 92(3):1393-478.

Vasudevan, S.

2012 Posttranscriptional upregulation by microRNAs. Wiley Interdiscip Rev RNA 3(3):311-30.

Vasudevan, S., and J. A. Steitz

2007 AU-rich-element-mediated upregulation of translation by FXR1 and Argonaute 2. Cell 128(6):1105-18.

Vegter, E. L., et al.

2016 MicroRNAs in heart failure: from biomarker to target for therapy. Eur J Heart Fail 18(5):457-68.

Wang, D., et al.

2018a MiR-362-3p functions as a tumor suppressor through targeting MCM5 in cervical adenocarcinoma. Biosci Rep 38(3).

Wang, N., et al.

2018b miR-362-3p regulates cell proliferation, migration and invasion of trophoblastic cells under hypoxia through targeting Pax3. Biomed Pharmacother 99:462-468.

Wang, Qi, et al.

2013 MiR-17-5p impairs trafficking of H-ERG K+ channel protein by targeting multiple er stress-related chaperones during chronic oxidative stress. PloS one 8(12):e84984-e84984.

Wang, Y., et al.

2015 Arsenic trioxide inhibits breast cancer cell growth via microRNA-328/hERG pathway in MCF-7 cells. Mol Med Rep 12(1):1233-8.

Warmke, J. W., and B. Ganetzky

1994 A family of potassium channel genes related to eag in Drosophila and mammals. Proc Natl Acad Sci U S A 91(8):3438-42.

Wong, Lee Lee, et al.

2016 MicroRNA and Heart Failure. International journal of molecular sciences 17(4):502-502.

Wu, S., et al.

2010 Multiple microRNAs modulate p21Cip1/Waf1 expression by directly targeting its 3' untranslated region. Oncogene 29(15):2302-8.

Xie, B., et al.

2013 miRCancer: a microRNA-cancer association database constructed by text mining on literature. Bioinformatics 29(5):638-44.

Yap, Y. G., and A. J. Camm

2003 Drug induced QT prolongation and torsades de pointes. Heart 89(11):1363-72.

Yekta, S., I. H. Shih, and D. P. Bartel

2004 MicroRNA-directed cleavage of HOXB8 mRNA. Science 304(5670):594-6.

Zealy, R. W., et al.

2017 microRNA-binding proteins: specificity and function. Wiley Interdiscip Rev RNA 8(5).

Zhang, M., J. Liu, and G. N. Tseng

2004 Gating charges in the activation and inactivation processes of the HERG channel. J Gen Physiol 124(6):703-18.

Zhang, Q. H., et al.

2015 Anti-miR-362-3p Inhibits Migration and Invasion of Human Gastric Cancer Cells by Its Target CD82. Dig Dis Sci 60(7):1967-76.

Zhi, D., et al.

2017 miR-493 inhibits proliferation and invasion in pancreatic cancer cells and inversely regulated hERG1 expression. Oncol Lett 14(6):7398-7404.

Zhou, Z., et al.

1998 Properties of HERG channels stably expressed in HEK 293 cells studied at physiological temperature. Biophys J 74(1):230-41.

Zito, R. A., and P. R. Reid

1978 Lidocaine kinetics predicted by indocyanine green clearance. N Engl J Med 298(21):1160-3.

Zou, X., et al.

2016 miR-362-3p targets nemo-like kinase and functions as a tumor suppressor in renal cancer cells. Mol Med Rep 13(1):994-1002.